Statistical Shape Analysis for the Human Back

ARIF REZA ANWARY

A thesis submitted to the department of Engineering and Technology in partial fulfilment of the requirements for the degree of Master of Philosophy in Production and Manufacturing Engineering at the University of Wolverhampton

The research was carried out with the Research and Teaching Centre of the Royal Orthopaedic Hospital, Birmingham

May 2012

Statistical Shape Analysis for the Human Back

ARIF REZA ANWARY

MAY 2012

This work or any part thereof has not previously been presented in any form to the University or to any other body whether for the purpose of assessment, publication or for any other purpose (unless otherwise indicated). Save for any express acknowledgements, references and/or bibliographies cited in the work, I confirm that the intellectual content of the work is the result of my own efforts and of no other person.

Signature :_____

Date : _____

Abstract

In this research, Procrustes and Euclidean distance matrix analysis (EDMA) have been investigated for analysing the three-dimensional shape and form of the human back. Procrustes analysis is used to distinguish deformed backs from normal backs. EDMA is used to locate the changes occurring on the back surface due to spinal deformity (scoliosis, kyphosis and lordosis) for back deformity patients.

A surface topography system, ISIS2 (Integrated Shape Imaging System 2), is available to measure the three-dimensional back surface. The system presents clinical parameters, which are based on distances and angles relative to certain anatomical landmarks on the back surface. Location, rotation and scale definitely influence these parameters. Although the anatomical landmarks are used in the present system to take some account of patient stance, it is still felt that variability in the clinical parameters is increased by the use of length and angle data. Patients also grow and so their back size, shape and form change between appointments with the doctor. Instead of distances and angles, geometric shape that is independent of location, rotation and scale effects could be measured. This research is mainly focusing on the geometric shape and form change in the back surface, thus removing the unwanted effects.

Landmarks are used for describing back information and an analysis of the variability in positioning the landmarks has been carried out for repeated measurements.

Generalized Procrustes analysis has been applied to all normal backs to calculate a mean Procrustes shape, which is named the standard normal shape (SNS). Each back (normal and deformed) is then translated, rotated and scaled to give a best fit with the SNS using ordinary Procrustes analysis. Riemannian distances are then estimated between the SNS and all individual backs. The highest Riemannian distance value between the normal backs and the SNS is lower than the lowest Riemannian distance value between the deformed backs and the SNS. The results shows that deformed backs can be differentiated from normal backs.

EDMA has been used to estimate a mean form, variance-covariance matrix and mean form difference from all the normal backs. This mean form is named the standard normal form (SNF). The influence of individual landmarks for form difference between each deformed back and the SNF is estimated. A high value indicates high deformity on the location of that landmark and a low value close to 1 indicates less deformity. The result is displayed in a graph that provides information regarding the degree and location of the deformity.

The novel aspects of this research lie in the development of an effective method for assessing the three-dimensional back shape; extracting automatic landmarks; visualizing back shape and back form differences.

Table of Contents

List of Figures

List of Tables

Acknowledgments

I would like to express my gratitude to my first supervisor, Dr. Fiona Berryman, whose expertise, understanding, and patience, added considerably to my research experience. I appreciate her vast knowledge and skill in many areas (e.g., medical, engineering, statistics), and her assistance in writing reports (i.e., annual report and this thesis). I would like to thank my second supervisor Professor Paul Pynsent for his support and guidance provided at all levels throughout the research project. Finally, I would like to thank Professor Diane Mynors for taking time out from her busy schedule to serve as my other supervisor. Special thanks go to Dang C. Zheng for her motivation and encouragement during my research. I also would like to acknowledge Hayley Everett for her assistance in accessing the research room during the weekend.

I must also acknowledge Dr. M. Fayyaz Khan (Head of EEE, United International University, Bangladesh) and Dr. Iftekhar Anam (Associate Professor, The University of Asia Pacific, Bangladesh) who truly made a difference in my life. It was under their tutelage that I developed an artificial intelligent robot and became interested in back shape analysis. They provided me with direction and support and became more of a mentor and friend, than a professor. It was through their persistence, understanding and kindness that I completed my undergraduate degree and was encouraged for further study. I doubt that I will ever be able to convey my appreciation fully, but I owe them my eternal gratitude.

I would like to thank my friends particularly Shimon Ferdous, Enamul, Sujon, Bony, Farzana and Asamta for exchanging of knowledge, skills and venting of frustration during my research work, which helped enrich the experience.

Very special thanks go to my parents for their endless support to me throughout their lives. May Allah grant them entrance into Paradise by Allah's infinite mercy. Without their love and passion I would never be able to reach here and I dedicate this work to my parents.

In conclusion, I recognize that this research would not have been possible without the financial assistance of the trustees of the ROH Orthopaedic Charity.

Nomenclature

B_i	Wishart distribution independent of nuisance parameters
$B(X)$	centred inner product matrix
c_i	uniform scaling
D	number of dimensions
E	sum of squares of residuals
E_i	error matrix with Gaussian distribution
$Eu(x)$	matrix of squared distances
$F(X)$	Euclidean distances between all landmarks
G_i	centroid matrix
H	centring matrix
j	unit vector
k	number of dimensions
K	number of landmarks
L	number of pair-wise distances of upper or lower triangle from diagonal
m	number of configurations
M	mean form
O_i	rotation matrix
p	number of landmarks chosen from each configuration
P	number of clusters
R_s	residual sum of squares
S_r	diagonal matrix contains singular values from singular value decomposition
t_i	translation vector
^{T}	transpose of a matrix
$tr(A)$	trace operation of matrix A
$T(\cdot)$	maximal invariant under S space with the group rotation, translation and scaling of configuration

U_r	left singular vector where $U_r^T U_r = I_{r\times r}$ from singular value decomposition
V_r	right singular vector, U_r and V_r are orthogonal where $V_r^T V_r = I_{r\times r}$ from singular value decomposition
X_i	configuration containing landmark information
$\hat{X}_i$	transformations of scaling, rotation and translation
X^c	mean centered of X
X^*	rotation, translation of X
Y	consensus configuration or the new coordinates of the centroid of the group
Δ	residual, the length of mp
δ	Kronecker matrix
Λ	symmetric matrix
λ_{uv}	Lagrange multiplier
μ	population average configuration
$\otimes$	Kronecker product
Σ_K	variance and covariance of landmarks
Σ_D	variance and covariance of the perturbation with respect to the real space coordinate axes
Γ_i	rotation matrix
δ_{lm}	pair-wise Euclidean distance
e_{lm}	squared Euclidean distance between pairs of landmaks
ϕ_{lm}	scaling parameter
σ_{lm}	variance-covariance between pair of landmarks
λ_i	Eigenvalues

1 Introduction

1.1 Introduction

Assessment of the geometrical changes in human back is scientifically interesting and clinically important which can provide information to distinguish deformed backs from normal backs. This assessment of back shape in clinical practice has been deemed largely subjective and based on visual, non-standardized criteria and methods [1]. These can be subject to significant error and thus provide no objective or reproducible three-dimensional (3D) measurements. There are numerous computer systems (ISIS [2-4], ISIS2 [5], Quantec [6], laser beam [7] and Formetric [8] etc) available and those produce 3D surface information of human back. Although these systems are available for our use, yet data on normal adolescent back shape has so far been scarce [9-11]. Obviously, this is seriously affecting the clinical certainly with which they can establish an observed back deformity so as to initiate an appropriate treatment. The purpose of this study is to improve ISIS2 by using overall back surface information so that it could provide information for assessing back shapes in order to distinguish normal backs from deformed backs and locating the deformation location for back deformity patients.

1.2 Back deformity

A back deformity is a major difference in the shape of a back compared to the average back shape of human backs. There are various reasons (ribs tumours and/or osteoporosis etc [12]) for back deformity and deformities on the back are usually caused by abnormal development of the spine. The vertebrae are stacked together to form the spine. Hence, improper growth of a single vertebra changes the alignment of neighbouring vertebrae. Back deformity is often first noticed as small differences in the geometrical form of the back during the adolescence period. These differences may result in slight asymmetries of the shoulders, the

trunk or hips and the appearance of skin folds around the waist. A rib hump may also develop over time on the back. These changes on back surface occur over a period of months to years during the growth of the child. Sometime an abnormal lateral curvature or excessive backwards curvature of the spine can result in back deformity. The medical definition of the body planes is shown in Figure 1.1.

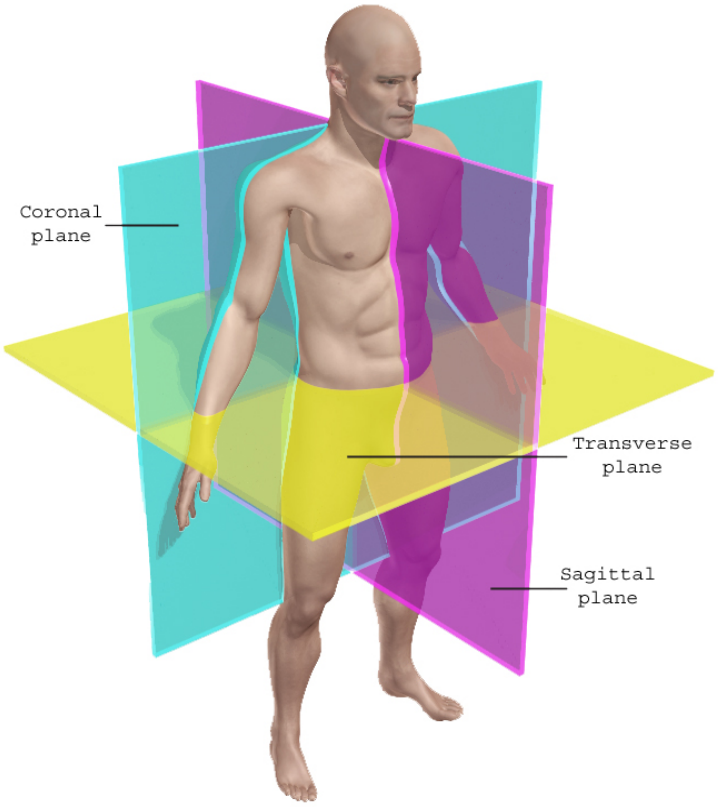

Figure 1.1: Coronal, sagittal and transverse planes of a normal back [13]

The sagittal plane divides the body into two sides, the coronal plane into front and back and the transverse plane into top and bottom. Back deformity can potentially affect all planes. The normal spine is straight in the coronal plane while a deformed spine has a curve in this plane and/or excessive curve on sagittal plane. A flat back (i.e. low curvature either in the thoracic region or the lumbar region) on sagittal plane can also be considered a deformity. Each normal curve on the spine is designed to efficiently transfer the weight of the body and distribute it down through the pelvis.

1.3 Causes of back deformities

Spinal deformity has great impact on the back surface; this is to say that whenever there is spinal deformity it usually results in back deformity. There are many different causes of spinal deformity. Some babies are born with spinal defects that might cause the spine to grow unevenly. Some children have nerve or muscle disease, injuries or other illness that can also cause back deformity (for example, cerebral palsy or myelomeningocele). Another reason for back deformity may involve genetic, neuromuscular, hormonal, biochemical or other abnormalities. Sometimes the back does not grow as straight as it should and the reason is unknown. This is the most common type of back deformity that is called “idiopathic”. A deformity of the back may also arise from tumours and infections of a vertebra. This can occur in any age group and its progression on back surface is dependent on the course of the tumour or infection.

1.4 Types of back deformities

Spinal deformity is a complex three-dimensional process. A normal spine looks straight when viewed from behind (coronal plane) and is curved when viewed from the side (sagittal plane). Based on the shape of spine, there are three basic types of back deformities. Those are scoliosis, kyphosis and lordosis.

1.4.1 Scoliosis

The term scoliosis originates from the Greek physician Galen [14] more than eighteen centuries ago and comes from the Greek word for “crooked”. It is a lateral deformation of the spine in the coronal plane. Although the spine does curve from front to back it should not curve sideways very much. A side-to-side curve is called scoliosis and may take the shape of an "S" (double curve) or a "C" (single curve). Scoliosis is more than just a curve to the side. The scoliotic spine is also rotated or twisted. As the spine twists it pulls the ribs along with it, so that one side of the chest becomes higher than the other, or the shape of the breastbone may change. To better understand this, compare the drawings of the

spinous process of a normal back (Figure 1.2 (a)) and a deformed back (Figure 1.2 (b)). The green line that represents the spinous process (from the vertebra prominens to the sacrum) is a spline curve fitted through the sticker locations on back surface. The red rectangle shows the anatomical sticker locations.

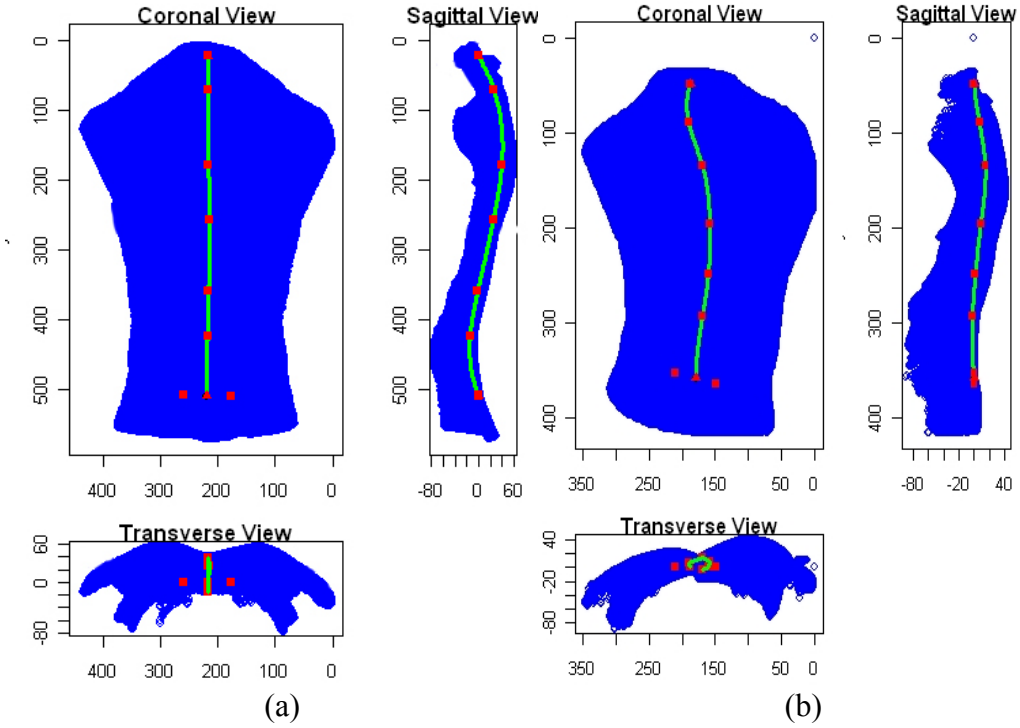

Figure 1.2: The spinal curve for normal back (NormalBack 1) and deformed back (DeformBack17)

Many people with scoliosis also have hypokyphosis (see Section 2.4.2.4). Because of all the possible combinations of curvatures, scoliosis can be very different in different people [15]. Orthopaedic surgeons refer to four different kinds of idiopathic scoliosis that is based on their age. Those are - i*nfantile idiopathic scoliosis, juvenile idiopathic scoliosis, adolescent idiopathic scoliosis and adult idiopathic scoliosis*.

1.4.1.1 Infantile idiopathic scoliosis

Infantile idiopathic scoliosis is not a common type of scoliosis. Infantile idiopathic scoliosis occurs from birth to less than four years of age. It is the only

type of scoliosis where the most common curve pattern is in the left thoracic region (upper spine) [16, 17].

1.4.1.2 Juvenile idiopathic scoliosis

Juvenile idiopathic scoliosis usually occurs from about age 4 to the onset of puberty (age 10 or 11 for girls and 12 for boys) [18].

1.4.1.3 Adolescent idiopathic scoliosis (AIS)

This type of scoliosis usually begins during early puberty, with the most rapid worsening occurring during the early adolescent growth spurt. It is the most common type of idiopathic scoliosis and the most common type of scoliosis overall which can present as curvature of the thoracic and lumbar spine. The North American Spine Society defines AIS as a persistent lateral curvature of the spine of more than 10 degrees in the upright or standing position [19]. It is a complex three-dimensional deformity associated with rotation of the spine, and different plane curvatures, although, its main component is the lateral curvature. There are many signs and symptoms of AIS including shoulder asymmetry (one shoulder higher than the other), waistline asymmetry or tilt, trunk shift (comparing the chest or torso to the pelvis) and limb length inequality. Most of the time, AIS is a painless deformity and the patients have no weakness or movement problems; the treatment recommendations for it are based on the magnitude of the curvature [20].

1.4.1.4 Adult idiopathic scoliosis

This is defined as a lateral curvature of the spine in a skeletally mature individual [21]. It does not start in adult life, and is usually recognized for the first time in adolescence and continued in to adulthood. It is marked by significant curve progression following the completion of physical maturity.

1.4.2 Kyphosis

Kyphosis is an excessive front-to-back curvature of the thoracic spine. This can be clearly seen when viewed from the side (see Figure 1.3). It causes the back to look rounded or humped. It is normal to have some kyphosis in the thoracic (chest area) spinal column. Too much kyphosis in the thoracic spine is called "hyperkyphosis," Scheurmann's kyphosis, or "round back." When there is not enough kyphosis in the thoracic spine (as is often the case with idiopathic scoliosis), it is called thoracic hypokyphosis.

1.4.3 Lordosis

Lordosis is an abnormal excessive front-to-back curvature of the lower spine (lumbar region). It can be seen in Figure 1.3. Sometime lordosis may be associated with poor posture, a congenital problem with the vertebrae, neuromuscular problems or hip problems. An exaggerated lordosis can be painful and it can also affect movement.

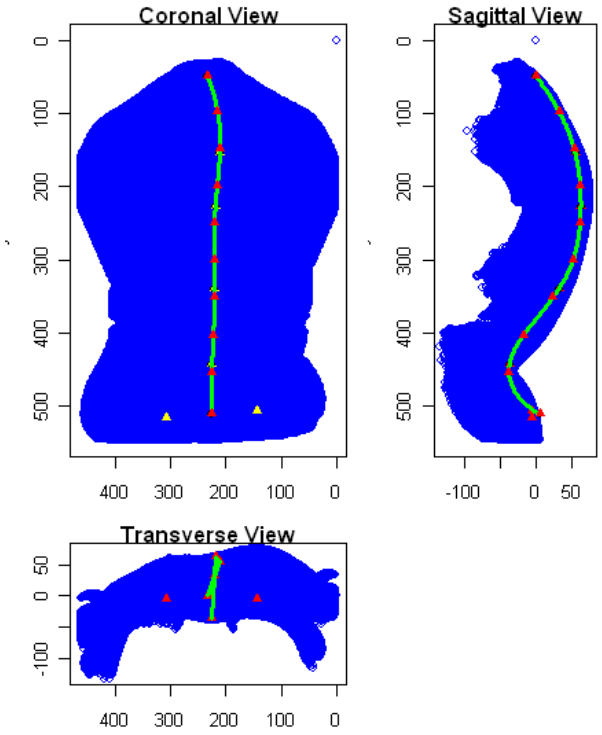

Figure 1.3: The spinal curvature for kyphosis and lordosis (Deform Back77)

1.5 Measuring techniques and devices of back deformities

Members of the International Research Society of Spinal Deformities (IRSSD) have been leaders in establishing different measurement techniques used to describe spinal deformities. The scoliometer [22, 23] and formulator contour tracer [24, 25] are both conducting manually applied instruments that are very slow to apply and give limited surface data (especially scoliometer) in the prone position. Moiré topography [26, 27] and various light-projection techniques including raster-stereography [11, 28, 29] are surface topography. Laser scanners have also been used for measuring surface topography [7, 30, 31]. However, these laser scanning methods tend to be time consuming for measuring back surface. During the measuring time the patient can change position. The shape of the back may change during the measurement time because of patient stance, breathing and muscle tension. Traditional radiography can certainly detect and diagnose spinal deformity, though it does not show what the back surface look like. The detection process of spinal deformity from radiograph is described in Section 1.5.1. Cosmetic concern is important for patient's psychological satisfaction. It also concerns the beauty of the body. Cosmetic deformity may also have a significant impact in the field social integration skills. Patients have a disturbed body image and affected psychological function. The health status of children and adolescents with back deformity determines the burden of the condition on the population and forms the baseline for determining the benefits of any intervention. It has been shown that back deformity causes a significant psychological disturbance to the majority of the patients involved [32]. The cosmetic shape of the back perhaps emphasising that the patient tends to be most interested in the surface shape. Surface topography equipment is expensive and requires considerable technical skill to set-up and to operate. This limited the wide-spread implementation and use of surface topography in the assessment of spinal deformities. With increasing computer power, commercially available surface topography systems such as ISIS [2, 3], Quantec [6, 33], and Formetric [8] were developed to

standardize patient positioning and descriptors of the deformity, and to reduce the labour and technical requirements.

There are now many additional tools beyond surface topography and plain radiographs to assess spinal deformity [34, 35]. Imaging modalities in use today, such as low dose 3D radiography [36], ultrasound [37], and MRI [34], can be used to model and visualize the spine in three dimensions. In spite of this, there is not yet a suite of commonly accepted and used 3D parameters for the routine clinical assessment of children with scoliosis and although all these methods are perfectly accurate, patient movement (sway), breathing and muscle tension can change the back shape and so a short while later the result can be different. For example, ISIS2 (Integrated Shape Imaging System 2) [5] system calculates clinical parameters based on lengths and angles measured from the three-dimensional surface but these can be affected by patient location, rotation and scale.

1.5.1 Radiography

Plain radiographs represent the initial diagnostic survey in evaluating the patient with back deformities [38]. Scoliosis can be viewed in the posteroanterior projection on the radiograph with the patient in the standing or upright sitting position. Most of the time radiographs are taken in the standing position. Sitting views will suffice for those patients who are unable to stand. Lateral projections are used to assess kyphosis and lordosis. The gold standard method of assessing back deformity in scoliosis is the Cobb angle. This was originated by John Cobb [38] to measure and quantify the magnitude of the coronal plane deformity on anteroposterior (AP) or posteroanterior (PA) plain radiographs in the classification of scoliosis. The diagrammatical representation of Cobb angle is shown in Figure 1.4.

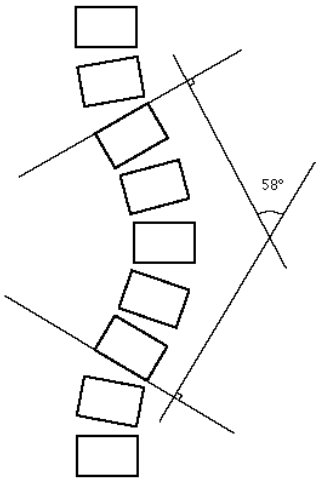

Figure 1.4: Measurement of Cobb angle [39]

A vast majority of children undergo multiple radiographic examinations during the adolescent growth spurt (when the progression of any curves is most likely to occur) for monitoring of back deformities. The use of radiographs has many disadvantages. First, the patient is exposed to frequent doses of radiation during longitudinal monitoring which increases the risk of breast cancer in late life [40-42]. Secondly, Cobb angle is a two-dimensional (2D) representation of a three-dimensional (3D) shape and is often not directly related to the rib hump. Radiography gives no information about back surface, which is of main interest to the patient, and the size of the rib hump that is very important to the patient is not measured at all in radiography. However, back deformities are three-dimensional complex processes and it is essential to quantify the three dimensional information to understand the mechanisms of back deformities.

1.6 Research problem

Initially radiographs of the spine, including a posteroanterior and lateral standing radiograph of the entire spine, are used to assess the degree of curvature for spinal deformity (scoliosis, kyphosis and lordosis). The degree of curvature is measured from the most tilted or end vertebra of the curve superiorly and inferiorly using the Cobb method. Radiography has many

disadvantages as discussed above in Section 1.5.1. A topographic system ISIS2 is available to calculate the shape of the back avoiding the problems caused by radiographs. The system measures three-dimensional shape by projecting a grid of horizontal lines onto the back, photographing the back and then using Fourier transform profilometry (FTP) to convert the distortions of the grid into a three-dimensional map of the back. All the clinical parameters from this system are based on distances and angles measured relative to certain anatomical landmarks on the back surface. Location, rotation and scale definitely influence these parameters. Although, anatomical landmarks are used in the present system to take some account of patient stance, it is still felt that variability in the clinical parameters is increased by the use of length and angle data. Patients also grow and so their back size changes between appointments with the doctor, leading to scale changes. Instead of distances and angles, geometric shape that is independent of location, rotation and scale effects could be measured. This research is mainly focusing on the shape changes in the back.

1.7 Statistical analysis of shape

Statistical shape analysis is a type of geometrical analysis that involves a set of visual shapes in which statistics are measured to describe shape components of similar or different shapes, for example, the difference between male and female gorilla skull shapes [43]. Some of the important aspects of shape analysis are to obtain a measure of distance between shapes, to estimate average shapes from a (possibly random) sample and to estimate shape variability in a sample [43]. Statistical shape analysis plays an important role in many kinds of biological studies [44-47]. Shape analysis is mainly automatic analysis of geometric shapes, for example using a computer to detect similarly shaped objects in a database or parts that fit together. For a computer to automatically analyze and process geometric shapes, the objects have to be represented in a digital form or mathematical representation. Kendall [44, 48] and Bookstein [45, 46] are two of the early pioneers of the statistical theory of shape. Subsequently, developments have led to a deep differential geometric theory of shape spaces [47], as well as

practical statistical approaches to analysing objects using probability distributions of shape and likelihood based inference. In this research, Procrustes analysis and Euclidean distance matrix analysis (EDMA) have been investigated for use in analysis human back deformity. These are discussed below.

1.7.1 Procrustes analysis

The method of superimposition, particularly the Procrustes superimposition, was originally developed and introduced to the biological sciences by famed anthropologist Franz Boaz and his student Eleanor Phelps [49]. Later, the idea of studying shape change using superimposition and deformation approaches has been seriously considered and further developed by many different researchers [43, 48, 50]. Goodall [51] reported Procrustes methods in the statistical analysis of shape. His methods are useful for estimating an average shape and for exploring the structure of shape variability in a dataset. Procrustes analysis has been used in a wide range of biological applications, for example assessing variation in gorilla skulls [43], assessing differences between Chinese and Caucasian head shapes [52] and assessing differences in body shape in horses [53]. Procrustes analysis can also be used for assessing the geometrical shape changes in the human back.

1.7.2 Euclidean distance matrix analysis

Lele and Richtsmeier [54] in 1991 used Euclidean distance matrix analysis (EDMA) for comparing two shapes using landmark data. EDMA allows form variation or growth differences to be examined through the comparisons of ratios of landmarks of equivalent configurations. This method can compare the form and/or growth of organisms that have been measured using two or three-dimensional coordinates. EDMA has been used to quantify form and growth differences for cebus apella skulls [54], the cranial growth of squirrel monkeys [55] and sexual dimorphism in macaques [56]. EDMA can also be used to quantify form and growth differences for human back deformity.

1.8 Research objectives

To provide a clear understanding of what this research entails, its objectives are outlined below

- Develop a method of quantifying the three-dimensional shape of the human back using statistical shape analysis to allow assessment and monitoring of deformities such as scoliosis, kyphosis and lordosis.
- Establish the normal population back shape and variability and compare this to the shape from patients with back deformities.
- Investigate the sensitivity of the new method to changes in back shape with time.

1.9 Research outcomes

In this work, a method is presented for landmark-based statistical analysis of back deformity for differentiating deformed backs from normal backs and locating the position of the deformation on the back surface. In addition to demonstration of a fully three-dimensional automatic feature extraction and statistical analysis, the research includes:

- Development of automatic landmark extraction procedure to extract landmarks from individual back surface obtained using ISIS2.
- Estimation of variability in landmarks for repeated intra and inter measurements.
- Demonstration of Procrustes shape differences between deformed backs and normal backs.
- Demonstration of EDMA for estimating the degree of deformity and locating the position of the degree of deformity relative to the standard normal form obtained from normal backs.
- A total of 117 (20 normal and 97 deformed) backs have been analyzed for this research.

1.10 Ethical clearances statement

Back surface data acquisition was approved by the Royal Orthopaedic Research Committee in 2006. The committee ruled that the project need not be presented to a Regional Ethics Committee because the patients would not be having any extra procedures that were not part of their normal treatment; ISIS2 scans would be carried out in any case with repeat measurements occurring regularly for audit purposes. Patient/parent information sheets were provided. All patients who were happy for their anonymised back surface data to be used for the research were asked to sign a consent form. These signed consent forms are stored at the Royal Orthopaedic Hospital. The inclusion criterion was simply all patients who were having ISIS2 scans as part of their normal treatment and who were happy for their data to be used. (No patients in wheelchairs, for example, would therefore be included because they were not suitable for normal ISIS2.)

The data were then acquired from 2006 to 2009 but it was late 2008 before finance was in place for a student to work on the data. The School of Applied Sciences Ethics Committee in the University of Wolverhampton approved the project for the MPhil student in May 2009.

It should be noted that all ISIS2 scans were carried out by NHS personnel. The student had no contact with any patients and only received anonymised back surface data for his research.

1.11 Outline of thesis

Chapter 2 explains details of the three-dimensional spinal deformities. It starts with the basic anatomy of the spine and continued with the surface anatomy of the back, prevalence of spinal deformity, curvatures of spine (scoliosis, kyphosis and lordosis) and the geometric description of spinal deformities. Chapter 3 explains the literature review on surface measurement techniques for clinical assessment. This chapter covers the importance of surface measurement, surface

measurement techniques available to use for clinical assessment, the shortcomings of available techniques and the reason for using ISIS2 for this research. Chapter 4 explains the literature review for statistical shape analysis. It starts with introductory shape analysis, the available statistical shape analysis methods, Procrustes analysis and Euclidean Distance Matrix Analysis (EDMA) etc. Chapter 5 describes the feature extraction and variability estimation for back shape analysis. This chapter includes the procedure for patient selection, feature extraction procedure, variability for the intra and inter landmark locations. Chapter 6 explains the implementation techniques of Procrustes analysis and EDMA for back shape analysis. This chapter descries the implementation of Procrustes and EDMA for backs, degree of deformity visualization and result interpretation. Chapter 7 discusses on Procrustes and EDMA. Chapter 8 presents the conclusions and future work. Chapter 9 is the reference list.

2 Three-dimensional spinal deformities

2.1 Introduction

Human back shape analysis starts with understanding of the geometrical properties on back surface. This chapter reviews of spinal and back deformities including their properties relevant to our application of statistical shape analysis for the human back. The chapter starts with the description of basic anatomy of the spine that includes the visual and palpable landmarks on the back surface. These landmarks are of a particular interest since they are the parts of the spine that generally protrude to the surface of the back forming bumps or dimples. The available surface measurements techniques to a large extend are dependent on these landmarks. Three types of back deformities are described details which are related with the spine called scoliosis, kyphosis and lordosis. The treatment of spinal curvature is also described. The conventional approach for assessing spinal deformities based on physical examination and radiographs does not provide complete description of the three-dimensional nature of the deformity. Based on the terminology developed by the Scoliosis Research Society, the three-dimensional measurements are described.

2.2 Spinal anatomy

The human spine is normally composed of 33 individual bones, 24 of those bones are called vertebrae. The vertebrae column is a flexible column made up of a series of bones that provides strength and support the entire upper body for the remainder of the human body. The vertebrae are stacked one on top of the other and form the main part of the spine running from the base of the skull to the pelvis. The spinal column is divided into five regions of vertebra: cervical, thoracic, lumbar, sacrum and coccyx. Figure 2.1 demonstrates of typical cervical, thoracic, lumbar, sacrum and coccyx vertebrae respectively, as seen from the front, in a side view and from the back. The first cervical vertebra

supports the globe of the head and it is named the atlas. Its chief peculiarity is that it has no body, and this is due to the fact that the body of the atlas has fused with that of the next vertebra. The thoracic vertebrae are intermediate in size between those of the cervical and lumbar regions. These vertebrae increase in size from above downward, the upper vertebrae being much smaller than those in the lower part of the region. The lumbar vertebrae are the largest segments of the movable part of the vertebral column. The sacrum is a large, triangular bone, situated in the lower part of the vertebral column. The coccyx is usually formed of four rudimentary vertebrae [57]. There are 7 vertebrae in the cervical region, 12 thoracic vertebrae, 5 lumbar vertebrae, 5 in the sacrum (fused) and 4 in the coccyx. Vertebral she and size vary in different regions of the spine. Each vertebra is distinguished by using a combination of a letter that describes the spinal region and a number that describes its location within that region. For example, C7 is the seventh cervical vertebra, T4 is the fourth thoracic vertebra and L5 is the fifth lumbar vertebra. The sacrum is simply referred to as S1 and the coccyx is not abbreviated or numbered. Inter-vertebral disks separate the individual vertebrae enabling spinal articulation and also act as dynamic shock absorbers.

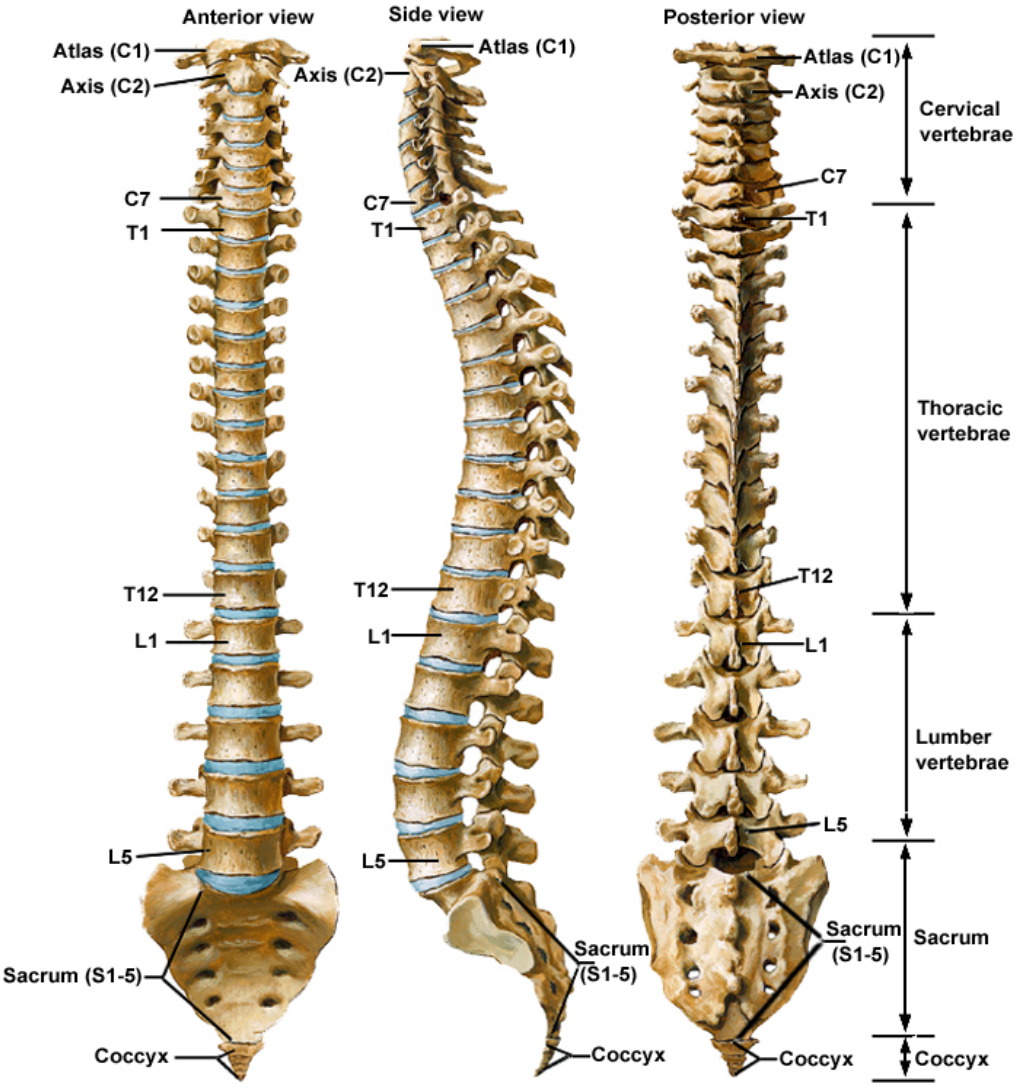

Figure 2.1 Illustration of typical cervical, thoracic, lumbar, sacrum and coccyx vertebrae [58]

Table 2.1 Spine vertebrae regions

Spine vertebrae region	Number of Vertebrae	Body area	Abbreviation
Cervical	7	Neck	C1-C7
Thoracic	12	Upper back	T1-T12
Lumbar	5	Low back	L1-L5
Sacrum	5 (fused)	Pelvis	S1-S5
Coccyx	4	Tailbone	None

When viewed from in front, the width of the bodies of the vertebra is seen to increase from the second cervical to the first thoracic; there is then a slight reduction in the next three vertebrae; below this there is again a gradual and progressive increase in low width. From this point there is a rapid diminution, to the apex of the coccyx.

2.3 Human back surface anatomy

According to Cramer and Darby [59], human back surface anatomy is defined as the configuration of the surface of the body, especially in relation to deeper parts. Although, information gathered by the eyes (inspection) and fingers (palpation) is often critical in the assessment of a back deformity patient, it is necessary to understand a thorough knowledge of human back surface anatomy for the proper performance of a physical examination.

2.3.1 Visible landmarks on human back

There is a longitudinal groove in the midline of the back which is known as median furrow (Figure 2.2). It starts at the external occipital protuberance (EOP) and continues inferiorlyu as the gluteal (anal, natal, or cluneal) cleft to the level of the S3 spinous tubercle, the remnants of the spinous process of S3. The furrow is shallow in the lower cervical region and deepest in the lumbar region, widening inferiorly to form a triangle with a line connecting the posterior superior iliac spines (PSISs), forming the base above and the gluteal cleft forming the apex of the triangle below. The PSISs are visible as a pair of dimples (denoted in this thesis as dimples of Venus) located about 3 cm lateral to the midline at the level of the S2 spinous tubercle [59].

Several muscles are commonly visible in the human back region. The trapezius is a large, flat, triangular muscle that originates in the midline from the EOP to the spinous process of T12 and inserts laterally onto the spine of the scapula. Several bony landmarks are usually visible in the human back. The spinous process of C7 (the vertebra prominens) is usually visible in the lower cervical

region. The C7 location can be found by moving fingers inferiorly over the spinous processes of the cervical vertebrae until it comes to the most prominent spinous process. When the patient's head is flexed, the spinous process of C6 is usually visible as well. The other cervical spinous processes are usually sunken. In the thoracic region the furrow is shallow and during stooping disappears, and then the spinous processes are more likely to be visible. In the lumbar region the furrow is deep and the spinous processes are frequently indicated by little pits or depressions, especially when the muscles in the loins are well-developed. In the sacral region the furrow is shallower, presenting a flattened area which ends at the most prominent part of the dorsal surface of the sacrum.

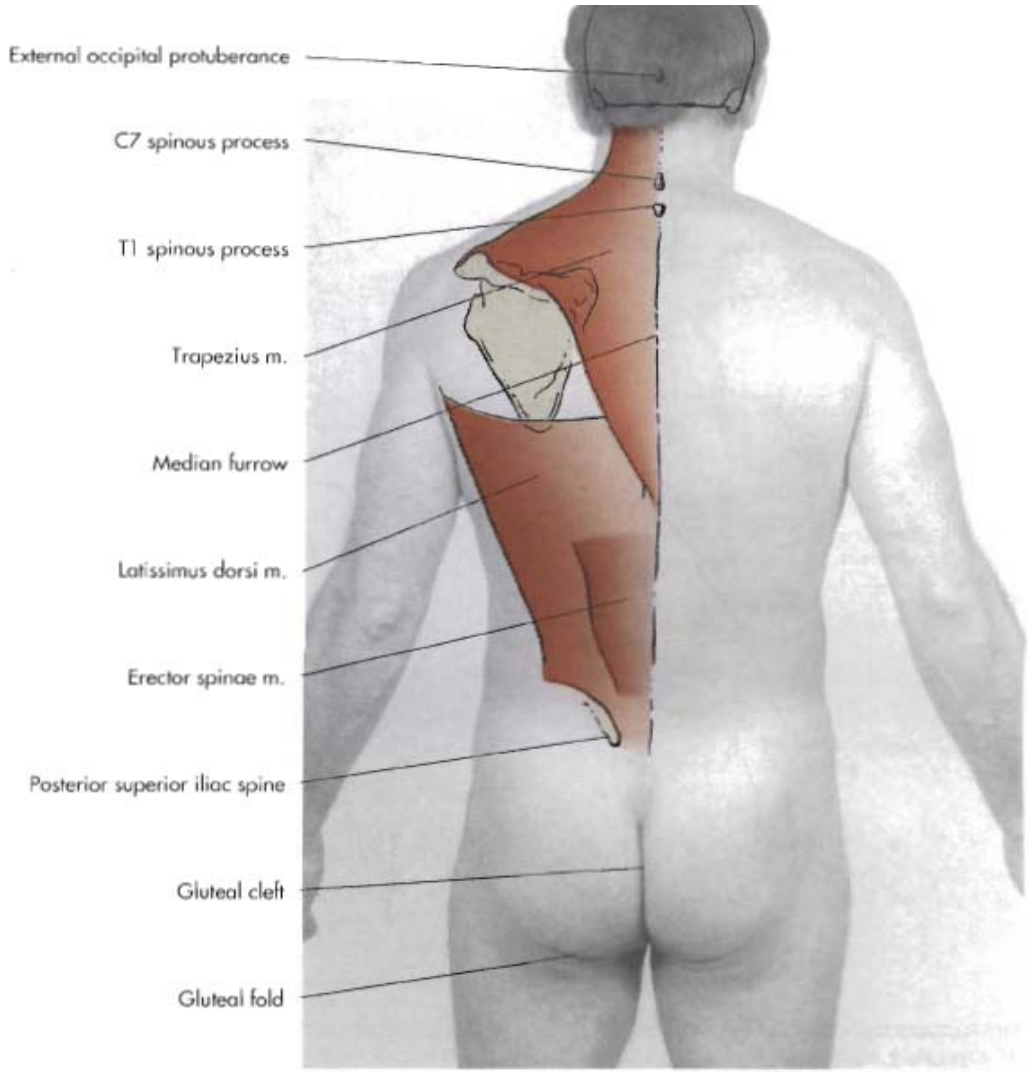

Figure 2.2 Visible landmarks on the back surface [59]

In the adult the vertebral column has several normal curves that are visible. In the cervical (lordotic), and in the thoracic and sacral areas it is posteriorly convex (kyphotic). Normally there is no lateral deviation of the spinal column, but when present this curvature is known as scoliosis.

2.3.2 Palpable landmarks of the back surface

In the cervical region, the spinous process of the C2 is the first readily palpable bone in the posterior midline below the EOP (Figure 2.3); the second being C7. The spinous process of C6 is usually palpable with full flexion of the neck. The other cervical spinous processes are generally more difficult to palpate. In the thoracic region, T1 is the third palpable spinous process. The spinous process of T4 is located at the extreme convexity of the thoracic kyphosis and is usually the most prominent spinous process below the root of the neck. The spinous processes of T9 and T10 are often palpably closer together; and the spinous process of T12 is roughly located between the level of the inferior angle of the scapula and the superior margin of the iliac crest. In the lumbosacral region, the spinous processes are horizontal and more squared in shape. The spinous processes of L4 and L5 are shorter than other spinous processes and difficult to palpate.

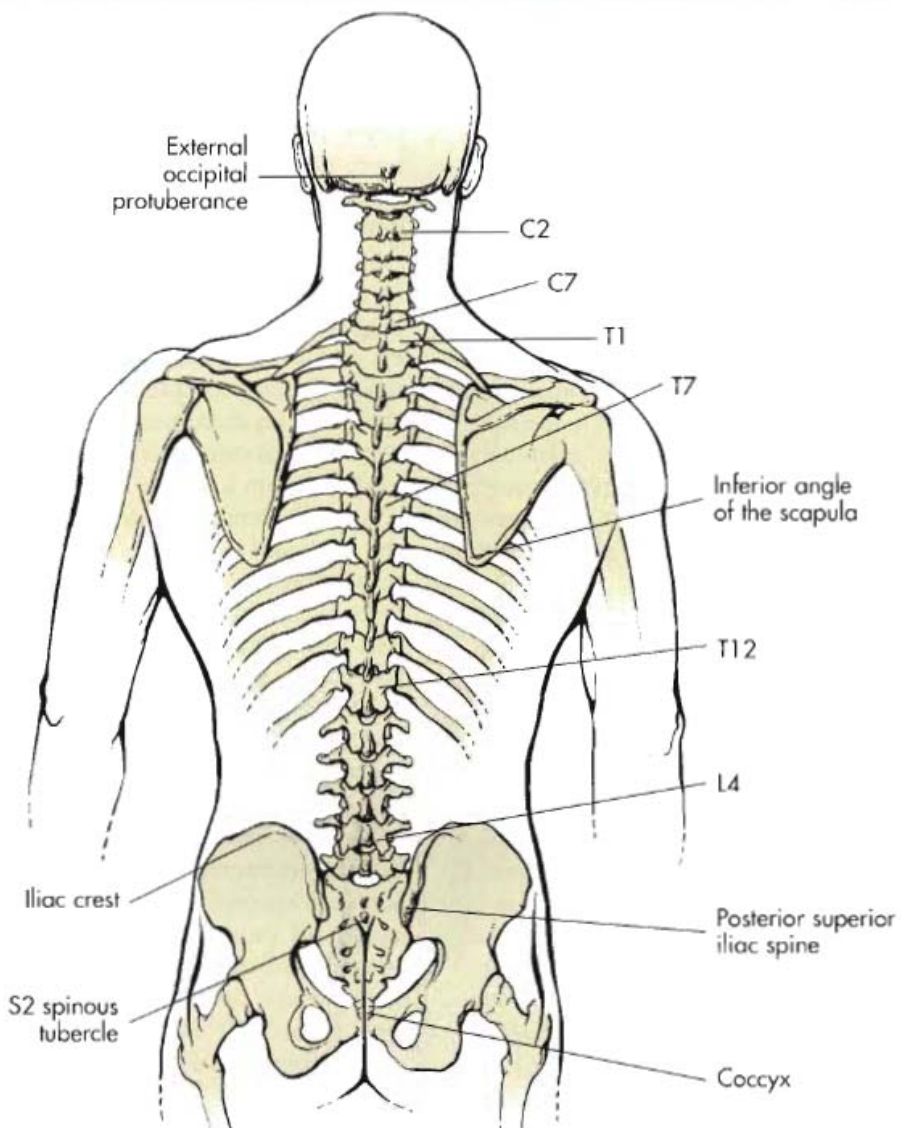

Figure 2.3 Palpable landmarks on the back [59]

2.4 Back deformity

Spinal deformity has a great impact on the back surface; this is to say that whenever there is spinal deformity it usually results in back deformity. A back deformity is a major difference in the shape of a back compared to the average human back. The skeletal distortions caused by scoliosis will almost result in the deformity of the back surface. The back surface deformity typically include prominent shoulder blade(s), rib hump, scapula asymmetry, pelvic asymmetry, a skin fold on the side of the concavity and a subtle twisting of the trunk [60]. There are various surface deformities caused by scoliosis that can be seen in

Figure 2.4, a) twisting of the whole trunk toward the side of the concavity; head not centred over trunk; right shoulder higher than the left; left pelvis higher than the right; and b) vertebra rotation causing rib cage distortion and the rib hump.

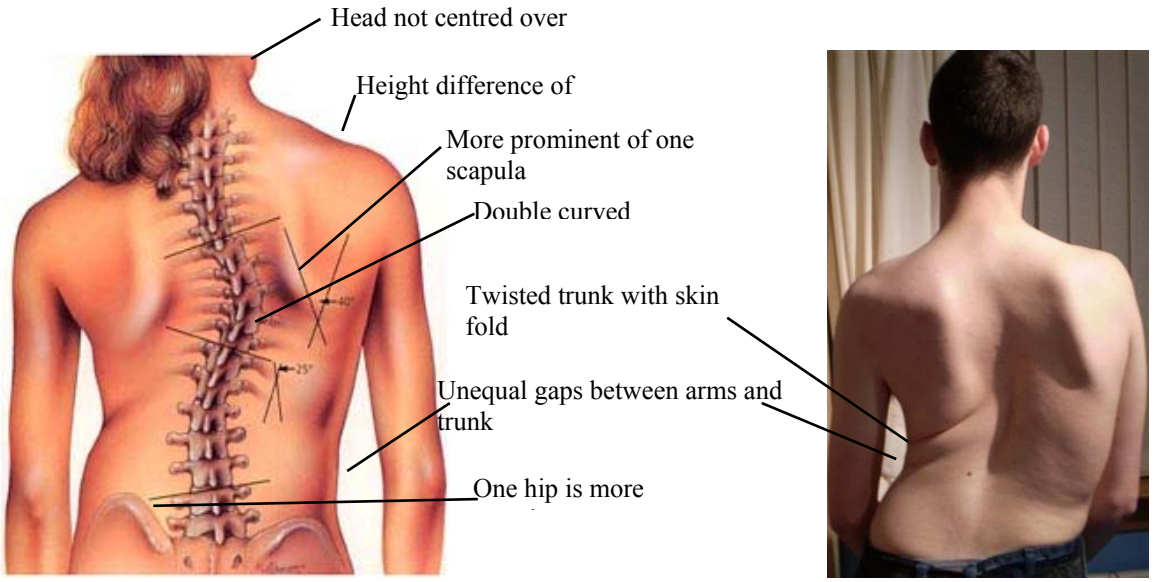

(a) Surface deformities due to scoliosis (b) Surface deformities due to

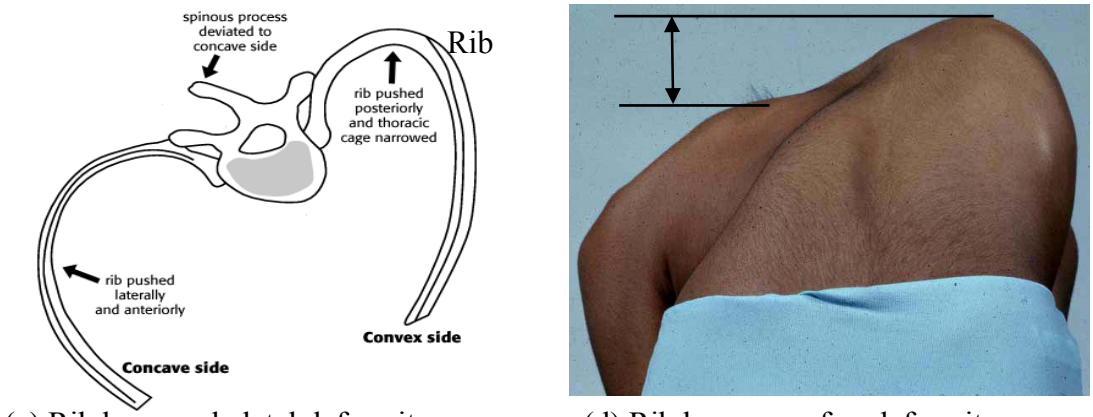

(c) Rib hump –skeletal deformity (d) Rib hump –surfacedeformity

Figure 2.4: Surface deformities of scoliosis [61]

2.4.1 Prevalence of back deformities

There are many different causes of spinal deformity. Some babies are born with spinal defects that might cause the spine to grow unevenly. Some children have nerve or muscle disease, injuries or other illness that can also cause back deformity (for example, cerebral palsy or myelomeningocele). A deformity of the back may also arise from tumours and infections of a vertebra. This can

occur in any age group and its progression on back surface is dependent on the course of the tumour or infection. Another reason for back deformity may involve genetic, neuromuscular, hormonal, biochemical or other abnormalities. Sometimes the back does not grow as straight as it should and the reason is unknown. This is the most common type of back deformity that is called "idiopathic". Roughly 80% of scoliosis patients suffer from the idiopathic scoliosis. Idiopathic scoliosis can occur at any age but it is the most commonly detected in childhood or early adolescence. This is called adolescence idiopathic scoliosis (AIS). Large numbers of people, perhaps as high as 10% of the general population, have minor curves (less than 10º) [62]; for curves greater than 10º the prevalence of AIS has been variously estimated [62-64] at between 1.5% and 3% of the population. However, only a small number of these patients (1–2/1000) have curves that progress to greater than 30º and seek treatment.

Scoliosis also includes axial rotation of the vertebrae, rotation of the plane of maximum curvature of the spine, and rotation and distortion of the ribs. As the deformity progresses, the vertebrae and spinous processes rotate toward the concavity of the curve. On the concave side of the curve, the ribs are close together. On the convex side, they are widely separated. As the vertebral bodies rotate, the spinous processes deviate more and more to the concave side and the ribs follow the rotation of the vertebrae that can be seen in Figure 2.4 (c). The posterior ribs on the convex side are pushed posteriory, causing the characteristic rib hump seen in thoracic scoliosis. The anterior ribs on the concave side are pushed anteriorly [65].

There are various other reasons (ribs tumours and/or osteoporosis etc [12]) for back deformity and deformities on the back are usually caused by abnormal development of the spine. Hence, improper growth of a single vertebra changes the alignment of neighbouring vertebrae. Back deformity is often first noticed as small differences in the geometrical form of the back during the adolescence period. These differences may result in slight asymmetries of the shoulders, the trunk or hips and the appearance of skin folds around the waist. A rib hump may

also develop over time on the back. These changes on back surface occur over a period of months to years during the growth of the child.

The surface deformity enables surface assessment to be carried out. The cosmetic deformity of the trunk surface is actually more important to the patient and family, and is what frequently motivates them to seek treatment [60].

2.4.2 Types of back deformities

Spinal deformity is a complex three-dimensional process. A normal spine looks straight when viewed from behind (coronal plane) and is curved when viewed from the side (sagittal plane). Based on the shape of spine, there are three basic types of back deformities. Those are scoliosis, kyphosis and lordosis.

2.4.2.1 Human body planes

The medical definition of the body planes is shown in Figure 2.5.

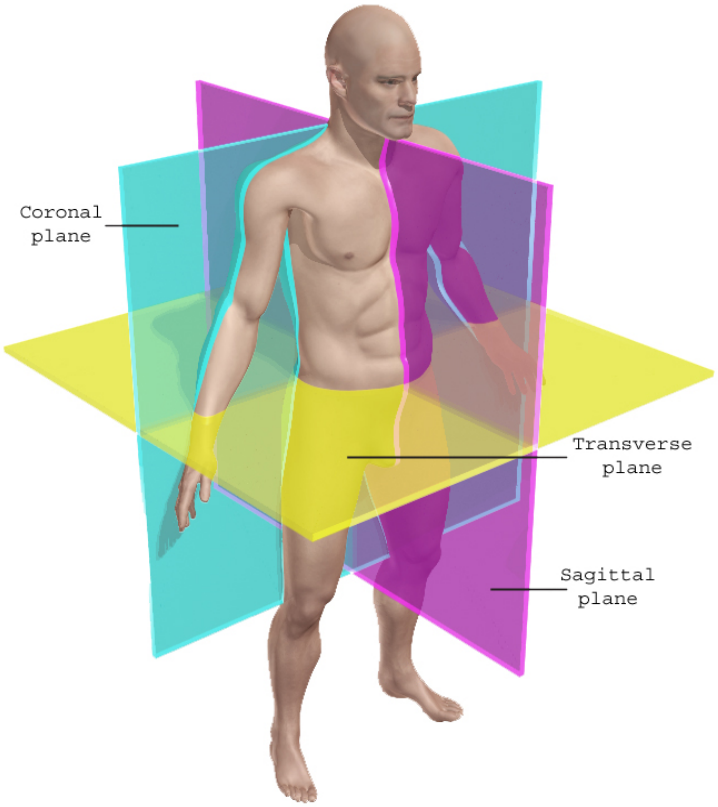

Figure 2.5: Coronal, sagittal and transverse planes of a normal back [13]

The sagittal plane divides the body into two sides, the coronal plane into front and back and the transverse plane into top and bottom. Back deformity can potentially affect all planes. The normal spine is straight in the coronal plane while a deformed spine has a curve in this plane and/or excessive curve in the sagittal plane. A flat back (i.e. low curvature either in the thoracic region or the lumbar region) in the sagittal plane can also be considered a deformity. Each normal curve on the spine is designed to efficiently transfer the weight of the body and distribute it down through the pelvis.

2.4.2.2 Scoliosis

The term scoliosis originates from the Greek physician Galen [14] more than eighteen centuries ago and comes from the Greek word for “crooked”. It is a lateral deformation of the spine in the coronal plane. Although the spine does curve from front to back it should not curve sideways very much. A side-to-side curve is called scoliosis and may take the shape of an "S" (double curve) or a "C" (single curve). Typically, a scoliotic spine will exhibit either a single or double structural curve and will be accompanied by compensatory curves above and below the structural curves to maintain the general position of the individual. Scoliosis is more than just a curve to the side. The scoliotic spine is also rotated or twisted. As the spine twists it pulls the ribs along with it, so that one side of the chest becomes higher than the other, or the shape of the breastbone may change. To better understand these complex three- dimensional problems, compare the drawings of the green line passing through anatomical sticker locations on back surface for a normal back (Figure 2.6 (a)) and a deformed back (Figure 2.6 (b)). The green line (drawn from the vertebra prominens to the sacrum) is a spline curve fitted through the sticker locations on back surface. The red rectangle shows the anatomical sticker locations.

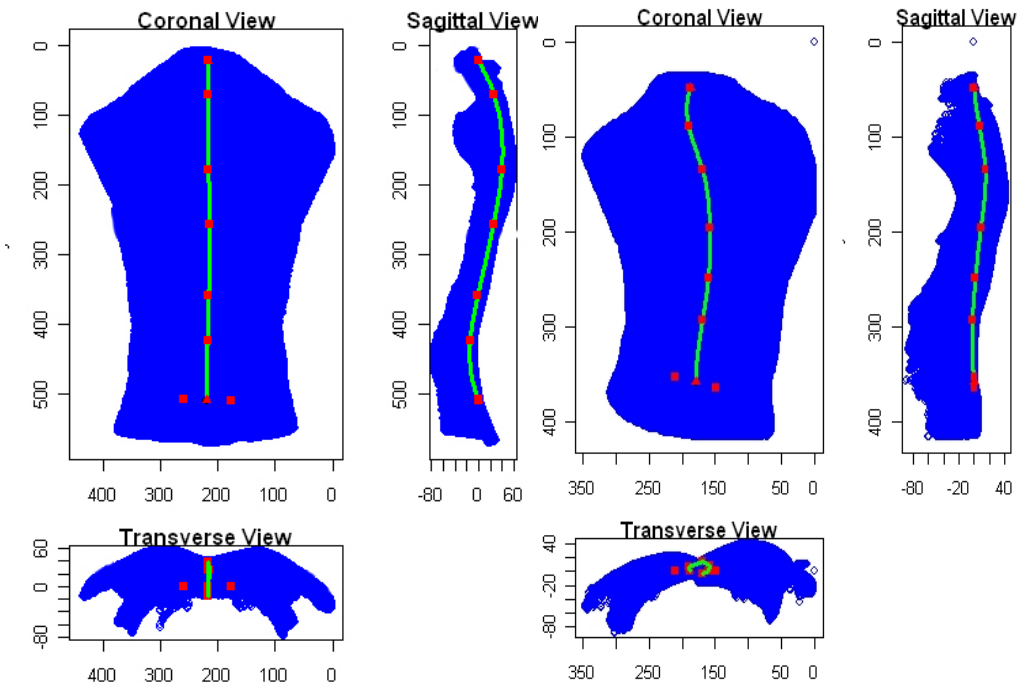

Figure 2.6: The spinal curve for normal back (NormalBack 1) and deformed back (DeformBack17)

Many people with scoliosis also have hypokyphosis (see Section 2.4.2.4). Because of all the possible combinations of curvatures, scoliosis can be very different in different people [15]. As scoliosis is a complex three-dimensional process, the Scoliosis Research Society (SRS) in the USA developed a three-dimensional terminology of scoliosis covering the geometrical properties of the vertebrae and the spine [66].

2.4.2.3 Treatment of scoliosis

When scoliosis is mild, non-structural and poses no real health threat to the patient, it may require no treatment other than monitoring for progression. Treatment for AIS patient depends on the physiological age, the curve severity, pattern, magnitude and location, and bone maturity. Children who have mild AIS may need checkups every four to six months to see if there have been changes in the curvature of their spines. While there are guidelines for mild,

moderate and severe curves, the decision to begin treatment is always made on an individual basis.

For structural scoliosis that requires treatment, a number of options are available. One option is bracing where the patient wears a rigid brace which exerts pressure on one side of the body in an attempt to correct the deformity. Bracing is normally prescribed when the patient is still growing and the scoliosis has the tendency to progress. The purpose of wearing the brace is to keep the curve in spine from getting worse as the patient continues to grow; however, it is usually not intended to reduce the amount of curve that already have. Many studies included patients whose risk of progression was small within their test cohort and often the follow-up period after bracing ceased was relatively short. One study was done using hidden compliance equipment [67] and it showed that true compliance was significantly less than the estimation by the patient or by the consultant based on brace soiling and skin condition. The orthopaedic community is divided on the use of bracing, with some being very much in favour [68, 69] and others very much against [70, 71]. Regardless of whether bracing is used or not patients will still need to be examined regularly every three to four months throughout the growth period for monitoring scoliosis.

The final alternative, but more severe option is to intervene with spinal surgery to hold progression of the deformity and where possible to straighten the curve without injury to the spinal cord. Many surgical techniques exist; the main procedure being correction, stabilization, and fusion of the curve.

2.4.2.3.1 Curvature angle

The most commonly used method for measuring the curvature angle of the spine is the Cobb angle. The Cobb angle was developed by John Cobb [72] to measure and quantify the magnitude of the coronal plane deformity on anteroposterior (AP) or posteroanterior (PA) plain radiographs in the classification of scoliosis. This method is regarded as the standard method of assessing the degree of deformity in scoliosis. First locate the upper and lower end-vertebrae at the

extremes of the curve (vertebrae with the most tilted endplates). One parallel line to the highest vertebral endplate is drawn at the top of the curve and a second parallel line to the lower vertebral endplate is drawn at the bottom of the curve. The Cobb angle is found by projecting perpendiculars from these two lines, and measuring the angle α of intersection that can be seen from Figure 2.7. The Cobb angle, however, only measures the angle of the spine and represents two-dimensional information of a three-dimensional problem, it has been shown not to be directly related to the shape of the back [73]. Interobserver and intraobserver variations in the measurement of Cobb angle have also shown to be variable [74], often as high as the change in Cobb angle considered to be clinically significant.

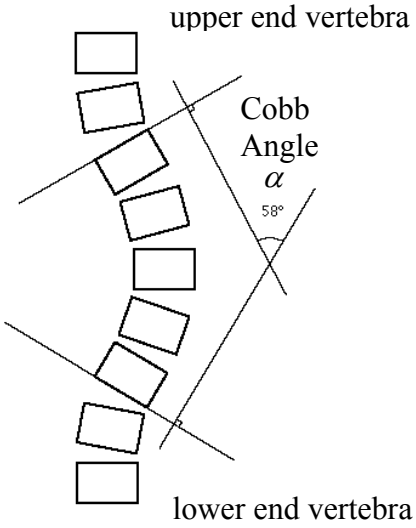

Figure 2.7: Measurement of Cobb angle [39]

2.4.2.4 Kyphosis and Lordosis

Kyphosis is an excessive front-to-back curvature of the thoracic spine. This can be clearly seen when viewed from the side (Figure 2.8(a)). It causes the back to look rounded or humped. It is normal to have some kyphosis in the thoracic (chest area) spinal column. The SRS defines kyphosis as a curvature of the spine measuring 45° or greater on a radiograph (SRS, 2000). The normal spine typically has thoracic kyphosis of 20°-45°. Too much kyphosis in the thoracic

spine is called "hyperkyphosis," Scheurmann's kyphosis, or "round back." When there is not enough kyphosis in the thoracic spine (as is often the case with idiopathic scoliosis), it is called thoracic hypokyphosis. Lordosis is an abnormal excessive front-to-back curvature of the lower spine (lumbar region) and can be seen in Figure 2.8(b). Sometime lordosis may be associated with poor posture, a congenital problem with the vertebrae, neuromuscular problems or hip problems. An exaggerated lordosis can be painful and it can also affect movement.

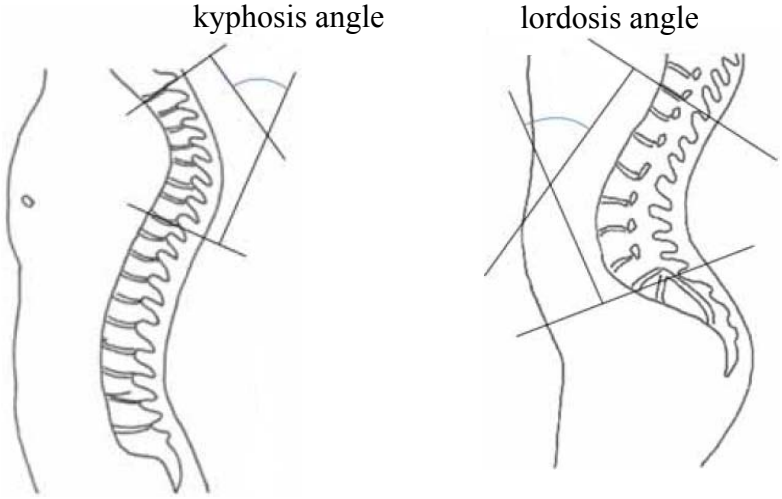

Figure 2.8: Kyphosis and lordosis angles

2.5 Three-dimensional spinal and surface measurements

The traditional definition of scoliosis as an abnormal lateral curve to the vertebral column does not provide sufficient description of the three-dimensional nature of the deformity on the back surface. For the purpose of research and management, a more comprehensive description is required. The SRS has developed three-dimensional geometric terminology of the spine which provides the basis for deriving surface measurements. The spinal measurements include linear, angular, area and volume measurements. The three-dimensional measurements include the measurement of three-dimensional spinal length or a specific region of the spine and volume of spinal bounding box. The surface measurements include the maximum area on the back surface. The research has

presented in this thesis investigated the quantification and analysis of the three-dimensional back surface.

2.6 Summary

This chapter covers the literature review on spinal and back deformities. The basic anatomy of the spine is discussed, including the visual and palpable landmarks of the back surface. These landmarks are of particular interest in this investigation since the success of surface measurement techniques to a large extent depends on these anatomical landmark locations. Types of back deformities related to the spine called scoliosis, kyphosis and lordosis are discussed. The traditional approach of quantifying spinal deformities by using the Cobb angle method does not provide the three-dimensional nature of the deformity, which is noted in the last section of this chapter and this will be discussed in details in the next chapter.

The next chapter will cover the fundamental methods that have been developed for back surface measurements.

3 Surface measurement methods

3.1 Introduction

This chapter discusses different surface measurement systems that have been developed for back surface analysis. It starts with the description of necessity for surface measurements. Various back surface measurement systems and imaging modalities have been proposed over past few decades. The underlying measurement technique and its application for each method have been briefly outlined. The limitations and advantages of each method have been pointed where necessary. Recent advances in hardware and software technology have now enabled fast and accurate three-dimensional back surface information acquisition of both image and coordinates. The ISIS2 has been described details as the back surface information for this research has been collected using this system.

3.2 Necessity of surface measurement

There are three primary reasons for assessing spinal deformities from surface measurements. First, the drawback of radiographic assessment is the radiation hazards associated with exposure to radiographs. Initially radiographs of the spine, including a posteroanterior and lateral standing radiograph of the entire spine, are used to assess the degree of curvature for spinal deformity (scoliosis, kyphosis and lordosis). The degree of curvature is measured from the most tilted or end vertebra of the curve superiorly and inferiorly using the Cobb method. During the assessment of spinal deformities, it is often required to monitor a patient at regular intervals over a period of time, to assess progression of the condition or even to assess the effect of treatment methods. A vast majority of children undergo multiple radiographic examinations during the adolescent growth spurt (when the progression of any curves is most likely to occur) for monitoring of back deformities. The use of radiographs has many disadvantages. The patient is exposed to frequent doses of radiation during longitudinal

monitoring which increases the risk of breast cancer in late life [40-42]. Second, structural deformity of the spine will almost result in corresponding deformity of the back surface (see Section 2.4). Studies indicate that it is the cosmetic deformity of the trunk surface which is more important to the patient and family, and is what frequently motivates them to seek treatment [75]. It has been shown that back deformity causes a significant psychological disturbance to the majority of the patients involved [32]. The cosmetic shape of the back perhaps emphasising that the patient tends to be most interested in the surface shape such as the rib hump. Clinically, the back or trunk surface is important not only because of its cosmetic relevance, but also because it is the interface for some treatment methods such as bracing. Assessment methods should therefore allow the quantification of the surface deformity in addition to the spinal deformity. Third, Cobb angle is a two-dimensional representation of a three-dimensional shape and is often not directly related to the rib hump. Radiography gives no information about back surface, which is of main interest to the patient, and the size of the rib hump that is very important to the patient is not measured at all in radiography. However, back deformities are three-dimensional complex processes and it is essential to quantify the three dimensional information to understand the mechanisms of back deformities.

3.3 Surface measurement methods

Members of the International Research Society of Spinal Deformities (IRSSD) have been leaders in establishing different surface measurement methods used to describe spinal deformities.

3.3.1 Scoliometer

A scoliometer was developed by Bunnell [22, 76]. It is an instrument used to estimate the spinal rotation, i.e the amount of spine twists in a person's spine. This rotation of the spine cannot be seen in an X-ray. This curvature of the spine is expressed as an angle of trunk inclination (ATI). The ATI is defined by the SRS as the angle between the horizontal and the plane across the back at the

greatest elevation of a rib prominence or lumbar prominence, as measured by an inclinometer or Scoliometer (SRS, 2000). For measuring the ATI angle, the patient is asked to bend over (Adam's forward bending position) with arms dangling and palms pressed together, until a curve can be observed in the thoracic area (the upper back) that can be seen in Figure 3.1. The Scoliometer is then placed on the back to measure the apex (the highest point) of the curve. The patient is then asked to continue bending until the curve in the lower back can be seen; the apex of this curve is then measured. The results of the scoliometer can indicate problems and the measurement is not sufficient to use for determining patient diagnosis and management [77].

The scoliometer shows very sensitive to false negative results [78]. In Bunnell's study [22], over half the patients with minor scoliosis (Cobb angle less than 20°) had been determined as positive by the scoliometer method, and thus were false-positives. Another study by Karachalios et al. [79] found it resulted in 27 false-negatives out of 2,700 students screened (1%), and 419 false-positives (15.5%). They calculated the scoliometer's sensitivity to be 90.62% and specificity of 79.76%. However, some experts believe it is a useful device for widespread screening [80, 81].

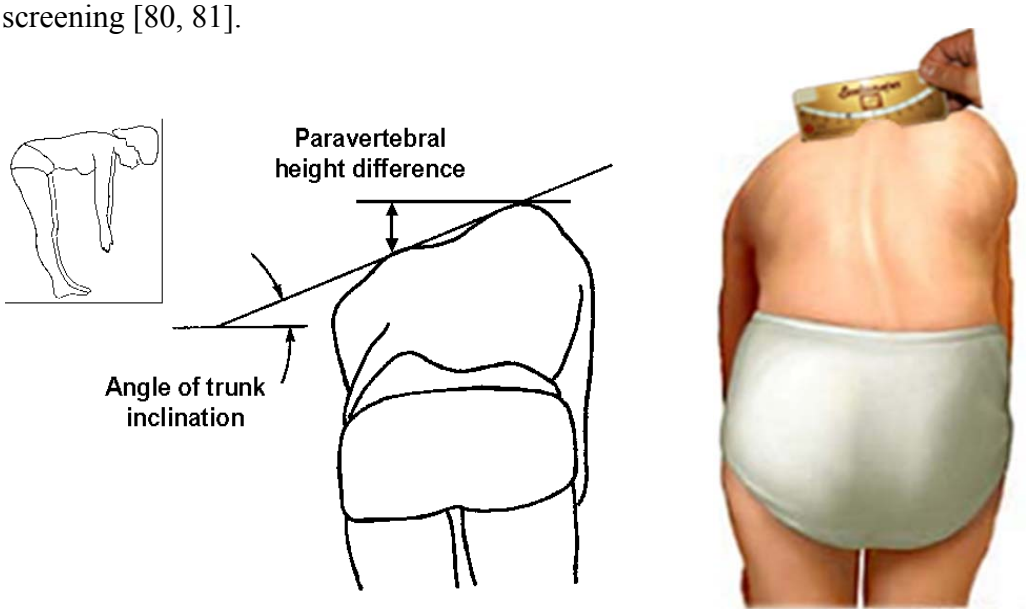

a) ATI definition b) ATI scoliosis

Figure 3.1: ATI definition and measurement using scoliometer

3.3.2 Contour devices

Different contour devices have been developed and tested over the years for measuring the shape of rib hump. Thulbourne and Gillespie's rib measuring device [24], the flexible curve instrument reported by Pun [25] and the Formulator Body Contour Tracer (FBCT) [82] are all similar devices. The FBCT device allows a more accurate recording of the cross-sectional profiles of the back surface and it consists of a simple matrix of rods that are placed parallel to the coronal plane across the surface of the back (usually in the forward bending position). The rods assume the profile of the back as shown in Figure 3.3. To use the FBCT, the spinous processes are first palpated and marked with markers. The FBCT is then placed on the back of the subject in Adams's forward bending pose with its central rod coinciding with the spinous process marker. The rods are then allowed to fall under gravity to assume the contour of the back and then locked by tightening a winged nut on their housing and removed from the patient.

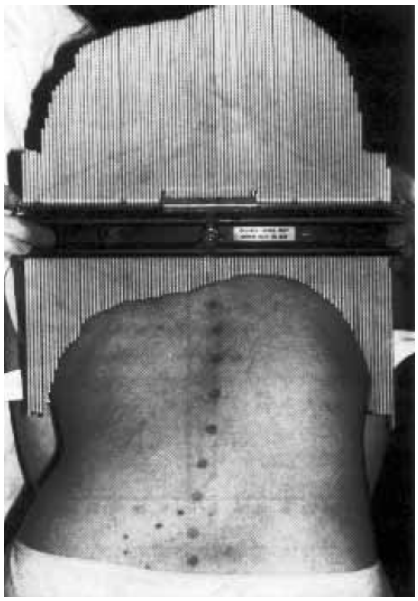

Figure 3.2: Measurement of the back profile of a subject using FBCT [82]

The resulting cross-sectional profile of the FBCT is then transferred onto paper by tracing out the edges of the rods. A linear measurement known as Trunk Asymmetry Score (TAS) is calculated by sub-diving each half of the contour profile into five sections and measuring the distance from the contour to a datum

line. The differences between corresponding left and right distances are summed, termed Crude Trunk Asymmetry Scores (CTAS). For comparison of different subjects, the CTAS values are standardised to a mean trunk diameter of the study group, giving Standardised Trunk Asymmetry Score (STAS).

The main problem with contact measurement devices is that the analysis is carried out manually. The measurement is done by hand. The time and concentration needed to measure the trunk shape, transfer it to paper, and then carry out the analysis make this method impractical in most hospitals. Moreover, contact of the device with the back may cause the subject to become tense or flinch, resulting in a change of body posture which can affect the measurement [83]. It also does not provide a useful method for long-term monitoring of the shape progression of the back. In general, contact devices are manually operated, less accurate and time-consuming. For these reasons, non-contact measurements methods are necessary.

3.3.3 Moiré Topography

Moiré topography is one of the earliest 1970s [26, 27, 84-86] non-contact optical techniques which gained widespread clinical use in the assessment of the back shape. It is most valuable as a non-radiographic monitoring tool for detecting scoliosis progression. It is widely used for back surface screening and reduces radiation exposure. In 1970, Takasaki [87] demonstrated the clinical application of moiré topography to measure deformity of the body surface and this has been used for scoliosis screen in Japan [88] and in Canada [26]. They found that moiré topography was more sensitive than the Adam's forward bend test. It has an advantage over the forward bend test in that permanent records can be stored for future analysis or longitudinal review. A moiré topograph (or topogram) provides a contour map which can be easily understood by a human observer. In Figure 3.3 shows an example of moiré topogram of a scoliosis patient.

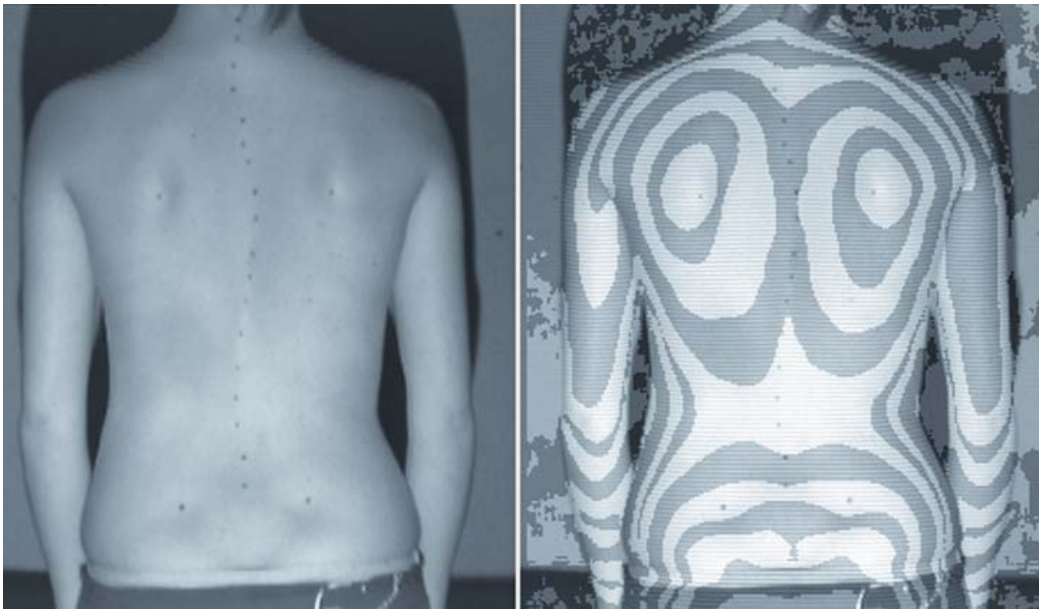

Figure 3.3: Examples of Moiré topogram of a scoliosis patient [89]

Although moiré topographs encode information is easily recognizable for clinical use, moreover accurate quantitative information is not readily available. Several authors have analysed moiré topograms using various techniques in an attempt to quantify back shape deformity based on the fringes [27, 73, 90, 91]. The basic advantage of moiré topographs is to overcome the fundamental limitation of conventional photographs in that each image is not solely a two-dimensional projection of a three-dimensional, but it is actually a three-dimensional 'map' of the surface. Quantitative analysis of moiré fringes typically involves comparison of corresponding left and right fringes, and derivation of some quantitative angular and/or linear measures.

Stokes *et al.* [73] analysed moiré topographs of scoliosis patients by constructing lines tangentially across corresponding fringes on each side of the back midline (Figure 3.4). The objective of this study was to determine the extent to which moiré topographs and rasterstereography (Section 3.3.3) could be used to detect the presence, magnitude, side and anatomic level of spinal deformity. The angle between each line and the horizontal was measured and termed ‘moiré fringe angles’. Each angle was interpreted as a measure of both

side-to-side asymmetry and sagittal curvature. The vertical height position of each fringe angle was measured relative to skin marks attached to each patient at levels T1 and L5 spinous processes.

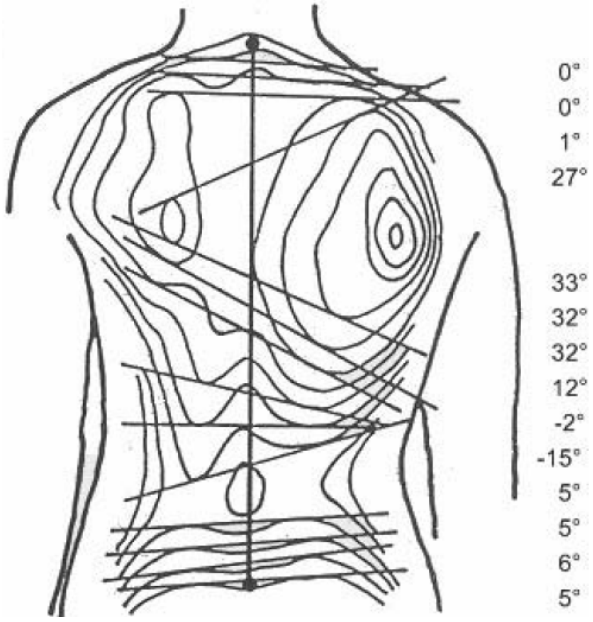

Figure 3.4: Moiré topograms analysis. Double tangent lines are drawn for corresponding contours and the angles between these contours and the horizontal measured [73].

The moiré fringe angles were plotted as a function of the vertebral level of the back at which they were measured and compared with graphs of 'back surface rotation' determined from raster-stereography (see Section 3.3.4) and axial rotation of the vertebrae measured from radiographs (see Section 1.5.1), with the radiographic measurements used as the standard for comparison. The result showed that the presence or absence of scoliosis and the number of curves were correctly identified in 68% of the patients (mean Cobb 24°, range 5-61°). In 22% of the patients, there were missed curves or false positives by both surface methods (mean Cobb 14°, range 0-42°). In the other 10% (mean Cobb 8°, range 5-11°), both surface methods gave incorrect results.

Although moiré topography visualizes the contour of back surface, but it has a number of problems which makes it unsuitable for objective back shape measurements. The major problem with moiré topography is that it requires the

absolute order of the fringe to be analyzed. The formation of the moiré fringes depends on body shape and the patient positioning. A slight change in patient position can produce considerable changes in the moiré topogram. Thus a direct inspection of moiré fringes may be misleading, as has been confirmed in several studies. Therefore, a careful positioning of the patient relative to the moiré screen is needed and patients are often brought into standardised positioning pads or other fixing elements to control patient posture. Another problem with the moiré topography is the automation of analysis. The contour patterns of a depression and a peak are the same and it is very difficult to distinguish between them automatically. Several authors have attempted to automate the technique and have reported a number of problems that make automation difficult [92-94].

3.3.4 Quantec

The Quantec system [6, 95] employs raster stereography to produce a three-dimensional surface representation from a single video photographic image of a fringe pattern projected onto the subject's back. Marker dots are placed over T1, T12, dimples of Venus, and occasional additional spinous processes in between. An equivalent angle to the Cobb angle is accessed and also kyphosis and lordosis angles. The system is complex and relies on surface topography that has been known to contribute to inaccuracies [96].

The system does not seem to consider the orientation of the patient to the camera/reference plane axes. Therefore, all clinical parameters are calculated relative to the reference plane axes external to the patient. This is likely to give rise to variations in results between measurements, even those taken only a short time apart. Some users have overcome this problem by averaging a number of measurements [97-99].

A comparative study has been carried out for comparing the Quantec parameters with Cobb angle, Perdriolle measurement of rotation, and scoliometer; a conclusion is derived that Quantec parameters can be used instead of these other measures [33, 100, 101]. However, the use of the Quantec parameters in clinical

practice has not been widely published. The Quantec equipment is still used in some centres by enthusiasts.

3.3.5 ISIS

ISIS (Integrated Shape Imaging System) system was developed in the mid 1980s at the Oxford Orthopaedic Engineering Centre at the Nuffield Orthopaedic Centre [102]. It was an early and widely used optical scanning system for measuring human back shape in a clinical environment and commercialised by Oxford Metrics Limited, Oxford, UK [2, 3, 103, 104]. The ISIS system used structured white light projector. A 35 mm projector is used to project a horizontal blade of light which is swept over the back from neck to buttocks. A camera, mounted below the projector, captures the position of the light blade on the back and transfers the coordinates to a PDP11 computer. The three-dimensional shape information is then extracted from knowledge of the geometry of the illumination/camera system and the coordinates of the blade of light.

The system had been well validated in the late 1980s and early 1990s and it produced a printed report that was useful to the clinician [105, 106]. However, the ISIS system was very old and data acquisition was very slow (several seconds, thus allowing the possibility for movement errors to creep in) and calculation time before the report was printed was of the order of ten minutes. The system is then modified and redesigned with new clinical parameters and named ISIS2.

3.3.6 ISIS2

The ISIS2 [5] system is developed by Fiona Berryman *et al* about five years ago and has been in regular use at the Nuffield Orthopaedic Centre (NOC), Oxford since 2006 and at the Royal Orthopaedic Hospital, Birmingham since 2008. ISIS2 is a low-cost automated non-invasive system to measure the three-dimensional shape of the back.

Mechanical design

The system is equipped with a standard projector, camera, patient stand, telescopic actuator and computer etc that can be seen in Figure 3.5.

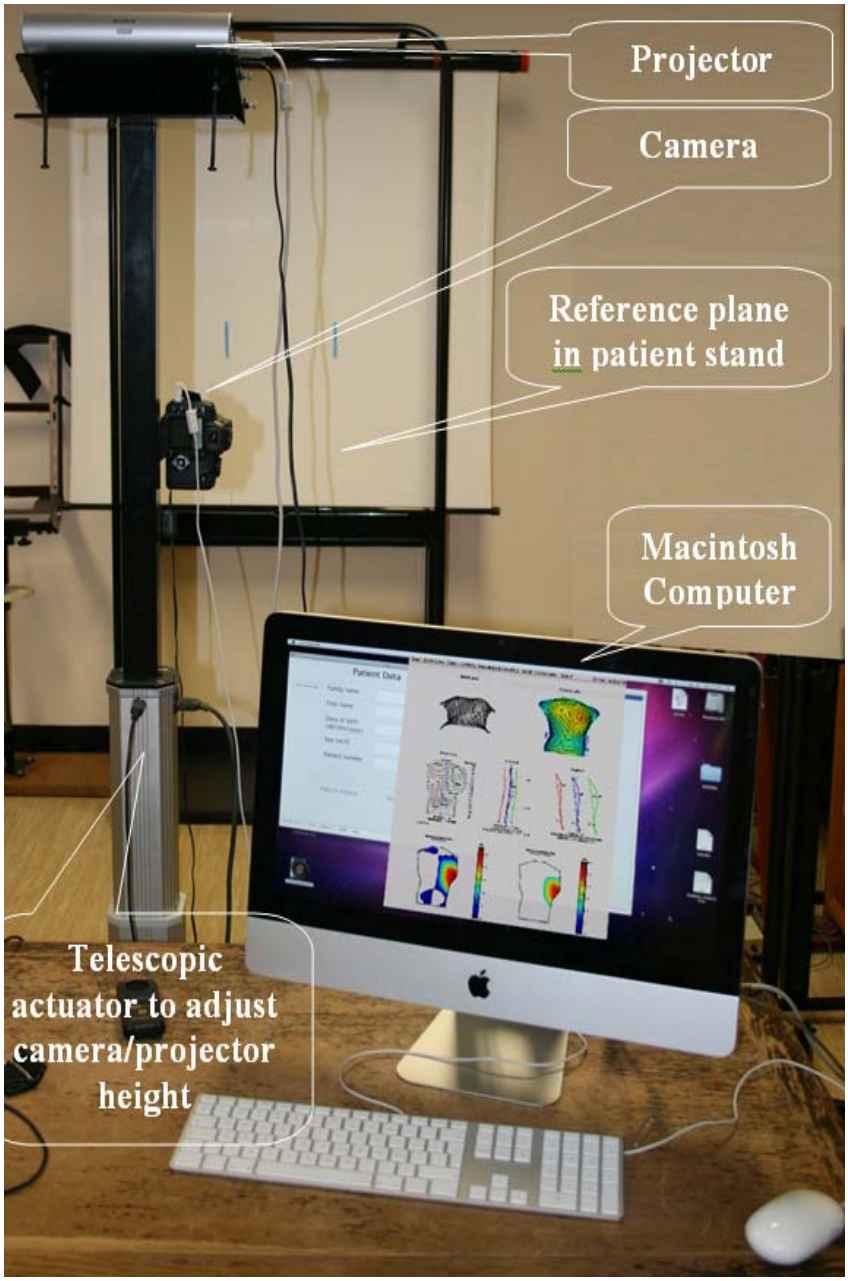

Figure 3.5: ISIS2 system

From the above figure, it can be seen that the mechanical part of the ISIS2 system consists of a camera/projector stand and a patient stand. The projector is mounted directly above the camera and projects a horizontal fringe pattern onto the patient's back. The camera/projector arrangement is mounted on a telescopic actuator which allows the camera to be centred on the patient's back regardless of patient height. The patient stand is used to help minimise postural variations and provide the reference plane. The reference plane is a retractable screen that is mounted above the patient's head, along the top of the frame.

Operating principle

Initially, the projector projects a grid of horizontal black lines onto the reference plane. An ordinary digital camera is used to take a photograph of the reference plane. During the measurement of the patient's back, a black velvet curtain is hung down the back of the patient stand frame so that the patient is silhouetted against a black background. The patient is asked to put on a black neckband and apron to provide clear limits for the area of the photograph to be analysed. Small coloured paper stickers are placed by an expert clinician on the patient's back, on the vertebra prominens, the dimples of Venus and a number of spinous processes. The stickers size is approximately 9×15 mm^2 and the numbers of stickers are typically seven to twelve in total [5]. The projector projects a grid of horizontal black lines onto the patient's back. A photograph of the patient's back is taken. A high speed Macintosh computer is used for receiving photo of patient and reference plane and mathematical analysis. Fourier transform profilometry is used to convert the distortion of the grid lines into a three dimensional surface map of the back [107].

A contour plot of a typical surface data matrix can be seen in Figure 3.6.

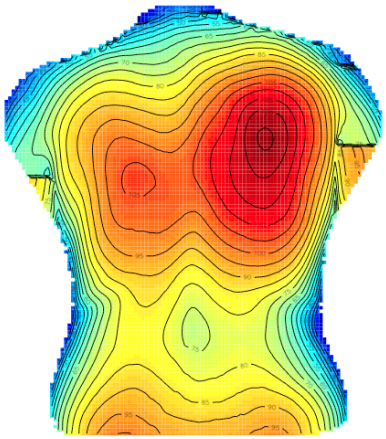

Figure 3.6: Contour map of back height

The full array includes areas of the photo that are off the back but the value in the matrix in these non-back regions is set to NaN. The stickers location data are stored in a two-dimensional matrix, the values in the matrix giving the *x* and *y* locations of each stickers. The matrices containing back surface information, the anatomical sticker locations and the pixel size are then stored in an R data file. This system calculates clinical parameters based on lengths and angles that are measured from the three-dimensional surface of the back. A diagrammatical representation of the ISIS2 analysis scenario can be seen in Figure 3.7.

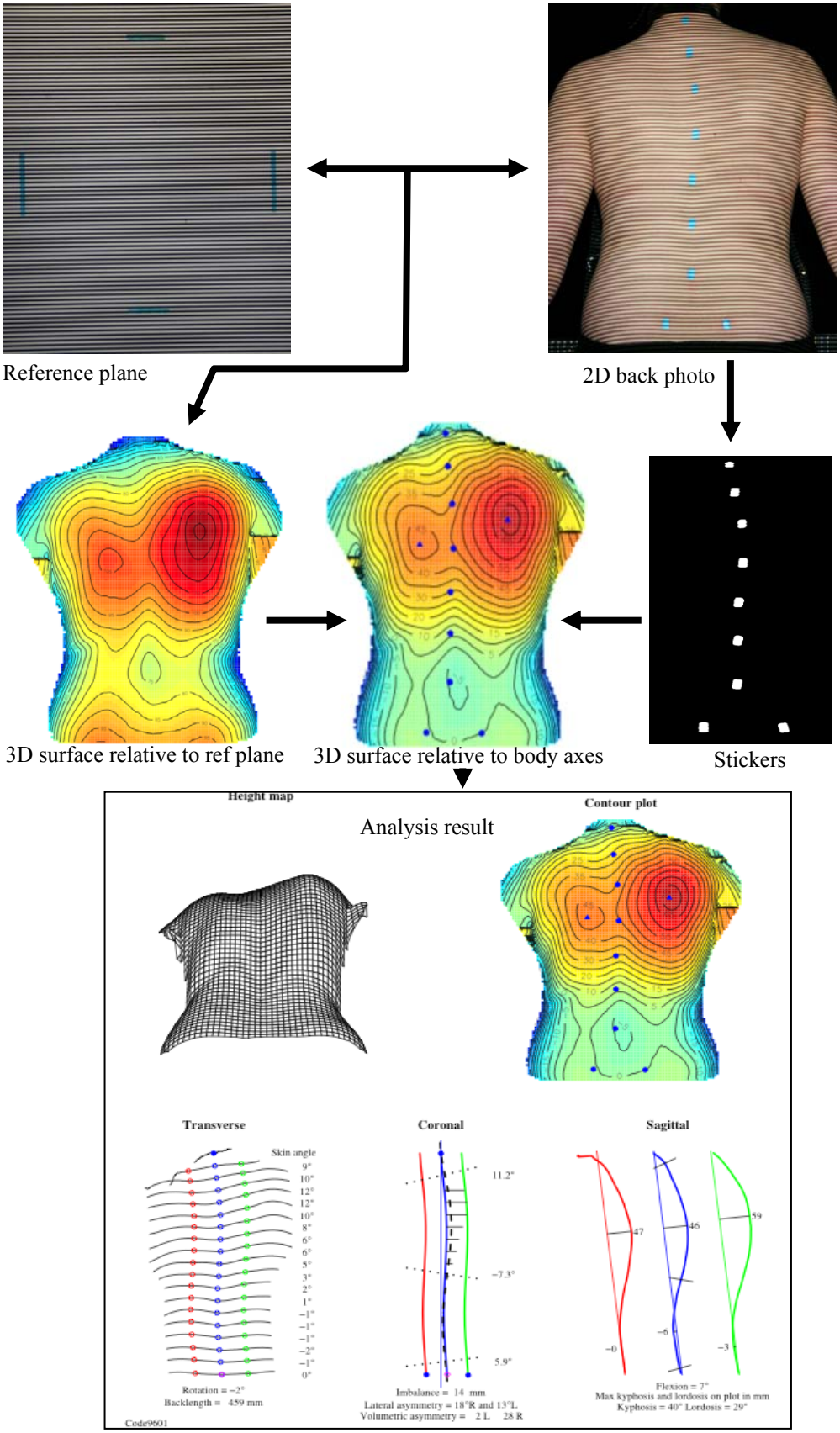

Figure 3.7: Analysis summary of ISIS2 [5]

Storing information

The surface data originates from a photograph stored as a two-dimensional matrix. The back height data is also in that format. The row and column position give the *x* and *y* locations of a particular pixel and the data stored in the matrix at that row and column gives the height (*z* value). The typical pixel sizes (i.e. the *x* and *y* axes) are approximately $0.5\,\text{mm} \times 0.5\,\text{mm}$ and the height (i.e. the *z* axis) is accurate to $\pm 1\,\text{mm}$ [5]. The ISIS2 analysis is carried out using the statistical language software R [108]. R is a language and environment particularly designed for data manipulation, calculation and graphical display which includes a wide variety of techniques such as effective data handling, graphical facilities for data analysis and storage facility. This software is free and many statistical analysis packages built in. These are the major reasons of choosing R for the analysis of this thesis.

Clinical parameters

A paper report is printed out after the analysis using ISIS2. It gives height map, contour plot, transverse, coronal and sagittal information that can be seen in Figure 3.7.

A height map is a wire-frame plot. It gives the three-dimensional shape of the back which is viewed from below to see exaggerated of any rib humps.

A contour plot represents the back shape using contour lines where the blue colour represents lowest and red colour represents highest value. The marker locations (solid blue circles) and the most prominent points on the two shoulder blade areas (solid blue triangles) are also indicated.

In transverse plot, the shape of the transverse section is divided 19 equally spaced levels from the vertebra prominens to the sacrum. It gives information of rotation angle, back length and the skin angle at each level. The open blue circles indicate the location of the spine at each level. A solid blue circle

indicates the vertebra prominens and a magenta diamond indicates the sacrum. The green and red circles are on the paramedian lines at 10% of the back length to the right and left of the spine.

The coronal plot shows a fifth order polynomial curve which fitted through the spinous process markers (thick blue curve) and similar curves at the paramedian locations to the right (green) and left (red). A fine blue line is dropped vertically from the vertebra prominens (gravity line). The horizontal distance between this line and the sacrum gives a measure of the imbalance. Imbalance is positive when the sacrum lies to the right of the vertical through the vertebra prominens. The heavy dashed black curve is calculated from the spinous processes curve and the skin angle at each transverse location (19 levels between vertebra prominens and sacrum). The angles of the perpendiculars to the points of inflection on this curve are calculated and used to compute the lateral asymmetry which is simulated Cobb angle(s).

The sagittal sections through the vertebra prominens and paramedian locations to the right and left are shown. The straight line from the vertebra prominens to sacrum is presented at the angle of flexion/extension. The numerical values for flexion, maximum kyphosis and lordosis in mm, and kyphosis and lordosis angles in degrees are stored in the database for longitudinal monitoring.

3.3.7 Other systems

A few other three-dimensional scanning systems are available for whole-body scanning (eg. Inspeck, Cyberware, TC2, Minolta Vivid, Vitus 3D, LASS, etc). Although these systems give whole-body information, these systems are not widely used because of the system price and the slow speed of scanning. There are few other systems for institutional use and not available commercially. For example, the Jozef Stefan Institute in Ljubljana, Slovenia has developed a Fourier transform-based system [109]. A group from the University of Alberta and the Glenrose Rehabilitation Hospital in Edmonton, Canada [110].

3.4 Clinical parameters for assessing normal and deformed backs

Back deformity analysis requires a thorough clinical parameters evaluation to completely assess the three-dimensional deformity. One can find quite a few back deformity evaluation indices, which are based on back surface data and are generally measured along the coronal, transverse and sagittal planes. However, there exists no coherent presentation of the underlying back deformity assessment to distinguish deformed backs from normal backs.

Generally speaking, the clinical parameters which have been used up to now are based on angle, length and anatomical location. These clinical parameters do not give a quantitative measure of back deformity based on the geometrical structure of back surface. A group of measuring back deformity includes indices which are specific to the measurement technique. These indices depend on the measurement technique, which means that cannot be measured and by other means. Such examples are the Cobb angle (see Section 1.5.1) and moiré fringe angles (see Section 3.3.3). Cobb angle is one of the great pioneers in the study and treatment of scoliosis. It is used to define and redefine curve patterns [111] and through arbitrary determined levels, to decide when treatment should commence and the type of treatment is needed. However, surgeons are divided for the decision to define the Cobb angle for back deformity. Some surgeons say a Cobb angle of greater than 10 degrees is scoliosis [112, 113], which means, if the Cobb angle is greater than 10 degree, it can be considered as deformed back and less than 10 degree can be considered as normal back. There are be plenty of people with curves greater than 10 degree who do not consider themselves to be “deformed” in any way. Kyphosis is even more disputable. There is no fixed way to define how kyphosis angle is measured. The range of vertebrae included in the measurement of kyphosis angle is varied widely, T1-T12 [114], T3-T11 [115], T4-T12 [116], T5-T12 [117], T4-T9 [118] and others allow free choice of end vertebrae [74]. The vertebrae are often not very clear in a sagittal radiograph and so the vertebrae used for the repeated measurement

also varies. An investigation has been carried out for the intra-rater variability in kyphosis radiographs and found that a change in kyphosis of 11° was necessary for 95% confidence limits covering 95% of the population [74]. Another method of detecting scoliosis is Adam's forward bending test and it has been used as a simple and effective [22]. Subjects exhibiting abnormal rib humps usually have been referred to a specialist for a more detailed examination. The severity of rib hump deformity justifying further examination is difficult to define, given that a rib hump is normally present [82, 119]. Some research has shown no relationship among specific indexes concerned with the rib hump and the degree of the Cobb angle [24]. Furthermore, the forward-bending test has been shown to be insensitive to the most common form of scoliosis, which occurs in the thoracolumbar region of the vertebral column [24]. There are many clinical parameters (rotation angle, imbalance, lateral asymmetry, volumetric asymmetry, flexion angle, kyphosis and lordosis angle etc) from ISIS2 system have been used for monitoring back deformity. However, these parameters are also based on angle, length and anatomical location; and unable to quantify normal backs from deformed backs.

Although the anatomical landmarks have been used in ISIS2 system to take some account of patient stance, it is still felt that variability in the clinical parameters is increased by the use of length and angle data. Patients also grow and so their back size, shape and form change between appointments with the doctor. Instead of distances and angles, geometric shape that is independent of location, rotation and scale effects could be measured. This research is mainly focusing on the quantification of three-dimensional human back shape based on geometrical structure of back surface using statistical shape analysis to allow assessment and monitoring for back deformities. This will also help to distinguish normal backs from deformed backs.

3.4.1 Classification of normal and deformed backs

From the literature review on backs, it can be concluded that there is no standard way to say whether a back is deformed or normal. It is a very subjective

decision. Although some surgeons say a Cobb angle of greater than 10 degrees is scoliosis [112], there will be plenty of people with curves greater than this who do not consider themselves to be "deformed" in any way. Kyphosis is even more disputable. There is no fixed way to define how kyphosis angle is measured. The vertebrae are often not very clear in a sagittal radiograph and so the vertebrae used for the measurement varies [120].

As there is no standard way to distinguish deformed backs from normal backs, for this research the classification of "normal" and "deformed" was carried out by an orthopaedic surgeon specialised in spinal deformity, making his decision based on clinical examination, ISIS2 scans and sometimes (but not always) radiography. For the volunteers, radiography was never part of the assessment.
All the patient data where there were repeat paired measurements, either intra-testing or inter-testing and some with both, were used for the research; this gave a total of 117 backs. Among all backs, one set of paired measurements was excluded because the patient had clearly moved between repeated measurements where the patient had great difficulty standing still. The patient had shoulders hunched in one photo and not in the other.

3.5 Summary

This chapter has described different surface measurement systems that have been developed for back surface analysis. The underlying measurement technique and its application for each method have been briefly outlined. The limitations and advantages of each method have been pointed where necessary. It is evident from the literature review that three dimensional surface data acquisition has now been developed to solve radiographic exposure and two dimensional problems. However, techniques to extract clinical parameters based on geometric structure on back surface for assessment of spinal and back deformities have not been widely developed. The three dimensional back surface information requires continuous research and development of methods and algorithms for interpretation and mathematical modelling to distinguish normal backs from deformed back. This investigation addresses this need and

attempts to develop processing techniques to extract useful information for the assessment back deformities.

The next chapter provides the mathematical foundation for the statistical shape and form analysis techniques that have been applied to back shape analysis in this investigation.

4 Statistical Shape analysis methods

4.1 Introduction

The mathematical basis for the shape and form analysis methods is presented in this chapter that has been used in this research for analyzing human backs. Anatomical shape, and its variation, has always been an important topic of medical research. Understanding the morphological changes caused by a particular disorder can help to identify the time of onset of a disease like back deformity, quantify its development and potentially lead to a better treatment. Unlike many industrial and real world objects, the human back is a relatively smooth surface, that is, there are no crisp features on the surface of the back. In this study, different statistical analysis of surface shape or form has been investigated for distinguishing deformed backs from normal backs and estimates the degree of deformation on each landmark location. Various shape measures that have been proposed in various applications of differential geometry are discussed.

4.2 Understanding of shape and form

The term shape is generally used to refer the appearance of an object. According to D.G Kendall [44], a shape is the geometrical information that remains when location, scale and rotational effects are filtered out from an object. It means that an object's shape is invariant under the Euclidean similarity transformations of translation, scaling and rotation. For example, the shape of human back consists of all the geometrical properties of the back that are unchanged when it is translated, rescaled or rotated in an arbitrary coordinate systems. Two backs have the same shape if they can be translated, rescaled and rotated to each other so that they match each other.

A form consists of geometrical representation of an object and a set of landmarks can represent that information. According to Richtsmeier et al. [49], the form of an object is the characteristic that remains invariant under any translation, rotation or reflection of the object. A form change of an object has occurred when differential change in magnitude occurs along various axes and there is difference in volume between the sphere surrounding the landmark in the reference form and the ellipsoid surrounding the landmark in the target form. To understand the form definition clearly, consider the simple situation of a triangle, defined by the location of three landmarks. Suppose the triangle is rotated or translated or reflected to an arbitrary amount. Any such movement of the triangle results in changes in the coordinate locations of the three vertices. Although no changes have been made regarding the relative location of the landmarks, a new set of coordinates is required to define the new location of the three landmarks once the triangle has been translated, rotated, or reflected. This means that the landmarks coordinate matrix changes upon reflection, translation, or rotation and that the landmark coordinate matrix is not invariant with respect to translation, rotation, and/or reflection. Considering landmarks of human back, the back can be rotated, translated or reflected by any arbitrary amount. Each such movement of the back results in changes in the coordinate locations of the back landmarks, although no changes have been made regarding the relative locations of the landmarks. This means that the landmarks coordinate matrix changes upon reflection, translation or rotation and that the landmark coordinate matrix is not invariant with respect to translation, rotation or reflection. Indeed, the terms shape and form have been used in this research as its origin and we are investigating shape and form techniques for human backs.

4.3 Statistical shape analysis

In 1960's and 1970's, researchers [121] illustrated that quantitative description of shape, combined with statistical analysis was adopted by biometricians to describe patterns of shape variations. Shape analysis plays an important role in many kinds of biological studies. It is mainly automatic analysis of geometric

shapes, for example using a computer to detect similarly shaped objects in a database or parts that fit together. For a computer to automatically analyze and process geometric shapes, the objects have to be represented in a digital form or mathematical representation. The statistical theory of shape began with the independent work of Kendall [44, 48] and Bookstein [45, 46]. Subsequently developments have led to a deep differential geometric theory of shape spaces [47], as well as practical statistical approaches to analysing objects using probability distributions of shape and likelihood based inference. Dryden and Mardia [43] have also played an important role and they concerned on the shapes of labelled point set configurations. Statistical shape analysis is a type of geometrical analysis that involves a set of visual shapes in which statistics are measured to describe shape components of similar or different shapes, for example, the difference between male and female gorilla skull shapes [43]. Some of the important aspects of shape analysis are to obtain a measure of distance between shapes, to estimate average shapes from a (possibly random) sample and to estimate shape variability in a sample [43]. Statistical shape analysis plays an important role in many kinds of biological studies [44-47].

A difference in shape or form between individuals such as scoliosis, kyphosis and lordosis occurs because of variety of biological processes. Shape analysis is one approach to understand those diverse causes of variation and morphological transformation. Differences in shape can be adequately summarised by comparing the observed shapes to more familiar objects such as rectangles, polygons or human backs. The human back can then be characterised as being more or less like a pentagon. The spine can look like “S”-shape or “C”-shape for scoliosis patients. Such comparisons can be extremely valuable because it helps to visualize and draw attention to the meaningful components of shape. Morphometrics is a quantitative way of addressing the shape comparisons. In general, the statistical studies of morphology are based on simple measurements of size, area and volume, which do not capture the entire complexity of shapes. These properties can provide some indication of normal variation and anomaly. However, the back shape surface data provides highly detailed shape

information. The way of extracting information from morphometric data involves mathematical operations rather than concepts rooted in biological intuition. Various methods have been studied for statistical shape analysis of human back.

4.4 Data representation

Shape analysis starts with extracting of shape attributes from the input data. A large number of shape descriptors have been proposed over the years for use in medical image analysis. Those descriptors are landmarks [46], dense surface meshes [122, 123], skeleton-based representation [124, 125] and deformation fields that define warping of a standard template to a particular input shape [126, 127]. The representation of shape depends on its application. In this research landmarks are used for feature extraction from back surface data obtained by ISIS2 system. Landmarks can be placed manually by a person who employs his/her knowledge of anatomy to identify special locations (known as anatomical landmarks), detected automatically using geometric properties of the outline surface (known as mathematical landmarks) or constructed points on an organism which are located either around the outline or in between anatomical or mathematical landmarks (known as pseudo landmarks). Those anatomical, mathematical and pseudo landmarks will then be used for statistical shape analysis.

4.5 Landmark based shape and form analysis methods

There are different shape and form analysis methods and a summary of the current methods is put forward by Richtsmeier et al. [128, 129], Marcus et al. [130] and Adams et al. [131]. Adapted from the classifying methods for form comparison used by Richtsmeier et al. [129], three main categories of form comparison methods are deformation methods, superimposition methods and methods based on linear distances. These methods are reviews in the following section.

4.5.1 Deformation methods

In these methods, a form is deformed correspond with the reference form [128, 129]. Three steps should be followed. Three steps are choose the reference object, employ elastic deformation of templates to deform the target object so that it matches the reference object exactly and study the deformation to quantify the form difference. Deformation methods include energy matrix [132], finite element scaling analysis (FESA) [133], free form deformation (FFD) [134] and thin plate splines (TPS) [135] etc.

FESA is widely used in engineering and it is required to subdivide the landmarks located on an object into groups to form so called “elements”. There exists a one to one correspondence between landmarks on the initial reference form and the target form. FESA determines the amount of “morphometric strain” required to produce the target model from the reference model [133]. One graphic technology of deforming the shape of objects smoothly by moving control lattice points set around the object , to analyze and classify the three dimensional foot forms of 56 Japanese females and faces for spectacles design carried out by Mochinaru et al. [134] using the FFD method. The distortion of the FFD control lattice points that transform the reference form into the target form is defined as the dissimilarity between two forms.

One limitation of deformation methods is that they lack of appropriate statistical procedures. Our research on back shape analysis needs proper statistical tests so that this method would not be suitable for out test.

4.5.2 Superimposition methods

According to some specific rules, landmark data of the reference shape and the target shape are arranged into one same coordinate space. Shape variation is determined by the displacement of landmarks in the target shape from the corresponding landmarks in the reference shape. There is not specific universal principium to choose the specified rule of superimposition and it depends on the

particular application [128]. According to Richtsmeier et al. [129], superimposition methods involves three steps. Those are fix one shape in a particular orientation and use it as the reference object, translate and rotate the other shape so that it matches the reference object according to some criterion and study the scaling value and direction of difference between shapes at each landmark. Based on different criteria for matching, superimposition methods consist of Procrustean approaches [51], Bookstein's edge matching [136] and roentgenographic cephalometry [137] etc. In this research, Procrustes analysis has been investigated for use in analysis human back deformity and is details discussed in Section 4.6.

4.5.3 Methods based on linear distances

In this category, methods compare linear distances that connect landmark pairs in one form with the corresponding linear distances in another form. Compare each linear distance of the form matrices as a ration, or an absolute difference or some other metric [129]. Study the matrix of linear distance comparisons to determine the difference between the forms. Examples include Euclidean distance matrix analysis (EDMA) [49] and its variations [138]. The statistics of EDMA have been formally developed [54]. Drawbacks of linear distance based methods have been argued by researchers from different aspects [129], e.g. the loss of geometric characteristic of the surfaces between landmarks, a great deal of physical effort in landmarks, short of providing the intangible graphics available from other methods. It has also been argued that the information contained within the form matrix is redundant [129]. . In this research, EDMA has been investigated for use in analysis human back deformity. A coloured scale graphical technique has been used to overcome the intangible graphics of EDMA. The EDMA is details discussed in Section 4.7.

4.6 Procrustes analysis

Shape analysis is an important aspect of visualizing and understanding of shape information. The analysis of shape plays a vital role, not only in determining the

differences between shape groups, but also in determining the location of differences among shapes. The form of statistical shape analysis used to analyse the distribution of a set of shapes in this work is Procrustes analysis [139]. According to Beinat and Crosilla [140], Procrustes analysis is a set of mathematical least-squares tools to directly estimate and perform simultaneous similarity transformations among the model point coordinates matrices up to their maximal agreement. Procrustes analysis is a rigid shape analysis that uses translation, isotropic scaling and rotation to find the best fit between two or more landmarks shapes [139]. It has variations and forms, of which are Orthogonal Procrustes analysis (OPA), Extended Orthogonal Procrustes analysis (EOPA), Weighted Extended Orthogonal Procrustes analysis (WEOPA), and Generalized Procrustes analysis (GPA) etc [51, 141-143]. In general, Procrustes analysis is a multivariate exploratory technique that involves transformations (i.e., translation, rotation, reflection, isotropic rescaling,) of individual data matrices to provide optimal comparability [141] i.e. it is the evaluation of many sets of configurations which can be aligned to one target shape or aligned to each other. GPA is used in several domains. For example, it can be used in sensory analysis before a preference mapping to reduce the scale effects and to obtain a consensus configuration. It also allows a comparison of the proximity between the terms that are used by different experts to describe products [144]. OPA, on the other hand, is used for matching two configurations [145].

Shapes and landmarks are two important concepts involved with GPA. Landmarks have their own role in the process of aligning shapes. Landmarks have been discussed in Chapter 2 Section 2.3.1. Dryden and Mardia [43] define shape as the geometrical information that remains when location, scale and rotational effects are filtered out from an object. By this definition of shape, there exists transforms that allow the shape to move so that the differences may be removed between two shapes while presenting the shape itself. The transforms used in aligning the shapes are; scaling, translation and rotation. Dryden and Mardia use the notation OPA to mean ordinary Procrustes analysis and this notation is what is used in the rest of this thesis.

The main objective of this research is to develop a method which will be able to distinguish deformed backs from normal backs based on full geometrical shape of the back and will be independent of location, rotation and scale effects. The present parameters of ISIS2 are based on lengths and angles, which can be affected by patient stance, breathing and muscle tension. An investigation of Procrustes analysis which would take into account the back shape more fully than lengths and angles was therefore undertaken.

4.6.1 Graphical representation of the Procrustes transformations

A representation of two configurations X and Y consisting of $n = 9$ landmarks on each object in $k = 2$ dimensional space can be seen in Figure 4.1(a). The landmarks are joined together by drawing lines between them to visualize the outline of two shape configurations. It can be seen that the two shapes are not aligned in the same way and they do not have the same origin. Their height and width are also different. The purpose of applying Procrustes analysis is to find the best fit between these two configurations. We can do this by superimposing the second configuration on to the first configuration and eliminating differences in scale and rotation. The result of the translation is shown in Figure 4.1 (b), Figure 4.1 (c) shows the result of scaling and the result of the rotation is shown in Figure 4.1 (d).

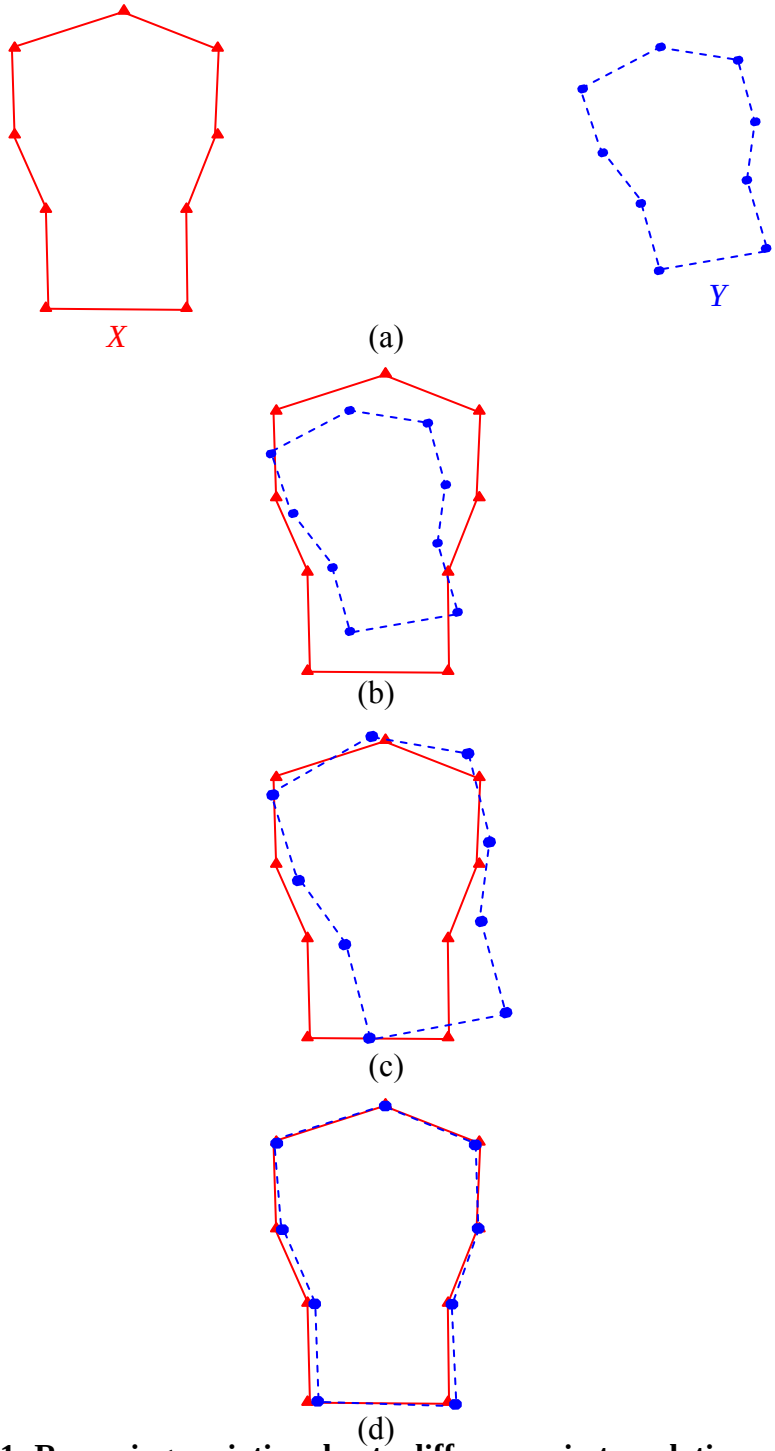

Figure 4.1: Removing variation due to differences in translation, scale and rotation (a) Original data of two configurations; (b) After translating the centroid of *X* to the centroid of *Y*; (c) After removing differences in scale; (d) After removing differences in rotation.

It is now important to understand mathematical formulae for these steps to implement this technique for back shape analysis.

4.6.2 Mathematical representation

Let X_i *(i=1,2,3,…,m)* be a series of *m* matrices that contain the coordinates of a set of *p* landmarks on the *m* shape configurations in *k* dimensions. According to Gower [141] translation, rotation and scaling of a configuration can be described as

$$\hat{X}_i = c_i X_i O_i + j t_i^T \tag{4.1}$$

Where $\hat{X}$ gives the new coordinates of the landmarks in the configuration. O_i is the rotation matrix, c_i is the scaling factor, t_i is the translation vector and *j* is the unit vector. The superscript ^{T} indicates the transpose of the matrix. For GPA, the configurations are translated, rotated and scaled until the sum of the squares of the distances between the equivalent landmarks are minimized to give the best possible match between all configurations. The function to be minimized is thus

$$E \equiv \mathrm{tr}\left\{\sum_{i=1}^{m}\sum_{q=i+1}^{m}\left[\left(c_i X_i O_i + j t_i^T\right)-\left(c_q X_q O_q + j t_q^T\right)\right]^T\left[\left(c_i X_i O_i + j t_i^T\right)-\left(c_q X_q O_q + j t_q^T\right)\right]\right\} \tag{4.2}$$

The procedure can be described pictorially [140] as shown in Figure 4.2 where the individual configurations are translated, rotated and scaled so that they can be “superimposed” on each other to achieve a “best” fit.

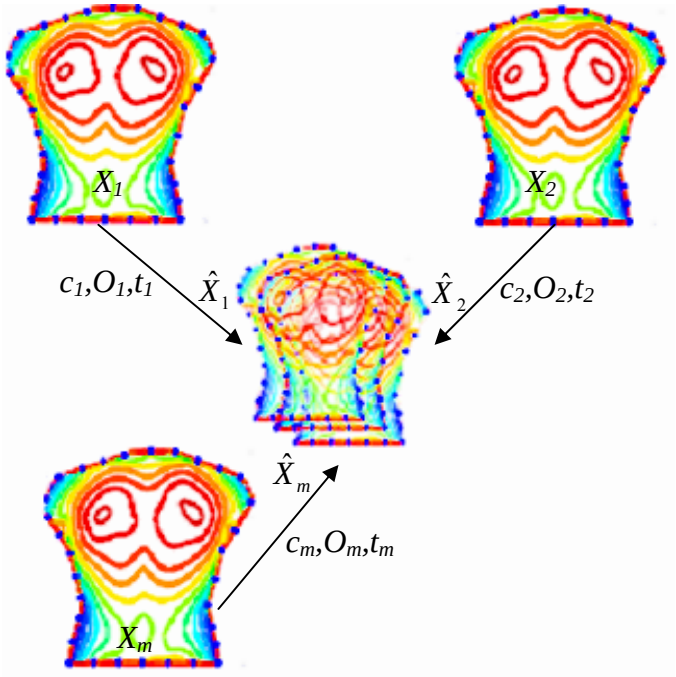

Figure 4.2: Concept of generalised Procrustes analysis

If the trivial solution found by setting all c_i to zero is excluded, another possible solution to the minimisation problem can be to select one configuration as the "norm" and scale all the other configurations relative to that one. However this means that fitting X_1 to X_2 does not give an identical result to fitting X_2 to X_1. It is more satisfactory to estimate all c_i parameters such that

$$\sum_{i=1}^{m} c_i^{\,2}\,\mathrm{tr}\left(X_i X_i^{T}\right) = \sum_{i=1}^{m} \mathrm{tr}\left(X_i X_i^{T}\right) \tag{4.3}$$

This means the sum of squares about the origin of the rotated, scaled and translated configurations is unchanged from the original value; in other words some configurations are increased in size while others are reduced so that the overall sum remains the same.

$$\sum_{i=1}^{m} \sum_{q=i+1}^{m} \left\| \bar{X}_i - \bar{X}_q \right\| = \min \tag{4.4}$$

Where the operator $\|.\|$ represents normal vector space or norm and $\bar{X}$ is mean.

Let us consider the sum-of-squares between each cluster of points $P_i^{(q)}$ where $i=1,2,3,\ldots m$ and their centroid is G_i which is summed over all P clusters. So the Euclidean distance between the pairs of points P_i and G_i is $\Delta(P_i^{(q)}, G_i)$. The mp lengths $\Delta(P_i^{(q)}, G_i)$ are termed residuals. The residual sum-of-squares R_s [141] is therefore

$$R_s = \sum_{i=1}^{p}\sum_{q=1}^{m}\Delta^2(P_i^{(q)}, G_i) \tag{4.5}$$

because of the identity of different configurations

$$\sum_{u<v}^{m}\Delta^2(P_i^{(u)}, P_i^{(v)}) \equiv m\sum_{u=1}^{m}\Delta^2(P_i^{(u)}, G_i) \tag{4.6}$$

Now it is required to estimate the scaling factor c_i, the rotation matrix O_i and the translation vector t_i so that the residual sum-of-squares of equation (3.5) is minimized.

There is no unique solution for O_i as equation (4.2) is invariant to orthogonal rotations of the total system of pm points. A unique solution can be determined by referring all final co-ordinates to the principal axes of the set of centroid points G_i where $i=1,2,3,\ldots,m$. Equation (4.2) can therefore be minimized subject to the constraints of equation (4.3).

Every O_i [141] is orthogonal can be represented by

$$\sum_{k=1}^{p} o_{uk}{}^{(i)} o_{vk}{}^{(i)} = \delta_{uv} \tag{4.7}$$

where δ_{uv} is the Kronecker-δ, for u ≤ v where $v=1,2,3,\ldots\ldots,p$

Associating with equation (4.3) the Lagrange multiplier μ and with equation (4.7) the $\frac{1}{2}mk(k+1)$ Lagrange $\lambda_{uv}{}^{(i)}$. Considering these as arranged in m

symmetric matrices Λ_i where $i = 1,2,3,\ldots,m$ with general elements $\lambda_{uv}^{(i)} (u \neq v)$ and $2\lambda_{uv}^{(i)}$ on the diagonal. Thus finally we have to minimize

$$E + \mu\left(\sum_{i=1}^{m} c_i^2 \operatorname{tr}(X_i X_i^T) - \sum_{i=1}^{m} \operatorname{tr}(X_i X_i^T)\right) + \sum_{r=1}^{m}\sum_{i \leq q}^{k} \lambda_{iq}^{(r)} \left(\sum_{l=1}^{k} o_{il}^{(r)} o_{qk}^{(r)} - \delta_{iq}\right) \tag{4.8}$$

4.6.2.1 Translation

The only terms involving the translation matrix, t_i, occur in equation (4.2)

$$E_o \equiv \operatorname{tr}\left[(m-1)\left(c_i X_i O_i + j t_i^T\right)\left(c_i X_i O_i + j t_i^T\right)^T - 2\left\{\sum_{j \neq i}^{m} \left(c_j X_j O_j + j t_j^T\right) t_i^T\right\}\right] \tag{4.9}$$

Now differentiating equation (4.9) [141] with respect to the elements of row vector t_i gives $\frac{\partial E_o}{\partial t_i} \equiv pmt_i$ which is the vector of column sums $\sum_{i=1}^{m} jt_i$. So the minimum is $t_1 = t_2 = t_3 \ldots = t_m$. It shows that all m configurations should be translated to have the same centroid. Thus the terms of equation (4.2) in t_i *(i= 1, 2, 3,…,m)* can be dropped from further consideration.

4.6.2.2 Rotation

Now differentiating equation (4.8) with respect to $o_{iq}^{(r)}$ (o_{iq} represents individual elements in O_i) gives

$$c_r\left\{c_1(X_r{}^T X_1 O_1)_{iq}+\cdots+c_{r-1}(X_r{}^T X_{r-1}O_{r-1})_{iq}+c_{r+1}(X_r{}^T X_{r+1}O_{r+1})_{iq}+\cdots+c_m(X_r{}^T X_m O_m)_{iq}\right\}$$
$$-\sum_{l\neq q}^{k}\lambda_{il}{}^{(r)}o_{il}{}^{(r)}-2\lambda_{iq}{}^{(r)}o_{iq}{}^{(r)}$$

(4.10)

Equating it to zero and expressing it in matrix terms gives [141]

$$c_r X_r{}^T(mY-c_r X_r O_r)=\Lambda_r O_r \tag{4.11}$$

where $r=1,2,3,\ldots,m$ and $Y=\frac{1}{m}\sum_{i=1}^{m} c_i X_i O_i$ are the co-ordinates of the centroid of the group or consensus configuration after rotation and scaling. Post-multiplying by $O_r{}^T$ and rearranging gives

$$(c_r X_r{}^T Y)O_r{}^T=(c_r{}^2 X_r{}^T X_r+\Lambda_r)\big/m \tag{4.12}$$

The singular value form of $c_r X_r{}^T Y$ is written as $U_r{}^T S_r V_r$ where U_r and V_r are orthogonal and S_r is diagonal. The right-hand-side of equation (4.12) is symmetric and thus equation (4.12) reduces to

$$O_r=U_r{}^T V_r \tag{4.13}$$

Therefore the rotation is completed by multiplying $U_r{}^T V_r$ by the X_i matrix in order to align it with the $\overline{X}_i$ matrix. Thus $\left|X_r O_r-\overline{X}_r\right|$ is minimized for the value O_r.

4.6.2.3 Scale

Differentiating equation (4.9) with respect to c_i and equating the result to zero gives

$$(m-1)c_i \mathrm{tr}(X_i X_i^T) - \mathrm{tr}\left\{ X_i O_i \sum_{\substack{l=1 \\ l \neq i}}^{m} c_l O_l^T X_l^T \right\} + \mu c_i \mathrm{tr}(X_i X_i^T) = 0 \quad (4.14)$$

or

$$(m-1)c_i \mathrm{tr}(X_i X_i^T) - \mathrm{tr}\left\{ X_i O_i \sum_{l=1}^{m} c_l O_l^T X_l^T \right\} + c_i \mathrm{tr}(X_i X_i^T) + \mu c_i \mathrm{tr}(X_i X_i^T) = 0 \quad (4.15)$$

Finally

$$m c_i \mathrm{tr}(X_i X_i^T) - m\mathrm{tr}(X_i O_i Y^T) + \mu c_i \mathrm{tr}(X_i X_i^T) = 0 \quad (4.16)$$

Multiplying equation (4.16) by c_i and summing over $i=1, 2,3, \ldots, m$ and recalling the constraints of equation (4.4) yields

$$(m+\mu)\sum_{i=1}^{m} \mathrm{tr}(X_i X_i^T) = m^2 \mathrm{tr}(YY^T) \quad (4.17)$$

and hence

$$c_i = \frac{\mathrm{tr}(X_i O_i Y^T)\sum_{i=1}^{m} \mathrm{tr}(X_i X_i^T)}{m \ \ \mathrm{tr}(X_i X_i^T)\mathrm{tr}(YY^T)} \quad (4.18)$$

The alternative form can be written as

$$c^2{}_i = \frac{\mathrm{tr}(c_i X_i O_i Y^T)\sum_{i=1}^{m} \mathrm{tr}(X_i X_i^T)}{m \ \ \mathrm{tr}(X_i X_i^T)\mathrm{tr}(YY^T)} \quad (4.19)$$

Because Y itself involves the scaling factors, the above formulae do not give a direct method for calculating c_i, but have to be used iteratively. However, equation (4.16) is the same equation for determining c_i as when given X_i,O_i are

to be scaled to fit *any* configuration Y and equations (4.18) and (4.19) still follow but with $tr(YY^T)$ replaced by $tr(\sum_{i=1}^{m} c_i X_i O_i Y^T)/m$.

Iterative procedures are used for the minimization process in GPA. The shapes are repeatedly scaled, rotated and translated until the sum-of-squares defining the distances between the equivalent landmarks on all shapes has been minimised.

4.6.3 Algorithm for GPA

The procedure to align the configurations using GPA is as follows:

1. Calculate the initial approximate mean with all centroids at the origin
2. Align all shapes to this mean:
    a. Calculate centroid for each shape
    b. Translate each shape to origin (common centroid)
    c. Scale each shape for best fit
    d. Rotate each shape for best fit
3. Calculate new approximate mean from aligned shapes.
4. If the approximate mean from 3 differs by more than a set tolerance from the previous approximate mean, then repeat steps 2 and 3.

4.6.4 Algorithm for OPA

Ordinary Procrustes analysis is a special case of GPA where the number of configurations is two. The second configuration is translated, scaled and rotated to find the best match on the first configuration.

4.7 Euclidean distance matrix analysis

Euclidean distance matrix analysis (EDMA) was developed by Lele and Richtsmeier [54] in 1991 for comparing two shapes using landmark data. They have described a method for comparing the forms of organisms that have been measured using the two or three-dimensional coordinates of homologous

landmarks. Homologous landmarks are those landmarks chosen to represent features on organisms that are similar due to a phylogenetic relationship. The organisms being compared thus share a common ancestor and the feature under study is present in all organisms under consideration due to each inheriting it from the common ancestor [49]. EDMA also allows form variation, shape or growth differences to be examined through the comparisons of ratios of landmarks of equivalent configurations. [54, 146-148].

The x and y landmark coordinates extracted from each back surface consist of variation due to the back length and back width. This variation is manifested as perturbations around the mean landmark configuration. These perturbations can vary in size and shape from landmark to landmark. A mean form is estimated from a set of twenty normal backs using EDMA. This mean form is considered to be the standard normal mean form. The standard normal mean form is then used to estimate the form difference from all backs. The variance and covariance are also estimated for individual landmarks. Two backs have the same form if their Euclidean matrices are identical. Two backs also have the same form if the Euclidean matrix describing one form is a constant multiple of the Euclidean matrix describing the second form.

4.8 The perturbation model for landmarks

Suppose $n=9$ two-dimensional landmarks have been selected on the back, then the landmarks data matrix for one subject will look as follows:

$$\begin{bmatrix} x_1 & y_1 \\ x_2 & y_2 \\ \cdots & \cdots \\ x_9 & y_9 \end{bmatrix}$$

where x and y denote the two-dimensional coordinates,

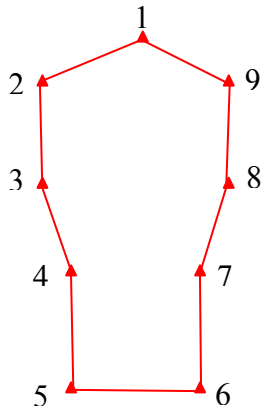

Figure 4.3: Diagram of a back indication the locations of 9 landmarks.

Assuming the configuration of these landmarks represents the form of a back as shown in Figure 4.3, the question is how to measure the variability among individuals that are represented by these two-dimensional landmark data. In statistical studies, when analyzing landmark data, variability is particularly difficult to characterize, because data on an individual is collected in a coordinate system specific to the orientation of that individual during data collection. This makes the problem statistically challenging. It is known that the general variance parameter is non-identifiable [146, 149]. For this analysis, a simple approach based on (EDMA) is used to estimate the parameters consistently.

Suppose K landmarks on a D-dimensional object are given. Then a matrix can be constructed of $K \times D$ whose j^{th} row consists of the D coordinates of the j^{th} landmark. Usually D is either 2 or 3 and K is assumed to be larger than D. All the information about the form of an object defined on the basis of landmark coordinates is summarized in the collection of all distances between pairs of landmarks. A matrix consisting of such a collection of distances is known as the form matrix. The number of unique pair-wise linear distances in a form matrix is L where $L=K(K-1)/2$. X_i can be considered as an individual configuration, denoting the $K \times D$ matrix of coordinates for the i^{th} individual. A $K \times D$ matrix is designated M which describes the mean for the population of backs, where each row represents the D dimensional coordinates of a single landmark. The

mean M is considered to be the standard normal back, which is a mathematical construction based on a set of twenty normal backs in this research. No single normal back is likely to be identical in form to the mean M and no two individuals are likely to be identical as normal backs also vary from person to person.

4.8.1 Perturbation model

Landmark data are commonly modelled using the perturbation model [51, 146] and it may be thought of as representing the following process. To generate a random geometrical object or equivalently, a K point configuration in D dimensional Euclidean space, nature first chooses a mean form (represented by matrix M) and perturbs the elements of this matrix by adding noise to this mean form according to a Gaussian distribution [146]. The distribution may vary from landmark to landmark. The K point configuration so obtained is then rotated and/or reflected by an unknown angle and translated by an unknown amount. Such perturbed, translated, rotated or reflected K point configurations are our data.

The above description can be put in a mathematical form as follows. Let M denote the $K \times D$ landmark coordinate matrix corresponding to the mean form. Let E_i be the $K \times D$ matrix representing the error for the i^{th} individual and assume E_i is Gaussian with mean matrix 0 and variance-covariance matrix $\Sigma_K \otimes \Sigma_D$ where Σ_K is a $K \times K$ positive definite matrix representing the variance among elements within the same column of E_i and Σ_D is a $D \times D$ positive definite matrix representing the variance among elements within the row of E_i. E_i also describes how X_i differs from mean M in the real data. The symbol $\otimes$ represents the Kronecker product. Σ_K describes the variances and covariances of the landmarks, while Σ_D describes the variances and covariances of the perturbation with respect to the real space coordinate axes. Let Γ_i be a $D \times D$ orthogonal matrix representing rotation and/or reflection of $(M + E_i)$ and

t_i, a $K \times D$ matrix with identical rows representing translation. Then the landmark coordinate matrix corresponding to the i^{th} individual may be represented as $X_i = (M + E_i)\Gamma_i + t_i$. It then follows that

$$X_i \sim MN_{K\times D}(M\Gamma_i + t_i, \Sigma_K, \Gamma_i^T \Sigma_D \Gamma_i) \tag{4.20}$$

for *i=1,2,…,n*. Here "*MN*" stands for "matrix normal". Parameters of interest are (M, Σ_K, Σ_D) and (Γ_i, t_i) are the nuisance parameters.

4.8.2 Eliminating the nuisance parameters

Before estimating the mean form *M* and the variance-covariance matrix Σ_K and Σ_D, it is important to eliminate the nuisance parameters first. The data can be transformed in such a way that the distribution of the transformed data is independent of the nuisance parameters. Lele [146] and Lele and McCulloch [149] use a maximal invariant statistic $T(\cdot)$ to eliminate nuisance parameters. They define the maximal invariant as follows. Let *S* denote the space of all $K \times D$ matrices and let $T(\cdot)$ be a function defined on this space such that for *X* and X^* in *S*, $T(X) = T(X^*)$ if and only if X^* is just a rotation, translation, and/or reflection of *X*. Then $T(\cdot)$ is called a maximal invariant defined on the space *S* under the group of rotation, translation and reflection of *X*.

$$\text{Let } H = \begin{bmatrix} 1-\frac{1}{k} & -\frac{1}{k} & \cdots & -\frac{1}{k} \\ -\frac{1}{k} & 1-\frac{1}{k} & \cdots & \vdots \\ \vdots & \vdots & 1-\frac{1}{k} & -\frac{1}{k} \\ -\frac{1}{k} & -\frac{1}{k} & \cdots & 1-\frac{1}{k} \end{bmatrix}$$

is a $K \times K$ centering matrix. Let $X^C = HX$, then the column of X^C sum to zero. The following theorem gives a maximal invariant of *X*, a $K \times D$ matrix of landmark coordinates.

Theorem 4.1. $T(X) = HXX^T H^T$ is a maximal invariant statistic, where X is a $K \times D$ matrix.

Proof:

1) $T(X)$ is invariant.

$$T(X\Gamma + t) = H(X\Gamma + t)(\Gamma^T X^T + t^T)H^T = HX\Gamma\Gamma^T H^T = T(X) \tag{4.21}$$

since t has identical rows and then $Ht = 0$.

2) $T(X)$ is maximal invariant.

To show that it is a maximal invariant, it is important to show that, given $T(X)$, it can be mapped back to a unique orbit in the original space. This can be proved using the fact that $T(X)$ is a centered inner product matrix and so there exists a unique (up to rotation, translation, reflection) mapping from the centered inner product matrix to a coordinate matrix [146, 149, 150]. Furthermore, it follows from standard multivariave normal distribution theory [151] that if $\sum_D = I$

$B_i = T(X_i) = X_i^C (X_i^C)^T \sim \text{Wishart}_K(D, \Sigma_K^*, MM^T)$ that is, the random variables B_is are $K \times K$ matrices and have a Wishart distribution independent of nuisance parameters, where $\Sigma_K^* = H\Sigma_K H^T$ is a $K \times K$ non-negative definite matrix of rank $K-1$ corresponding to the variance of the columns of X_i^C. Lele [146] shows that Σ_K^* and $X_i^C (X_i^C)^T$ are identifiable and provides a consistent estimator of Σ_K^* and $X_i^C (X_i^C)^T$ based on the method of moments. It can be noted that $T(M) = M_i^C (M_i^C)^T = HMM^T H$ is a centered inner product matrix corresponding to the mean form *M*. The second point of the proof of Theorem 4.1 establishes that estimation of $M_i^C (M_i^C)^T$ are equivalent to estimating the mean form. In

other words, given $M_i^C(M_i^C)^T$ one can construct M (up to translation, rotation and reflection).

4.8.3 The estimation of $M^C(M^C)^T$ and Σ_K^*

The following notations are used from [146]

(i) $F(X)=[F_{lm}]_{\substack{l=1,2,\ldots,k \\ m=1,2,\ldots,k}}$ where F_{lm} is the Euclidean distance between landmarks l and m. Euclidean distance is the straight line distance between two points that can be measured by the ruler.

(ii) $Eu(x)=[F_{lm}^2]=[e_{lm}]$ denotes the matrix of squared distances.

(iii) $B(X)=M^C(M^C)^T$ denotes the centered inner product matrix.

(iv) Let $\sum_K =[\sigma_{lm}]_{\substack{l=1,2,\ldots,k \\ m=1,2,\ldots,k}}$ be the variance-covariance matrix and,

$Eu(M)=[\delta_{lm}]_{\substack{l=1,2,\ldots,k \\ m=1,2,\ldots,k}}$ be the Euclidean distance corresponding to the mean form M.

The following theorems lead to the consistent moment estimator for δ_{lm}'s. The proof follows from the consistency of the sample moments and the consistency of a continuous function of sample moments. The properties of non-central χ^2 distribution follow from [152].

Theorem 4.2. $e_{l,m} \sim \phi_{lm}\chi_D^2(\delta_{lm}/\phi_{lm})$ that is, squared Euclidean distances between pairs of landmarks have a non-central χ^2 distribution with D degrees of freedom, non-centrality parameter δ_{lm} and scaling parameter ϕ_{lm}, where $\phi_{lm}=\sigma_{ll}+\sigma_{mm}-2\sigma_{lm}$.

Theorem 4.3. For a two-dimensional object,

$$E(e_{l,m}) = 2\phi_{l,m} + \delta_{l,m} = \alpha_1 \tag{4.22}$$

$$\mathrm{Var}(e_{l,m}) = 4\phi_{l,m}^2 + 4\delta_{l,m}\phi_{l,m} = \alpha_2 \tag{4.23}$$

and

$$\alpha_1 - \alpha_2 = (\delta_{l,m})^2 \tag{4.24}$$

We can then equate the sample moments to the population moments to obtain a moment estimator for δ_{lm}.

Theorem 4.4. Let e_{lm}^i denote the squared distance Euclidean distance between landmarks *l* and *m* in the i^{th} object.

$$\text{Let } \bar{e}_{l,m} = \frac{1}{n}\sum_{i=1}^{n} e_{lm}^i \tag{4.25}$$

$$S^2(e_{l,m}) = \frac{1}{n}\sum_{i=1}^{n} (e_{lm}^i - \bar{e}_{l,m})^2 \tag{4.26}$$

and

$$\hat{S}_{l,m} = [(\bar{e}_{l,m})^2 - S^2(e_{l,m}))]^{1/2} \tag{4.27}$$

then as $n \to \infty$,

$$\hat{\delta}_{l,m} \to \delta_{l,m} \text{ in probability}$$

We can now obtain the moment estimator of $\delta_{l,m}$ for three-dimensional objects.

Theorem 4.5.

$$E(e_{l,m}) = 3\phi_{l,m} + \delta_{l,m} = \beta_1 \tag{4.28}$$

$$\mathrm{Var}(e_{l,m}) = 6\phi_{l,m}^2 + 4\delta_{l,m}\phi_{l,m} = \beta_2 \tag{4.29}$$

and

$$\beta_1^2 - \frac{3}{2}\beta_2 = (\delta_{l,m})^2 \tag{4.30}$$

Theorem 4.5. Using the same notation as in Theorem 4.4, and

$$\hat{S}_{l,m} = [(\bar{e}_{l,m})^2 - 1.5S^2(e_{l,m}))]^{1/2} \tag{4.31}$$

it follows that as $n \to \infty$,

$$\hat{\delta}_{l,m} \to \delta_{l,m} \text{ in probability.}$$

The next theorem utilizes the estimators of $\delta_{l,m}$ to obtain a consistent estimator of the variance-covariance parameter Σ_K^*. The proof allows from Arnold [151] and consistency of moments and consistency of continuous function of moments from Theorem 4.1.

Theorem 4.6.

$$E(B(X)) = D\Sigma_K^* + B(M) \text{ and } \hat{\Sigma}_K^* = \frac{1}{D}\left[\frac{1}{n}\sum_{i=1}^{n} B(X)\right] - B(M) \to \Sigma_K^* \text{ in probability}$$

Following the theorems, the algorithm of obtaining and $\hat{M}$ and Σ_K^* can be shown as follows:

Step1. Calculate $B(M) = -\frac{1}{2}H\{Eu(M)\}H$ where $H = I - 1/K(1^T 1)$ is a $K \times K$ symmetric matrix such that its diagonal entrees are *1-1/K* and off diagonal entries are *–1/K*

Step2. Calculate the eigenvalues and eigenvectors of *B(M)*. Let the eigenvalues be $\lambda_1 > \lambda_2 > \cdots > \lambda_K$ and the corresponding eigenvectors be $h_1, h_2, \cdots, h_K$.

Step3. The estimator of the centred mean from $\hat{M}^C$ is given by:

For a two-dimensional object $\hat{M}^C = [\sqrt{\lambda_1 h_1}, \sqrt{\lambda_2 h_2}]$

For a three-dimensional object $\hat{M}^C = [\sqrt{\lambda_1 h_1}, \sqrt{\lambda_2 h_2}, \sqrt{\lambda_3 h_3}]$

Step4. The estimator of Σ_K^* is given by $\hat{\Sigma}_K^* = \frac{1}{D}\left[\frac{1}{n}\sum_{i=1}^{n} B(X)\right] - B(M) \to \Sigma_K^*$

This shows that $\Sigma_K^* = H\Sigma_K H^T$ is identifiable and estimable.

4.8.4 The estimation of Σ_K

However, our interest is to estimate Σ_K. Unfortunately, mapping from Σ_K^* to Σ_K is non-unique because the centring matrix H is singular and hence it is not invertible (recall that $\Sigma_K^* = H\Sigma_K H^T$). To make this mapping unique, conditions must be imposed on Σ_K. Let L be a $(K-1)\times K$ matrix whose first column consists of -1 s and the rest of the matrix an identity matrix of dimension $(K-1)\times(K-1)$. Let $\widetilde{\Sigma}_K = L\Sigma_K L^T$. It should be noted that Σ_K is a symmetric $K\times K$ matrix of full rank K while $\widetilde{\Sigma}_K$ is a $(K-1)\times(K-1)$ matrix of rank $(K-1)$. Lele and McCulloch [149] give the conditions under which Σ_K is a unique transformation of $\widetilde{\Sigma}_K$. Thus if $\widetilde{\Sigma}_K$ is estimable, then Σ_K is also estimable.

4.9 Summary

This chapter has presented different shape analysis methods. It has also presented mathematical foundation of the shape and form analysis methods applied in this study. The statistical shape analysis methods, data representation and landmark based shape and form methods are discussed. The Procrustes analysis and EDMA are discussed details because these have been used to distinguish deformed backs from normal backs and estimate the degree of deformity on each landmark location.

A crucial aspect of any form of data interpretation and analysis is how to deal with the presence of variations in the data. Every measurement process contains random variations, and if the measurements are to be useful, the methods of interpretation should properly account for these variations. The next chapter presents the techniques that have been used in this investigation to determine nature of these.

5 Feature extraction

5.1 Introduction

Shape analysis starts with extracting of shape attributes from the input data. A large number of shape descriptors have been proposed over the years for use in medical image analysis. Those descriptors include landmarks [46], dense surface meshes [122, 123], skeleton-based representation [124, 125] and deformation fields that define warping of a standard template to a particular input shape [126, 127]. The main objective of a feature extraction technique is to accurately represent the object information. The representation of shape depends on the application.

In this work landmarks are used for representation of back surface data obtained using the ISIS2 system. Landmark representation was chosen because of its simplicity, ease of use and the type of statistical shape analysis used in this research (Procrustes and EDMA) used landmark data only. The purpose of this chapter is to describe the detection of landmarks from individual back surface data and analyse the detected landmarks to estimate variation for repeated measurements from ISIS2.

5.2 Landmarks

Landmarks are useful features for describing a particular object. According to Acharya and Ray [153], an interesting way to describe a shape pattern is by defining a finite set of landmark points inside the object. Landmark points may be described as nodes or vertices of a polygon enclosing the shape pattern. Dryden and Mardia [43] define landmarks as points of correspondence on each object that match between and within populations and they classified landmarks into three subgroups, namely; anatomical landmarks, mathematical landmarks and pseudo landmarks. An expert clinician (who employs his/her knowledge of

anatomy) places anatomical landmarks to identify special locations (for example: vertebra prominens, dimples of Venus) on the back surface. Mathematical landmarks are detected automatically using geometric properties from the surface (for example: left and right scapulae maximum points). Sometimes constructed points are located in between anatomical or mathematical landmarks and these are known as pseudo landmarks (for example: the sacrum location can be estimated from the mid point of a line drawn between the dimples of Venus). These anatomical, mathematical and pseudo landmarks can be two-dimensional or three-dimensional coordinate points. For our analysis, three-dimensional landmarks are extracted from back surface data. The landmarks for this analysis are associated with *x*, *y* and *z* coordinates that represent back surface information and can be seen in Figure 5.1.

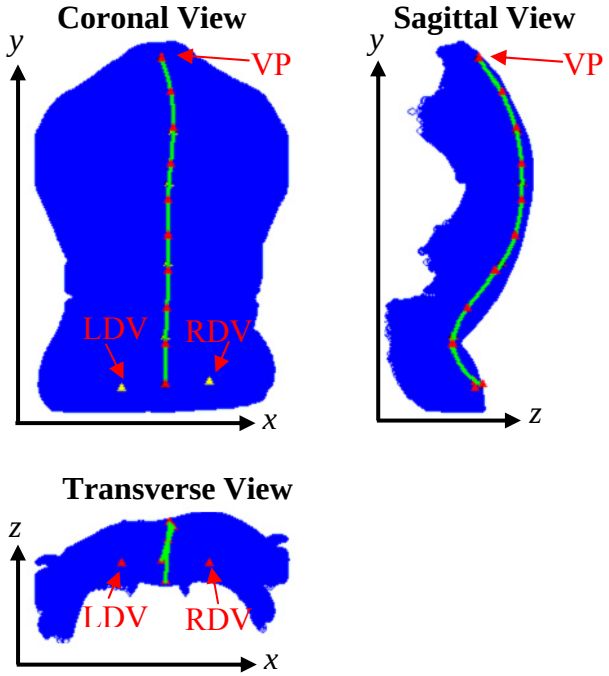

Figure 5.1: Body axes system; VP is vertebra prominens, LDV is left dimple of Venus and RDV is right dimple of Venus

The *x*-axis is horizontal and lies parallel to the line between the two dimples of Venus in the transverse plane, positive to the right. The *y*-axis runs vertically in the coronal plane, positive upwards. The *z*-axis is normal to the *x*-*y* plane and positive outwards from the back. These landmarks, which represent the features

of the back, can have variability for repeated measurements. The variability can occur because of variation in the patient's standing position, breathing, muscle tension, etc. Again, the back landmarks on the spine may vary if the patient changes his/her standing position forward or backward.

Statistical analysis is then necessary to examine the locations of the landmark points for repeated measurements of the same patient to understand their variability. First, a number of landmarks (x, y and z coordinate values) are extracted from the back surface, which gives most of the surface information of the back. The same procedures are then used to extract the landmarks for all backs. Second, a hypothesis test is applied to those landmark coordinate points to decide whether those repeated measurements landmarks are similar enough to have come from the same population or whether they are significantly different for the two groups. As the hypothesis test does not provide enough information about the data distribution, Euclidean distance between pairs of landmarks for repeated measurements are then estimated. The resulting information is displayed using histograms. This does not provide enough information about the agreement between repeated measurements. A Bland-Altman [154] plot (difference plot) is a statistical method to compare two measurements and analyse the agreement between them. The landmark coordinate points are then used for the Bland-Altman plots.

5.2.1 Landmark extraction from ISIS2 surface data

The extraction of back surface information using ISIS2 has already been discussed in Chapter 3. In this work, ISIS2 is used because it is capable of giving three-dimensional back surface information in which we are interested and also its availability.

A finite number of landmarks on each back have to be chosen to represent the geometrical information of the back surface obtained using ISIS2. These landmarks must be at corresponding points on all the back surfaces that are to be used in the analysis. The number of stickers placed on the spinous processes on

the back surface varies from patient to patient; the number of stickers is higher if the spine is much curved. The stickers are placed manually by an expert clinician. For the landmarks to correspond between backs a particular procedure is required. It is also important to extract the same number of landmarks and use the same procedure for extracting landmarks from all back surfaces. To extract the same numbers of equally spaced landmarks from the spine, a two-dimensional (x-y locations) spline curve is fitted through the sticker locations on the spinous processes (from the vertebra prominens to the sacrum). The position of the sacrum at the base of the spine is assumed to lie mid-way between the left and right dimples of Venus. This is taken as a pseudo landmark. The locations of ten equally spaced points between the vertebra prominens and sacrum are then calculated. The z value for each point is taken from the surface data. Initially, ten landmarks were chosen down the line of the spine. Three anatomical landmarks (vertebra prominens, left and right dimples of Venus) and three mathematical landmarks (sacrum, left and right scapulae maximum points) were also selected. In total twenty-four landmarks were selected, ten down the spine and seven on a line joining the scapula to the dimples of Venus as can be seen from Figure 5.2. In Figure 5.2(a), the white circles show the coloured sticker locations placed by the expert clinician and obtained using ISIS2. The red line from vertebra prominens to the sacrum through the stickers shows the fitted spline curve. The green triangles show the ten equally spaced points on the spline fitted curve. Seven equally spaced points from scapula to dimple of Venus are then extracted for both the left and right sides as shown in Figure 5.2(b). However, it was felt that these twenty-four landmarks exclude too much information about the back surface and so the number of landmarks needed to be increased.

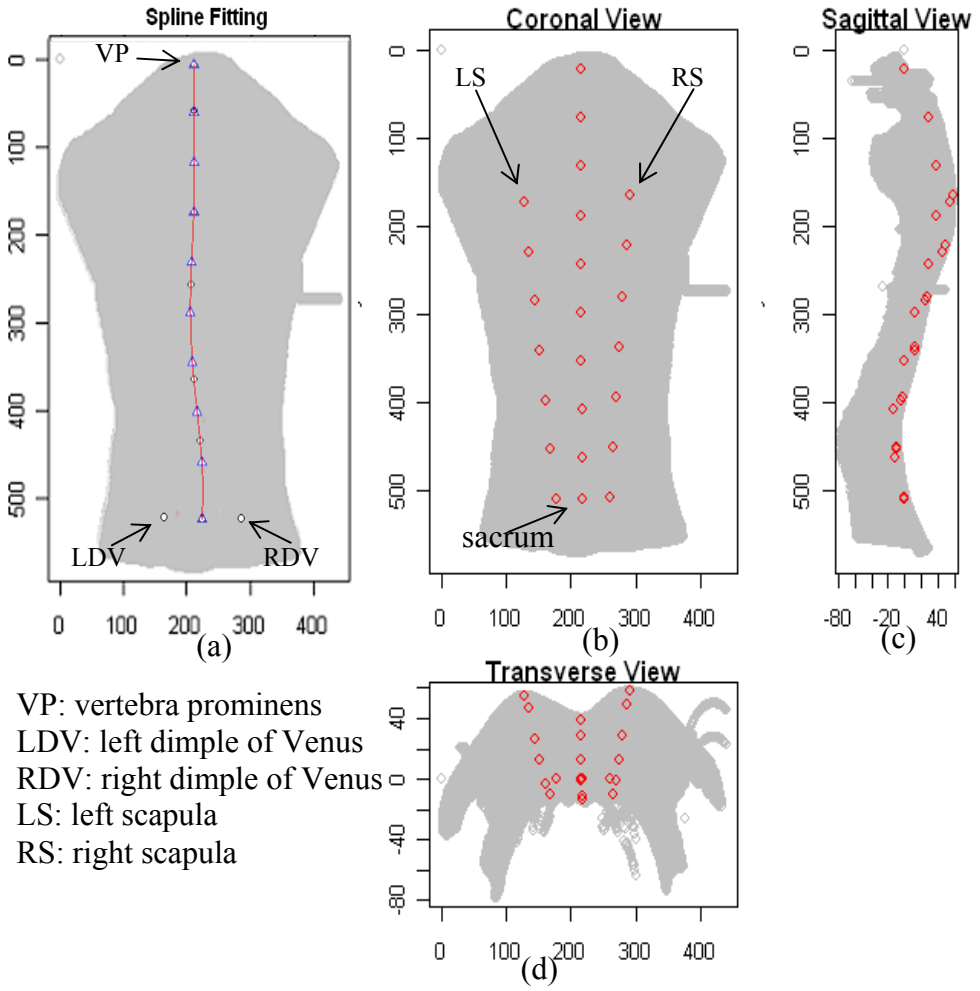

Figure 5.2: (a) Two-dimensional spline fitted through the stickers and the sacrum. The white circles represent the stickers locations obtained from ISIS2 and the blue triangles represent ten equally spaced landmark locations on the spine. (b) A total of twenty-four landmarks. (c) Sagittal view of twenty-four landmarks. (d) Transverse view of twenty-four landmarks.

The number of landmarks was therefore increased so that the landmarks are distributed over the back surface so that it gives more information about the surface of the back. The distance between the vertebra prominens and the sacrum is first measured which can be considered as the back length. To estimate the width of the back, the back length is multiplied by 0.54. The left width from the spine is 0.27 times of the back length and the right width is 0.27 times of the back length. As the original width of the back is different from upper area to lower area, it has been found that a width of 0.54 times the back

length covers most area on the back surface. In Figure 5.3, the area enclosed by the red line is the selected area for landmark distribution and the blue line shows the spine on the back.

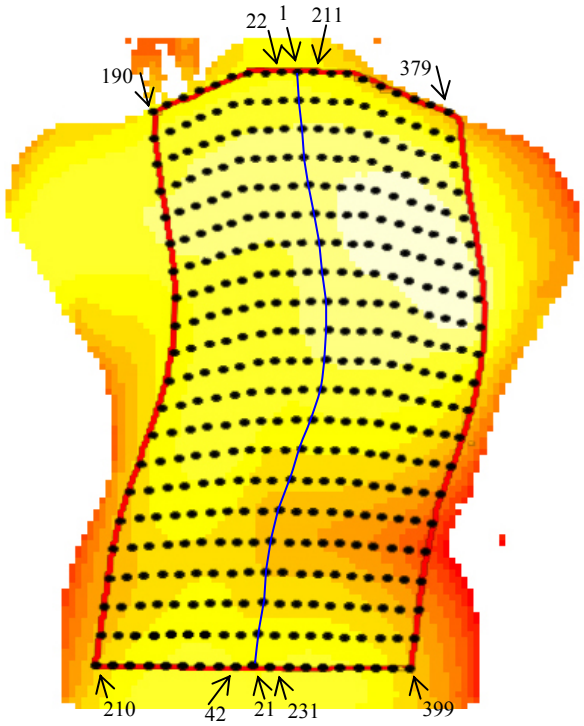

Figure 5.3: The arrangement of 399 landmarks on the back surface with indication of landmark numbering system.

A spline curve is fitted through the stickers of vertebra prominens to the sacrum and 21 equally spaced landmarks are extracted from that fitted line, 9 equally spaced columns (to both sides and which are spread across the 0.27 times of the back length) parallel to spine are then estimated. A spline curve is then fitted for each column and 21 equally spaced landmarks are extracted from each. In total, 399 landmarks have been selected, 21 landmarks down the spine and 9 columns to both sides of the spine. This makes a grid of 21 x 19 landmarks distributed over the back surface where these landmarks cover most of the information on back surface. Those 399 landmarks can be seen in Figure 5.3.

The positioning of the landmarks over the back surface is dependent on the positioning of the original stickers placed on the bony landmarks of the back by

the clinician at the time the back is measured using ISIS2. Variability in the 399 landmark locations is therefore dependent on variability in the spine fitted through the stickers and the sacrum. It was therefore decided to investigate the variability in the 21 landmarks calculated from the spine line from vertebra prominens to sacrum. As the sacrum location is calculated from the dimples of Venus locations, the two dimples of Venus locations are also considered for variability investigation. A total of 23 points have therefore been used in the analysis of variability. The 21 landmark points can be seen in Figure 5.3 and the dimples of Venus can be seen in Figure 5.2(a).

5.3 Variability in landmark locations

There is some variability in measurement results when a patient's back is measured several times. The main sources of measurement error are positioning of the patient, movement of the patient and placement of the stickers by the clinicians. These errors are quantified by repeated measurement of the same patient without the bony landmark stickers being replaced (intra variability) and repeated measurements with a different rater placing the stickers (inter variability). The position of landmark locations will change due to the position changes of sticker locations. As the landmark locations will be used for further analysis and it is important to investigate the variability in landmark locations. This involves two measurements variation, of which are intra and inter measurement variations.

5.3.1 Method of data collection

Once the three-dimensional landmarks, which represent the back surface, have been extracted from the back surface data, they are used to construct appropriate statistical tests to determine the variation in the detected locations of landmarks when a patient's back is measured several times. Locating the anatomical position, the clinician places small coloured paper stickers on the bony landmarks on the back of the patient and a photograph is taken of the patient's back. The back surface data are obtained from ISIS2 and stored in the database

together with the back image. The patient walks around the room and re-enters the patient stand and a second photograph is taken. This method of acquiring paired test data is known as intra measurement. The variations for intra measurement are positioning of the patient, patient stance, breathing and muscle tension. The landmarks are then extracted from individual back surface data using the procedure described in Section 5.2.1. The differences between the paired measurements of a total of 60 patients are then analysed.

Another measurement is conducted where the stickers on the bony landmarks are placed by different clinicians. The stickers are placed by one clinician and a photograph of the patient's back is taken, analyzed and stored in the database. The stickers are then removed and the patient walks around the room. New stickers are then placed by a second clinician and a second photograph is taken, analyzed and stored in the database. This method is known as inter measurement. The variations for inter measurement are positioning of the stickers on the back by the second clinician and all variations of the intra measurement. The same procedure is used to extract landmarks from individual back surface data which is described in Section 5.2.1. The differences between the paired measurements of a total of 37 patients are then analysed.

The *x*, *y* and *z* coordinates of the second observation landmark locations are translated relative to the first observation (considering vertebra prominens as reference) landmark locations for both intra and inter measurements data before the analysis.

5.3.2 Variability analysis for landmark locations

Multivariate statistical analysis is necessary to estimate the variability in the three dimensional landmarks (*x, y* and *z* coordinates). Student's *t*-test, Hotelling T^2 test [43], Goodall's F test [51] and analysis of variance (ANOVA) are familiar multivariate forms of statistical tests. Before starting statistical analysis for landmarks, it is essential to examine the distribution of the variation for skewness, kurtosis and spread of landmark coordinates. Information about each

of these parameters determines whether parametric or non-parametric tests need to be used. The data would not be considered a normal distribution, if the landmark coordinates have significant skewness or kurtosis. If a variable has a skewed distribution, the mean will give a biased estimate of the centre of the data.

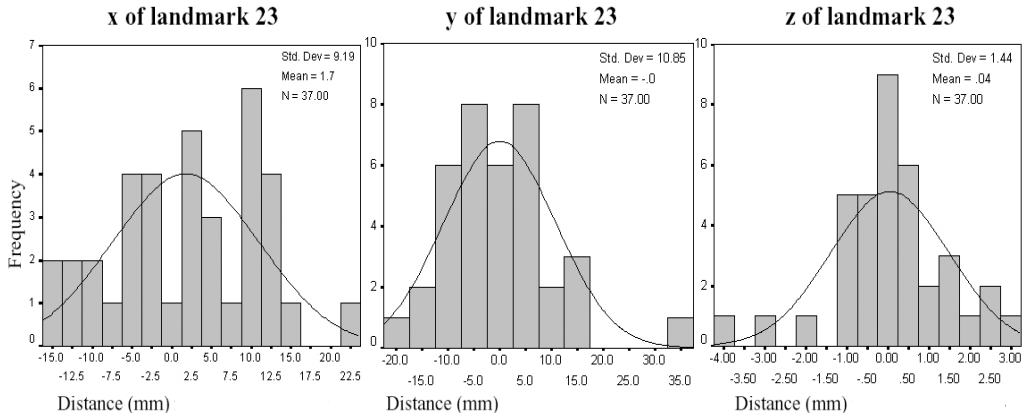

Figure 5.4: Histogram of *x*, *y* and *z* coordinates landmark 23 (inter)

It is important then to check for normality by examining whether the mean and the median values are close to one another for landmarks. The differences between the mean and the median have been investigated. The differences between the mean and median of *x*, *y* and *z* coordinate values for 23 landmarks in most cases are very close to 0. The large difference values are –1.9 mm (*y* of landmark 8), 1.83 mm (*y* of landmark 23) and –1.6 mm (*x* of landmark 22), etc for inter data. As the difference values of these landmarks are higher, these landmarks may have a non-normal distribution. Although, the difference between the mean and median are close to 0 in most cases, yet it can not be confirmed that the data is normally distributed. This is because, there might be a situation where the mean and median are very close to 0 but the distribution looks like an upside down bell shape or bimodal. It is therefore necessary to further examine those data to verify whether they are normally distributed or not. An inherent feature of a normal distribution is that most data values should lie in the area which is approximately two standard deviations from the mean (for example, see Schork and Remington [155]). It means that 95% of the data values should lie between –1.96 standard deviation and +1.96 standard

deviations from the mean. This will give an estimated range in which 95% of the values should lie. This analysis has been carried out for 23 landmarks and it has been found that most of the landmark data values lie in the area that is approximately two standard deviations from the mean. The mean ($\bar{x}$, $\bar{y}$ and $\bar{z}$) is estimated from the difference of coordinate values for repeated measurements, the 95% range (mean $\pm$ 1.96 $*$ standard deviation) is then estimated and the percentage of data lies in the 95% range is also calculated that can be seen in Tables A.1 and A.2 from Appendix A. A sample histogram of landmark 23 (inter) can be seen from Figure 5.4. The bell shaped black line in the histogram shows the distribution of the data. This indicates that the data distribution can be considered as normal. As the landmark coordinates are normally distributed, a parametric statistical test can be applied to compare the means of paired sample intra and inter measurements.

5.3.3 Hypothesis testing (*t*-test)

Three dimensional equally spaced *x*, *y* and *z* coordinates of 21 landmarks from the vertebra prominens to the sacrum on the spine and 2 anatomical landmarks of left and right dimples of Venus of 60-paired test intra measurement and 37-paired test inter measurement data are considered for hypothesis testing. The null hypothesis (H_0) and alternative hypothesis (H_1) for these data are as follows

H_0: $\mu = 0$; there is no difference in the *x*, *y* and *z* coordinate values (23 landmarks) between the first and second observations.

H_1: $\mu \neq 0$; there is a difference in the *x*, *y* and *z* coordinate values (23 landmarks) between the first and second observations.

A two-tailed test is used with 95% confidence interval for 23 landmark coordinates. For a two-tailed test, 2.5% of the rejection region lies in the positive tail of the distribution and 2.5% of the rejection region lies in the negative tail. The 95% confidence intervals of the differences are calculated from the mean paired difference $\pm$(1.96 $*$ standard error of mean paired

differences). The *t*-value is calculated as the mean differences divided by their standard error. The *t*-value increases as the sample size increases for the same mean difference. This is because the standard error becomes smaller as the sample size becomes larger. If the *t*-value gets smaller (approaches zero) the probability that the population means are the same gets larger and if the *t*-value gets larger (in either the positive or negative direction) the probability that the population means are the same gets smaller. If the computed *t*-value is the same as or smaller than the *t*-distribution tabled *t*-value, the null hypothesis will be accepted and a conclusion will be derived that the populations have the same mean. This can be done using standard errors and confidence intervals to see how precise the estimates are. The 95% confidence intervals can be calculated by finding the appropriate point of the *t*-distribution with the degrees of freedom and the confidence interval will be from the observed value plus and minus *t* standard errors of the observed value.

The numbers of degrees of freedom for the sample population is 59 for intra measurement data and 36 for inter measurement data. The level of confidence is $\alpha = 0.05$. The mean $\bar{x}_1, \bar{y}_1, \bar{z}_1$ and $\bar{x}_2, \bar{y}_2, \bar{z}_2$ have a normal distribution and the *t*-distribution is used for hypothesis testing. The *t*-distribution is also used to calculate the 95% confidence interval (from the *t*-distribution table, *t*-value is ± 2.000 for two-sided where degree of freedom is 59 and ± 2.028 where degree of freedom is 36) in this case. The analysis of variability for 23 landmark *x*, *y* and *z* coordinates for repeated examinations of patients' backs, the summary of the *t*-test hypothesis testing for 60-paired intra measurement and 37-paired inter measurement data are presented in Tables A3, A4 and A5 in Appendix A.

The mean differences at landmark 1 are zero because this is the common point between the two measurements. As the mean paired difference for landmark 1 is zero, an "NA" is put in the tables to indicate that the *t*-test has not applied there.

From the analytical results, it can be seen that there is a difference in the sample means. The coordinate *x* of landmark 22 (37- paired test intra measurement) has

the highest difference rather than the coordinates *y* and *z*. However, this difference is very small (in most cases) considering the variability of the measurement (standard errors of the mean). The *p*-values are always higher than the significant level. The *y* coordinate *p*-value of landmark 12 (37-paired test intra measurement) is 1 and that gives the strongest evidence that the difference in the *y* coordinate measurements between the repeated test is zero for landmark 12. The *t*-value is an indication of the probability that the first and second observations of intra and inter measurements data have the same mean and that the differences in two means are due to random fluctuation. As the computed *t*-value is always smaller than the tabled *t*-value (± 2.000 for intra measurement and ± 2.028 for intra measurement), there is no significant evidence to reject the null hypothesis. This means that there is no significant difference in the values of *x*, *y* and *z* coordinates for the 23 landmarks (intra and inter) between the first and second observations.

Although hypothesis testing shows that there is no significant difference in the locations of the landmarks between paired measurements, it does not give any quantitative measure of the differences found. The Euclidean distance between the pairs of landmarks from the first and second observation can be computed and a histogram can be plotted to get more information about the magnitude of the data.

5.3.4 Histogram of Euclidean distances for landmarks

Euclidean distance [156] is defined as the distance *d* between two points in three-dimensional space with coordinates x_1, y_1, z_1 and x_2, y_2, z_2 as follows:

$$d = \sqrt{(x_1 - x_2)^2 + (y_1 - y_2)^2 + (z_1 - z_2)^2} \tag{5.1}$$

This equation (5.1) only returns a positive number giving the length of the straight line drawn between two points. The Euclidean distance is then estimated for 60-paired intra measurement and 37-paired inter measurement data using

equation (5.1). The histograms are similar for all landmarks. As a sample, the histograms are plotted with frequency versus Euclidean distance for the landmarks 22 and 23, as shown in Figure 5.5 for the 60-paired intra and the 37-paired inter data.

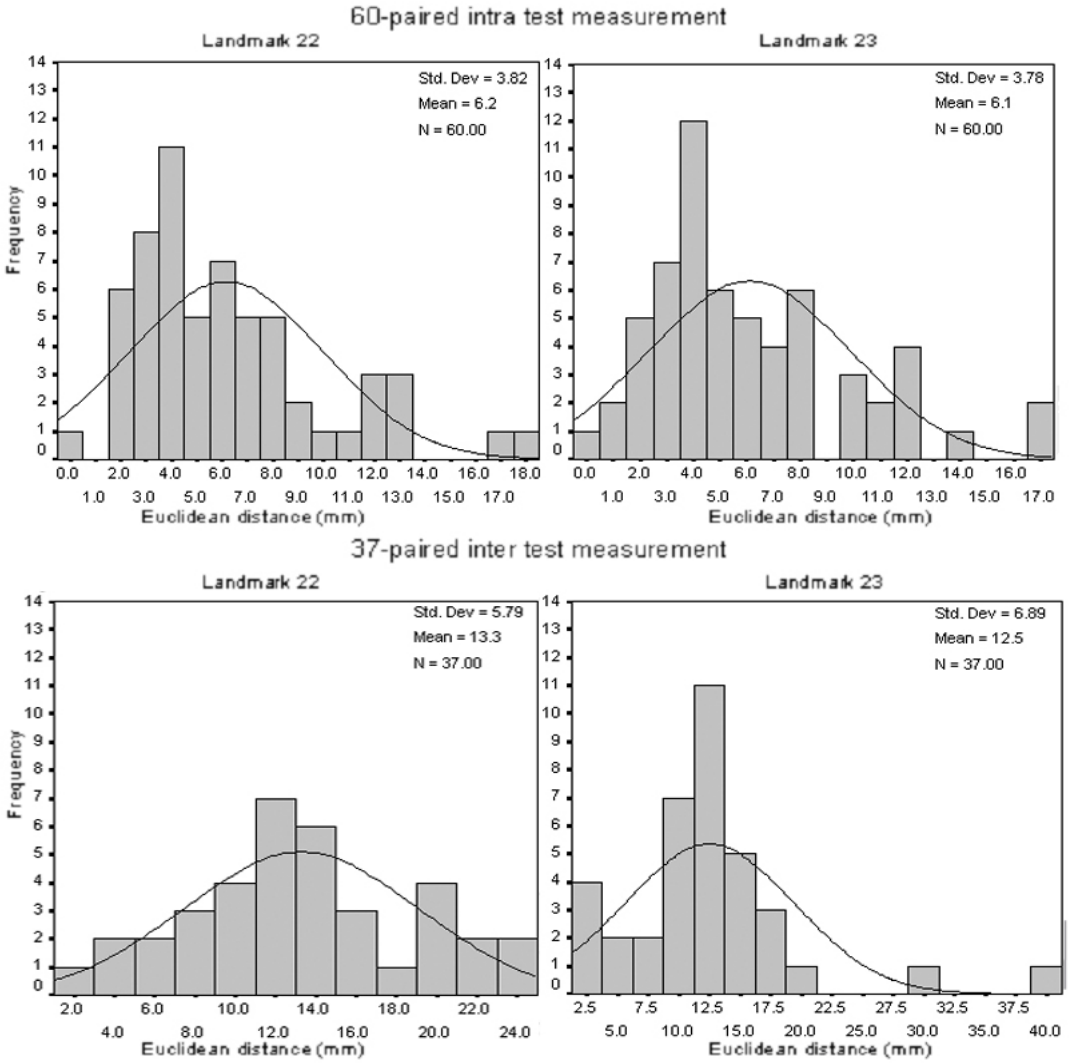

Figure 5.5: Euclidean distance histograms for intra and inter measurements

Landmark 22 and 23 are the left and right dimples of Venus. For the clinician placing the stickers, it is usually more difficult to locate the dimples of Venus than the spinous processes. For some patients whose pelvis in the dimple of Venus region is almost flat, it can be particularly difficult. It is not surprising, therefore, that the largest differences between the paired measurements occur at

the dimples of Venus (landmark 22 and 23). This is the reason for plotting histograms of only these two landmarks. The standard deviation for the intra measurements are lower than the standard deviation for the inter measurements. This suggests that the data points are closer to the mean for intra measurements than inter measurements. There is more variation in the inter measurement then the intra as indicated by the wider spread of Euclidean distances for landmark 22 and landmark 23. The histograms also show that the landmarks 22 and 23 are skewed to the right (something that is common when the data has a lower bound, as is the case here). This indicates that the Euclidean distances of individual landmarks are low for most cases. It also shows that there are few data with extreme values. Again, the standard deviation of landmark 23 for intra and inter measurements and landmark 22 of intra are close to half the mean, which indicates that the data points are not too far from the mean. Most of the data lie approximately two standard deviations from the mean. It can be considered a normal distribution, if most the data values lie between –1.96 standard deviations and +1.96 standard deviations from the mean. It indicates that the distribution of Euclidean distances for landmark 22 and landmark 23 are very close to normal distribution.

The difference between the first measurement and the second measurement of *x*, *y* or *z* coordinate value for each landmark can be either positive or negative. If the *x*, *y* or *z* coordinate value is high, it does not necessarily mean that the Euclidean distance will be high. Because Euclidean distance depends on all three coordinates and it can be assumed that the combined Euclidean distance error for individual landmarks will be like an ellipsoid. The Euclidean distance gives no indication of the direction of coordinate differences. These histograms also do not provide sufficient information to compare the differences in variations between repeated measurements. It can be a good idea to use a method for comparing repeated measurements where the method will allow determining agreement for repeated measurement.

5.3.5 Bland-Altman plots for landmark coordinates

The Bland-Altman [154, 157] plot is a very useful graphical technique for the examination of patterns of disagreement between repeated measurements. It consists of a scatter plot where the differences between paired measurements are plotted against their mean values. The magnitude of disagreement can be more easily assessed from this type of plot than from a regular scatter diagram. This method calculates the mean difference between two measurements (the 'bias') and 95% limits of agreement as the mean difference $\pm(1.96 * \text{standard deviation})$. It is expected that the 95% limits include 95% of differences between the two measurements. This 95% limits of agreement allow a visual judgement of how well the two measurements agree. The smaller the range between these two limits, the better the agreement.

In our situation, the *x*, *y* and *z* coordinate values of 23 landmarks are used assuming that the mean difference between the first measurement and the second measurements is 0. The standard deviation of *x*, *y* and *z* coordinate values are estimated. The mean $\pm 2 *$ standard deviation is referred to as the "95% limits of agreement". The bias is then estimated from the average of the differences. If the first measurement value is sometimes higher and sometimes the second measurement is higher then the mean of the differences will be very close to zero. If the mean of the differences is not close to zero, it indicates that there is a difference between repeated measurements. The Bland-Altman plots are similar for all landmarks and sample plots are shown in Figure 5.6 for *x*, *y* and *z* coordinates from landmark 23 where the differences between the pairs of measurement are plotted against the mean for 60-paired intra and 37-paired inter data.

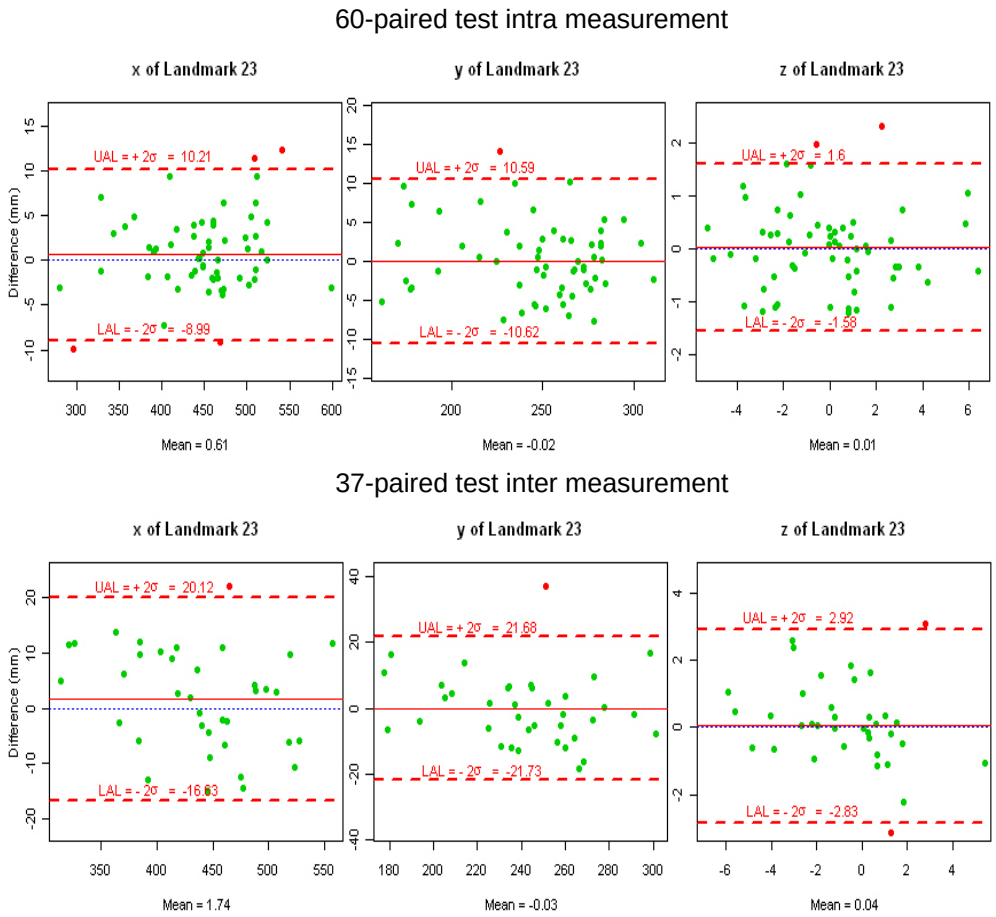

Figure 5.6: Bland-Altman difference plots of landmark 23 for intra and inter measurements

In Figure 5.6, the plots show the difference between the repeated measurements along the vertical axis and the mean of the repeated measurements along the horizontal axis. The red line shows the mean and the dashed red lines show the 95% limits of (upper and lower) agreement. The green dots indicate points lying in the limits of agreement region and the red dots show that these points lie outside the limits of agreement region. It can be seen clearly from the plots that the largest bias for the intra data (difference between the means) is only 0.61 mm for the *x* coordinate of landmark 23 (intra measurements) and the 95% limits of agreement are from –8.98 to 10.21 mm. This bias value of 0.61 mm, determined by the first measurement minus the second measurement, is close to zero. For the coordinates *y* and *z* of landmark 23 (intra measurements), the bias is very close to zero. The bias value is higher for the coordinate *x* compared to the coordinates *y* and *z*. The bias for the *x* coordinate of landmark 23 (inter

measurements) is 1.74 mm with the 95% limits of agreement from –16.63 to 20.12 mm. The bias is higher for the coordinate *x* rather than the coordinates *y* and *z,* similar to the intra measurements. This bias in the *x* coordinate can happen because one clinician places the stickers wider apart on the hips than the other clinician. A summary of the mean, standard deviation and limits of agreement ranges for all landmarks for the Bland-Altman analysis can be seen in Tables A.6, A.7 and A.8 in Appendix A for both intra and inter measurements.

It can be seen from those tables that the maximum bias for coordinate *x* can be seen for landmark 22 of intra measurement and the value is 3.28 mm. The average bias of the mean for the *x* coordinate of landmark 22 is 0.04 mm for intra measurements and 1 mm for inter measurements. The highest standard deviation is 10.85 mm for landmark 23 of *y* coordinate. Sometime *x* and *y* coordinates may vary for patients whose dimples of Venus points almost always flat. The important questions are how big is the variation, and can it be used for the analysis or is the variation too larger so that it can overlap to another landmark.

For the *x* coordinate of intra measurements, the average bias is 0.04 mm and the average bias 95% limits of agreement are –4.74 and 5.55 mm. Again the average bias is 0.86 mm and the average bias 95% limits of agreement are between –8.36 and 10.08 mm for the intra measurement. It indicates that on average, the horizontal axis can vary 10.29 mm for intra measurements and 18.44 mm for intra measurement. For the *y* coordinate, the average bias value is 0.25 mm for intra measurements and –0.38 mm for inter measurements. The average 95% limits of agreement are between –6.01 and 6.51 mm for intra measurements and between –14.25 and 13.49 mm for inter measurements. The *y* coordinate can vary 12.52 mm for intra measurements and 27.74 mm. The average bias for *z* coordinate is 0.19 mm for intra and 0.63 mm for inter measurements. The average 95% limits of agreement are between –5.62 and 6.0 mm for intra measurements and –8.05 and 9.30 mm for intra measurement. On average the *z*

coordinate can vary 11.62 mm for intra measurements and 17.35 mm for intra measurement.

It is mentioned earlier in Section 5.2.1 that landmark 22 and landmark 23 are the locations of dimples of Venus and these two landmarks are used to estimate the sacrum position which is considered as pseudo landmark. This pseudo landmark is used as landmark 21 for the 399 landmarks over the back. The spinal column represented by landmarks 1 to 21 is discussed in Section 5.2.1. As these 21 landmarks are used to estimate the remaining 378 landmarks which will be used for Procrustes analysis and EDMA, it is important to estimate the precision of the limits of agreement for the 21 landmarks. This can be done using standard errors and confidence intervals of *x*, *y* and *z* coordinate values. The results are shown in Tables A.3, A.4 and A.5 in Appendix A. The maximum standard error is 1.78 mm and 95% confidence interval are between –3.64 and 3.59 mm (see Table A.4 in Appendix A) for the *y* coordinate of landmark 23 (intra measurement). This means that the maximum variation is -3.64 to $3.59 = 6.73$ mm along the *y* axis. The rest of the values are rather small that will not have any effect for the analysis. The maximum standard error along *x* axis is 1.70 mm and 95% confidence interval are between –0.17 and 6.73 mm (see Table A.3 in Appendix A) for landmark 22 (intra measurement). This means that the maximum variation is -0.17 to $6.73 = 6.90$ mm along the *x* axis.

A set of 20 normal backs are available and this set contains male and female volunteers whose ages ranged between 13 and 53 years. The average back length (from vertebra prominens to the sacrum) is estimated for these normal backs and is 467.58 mm. As 21 landmarks are extracted from the vertebra prominens to the sacrum (back length), the vertical (*y* axis) distance between each landmark is $467.58/21 = 22.27$ mm which is high compared to the maximum variation (6.73 mm) measured in the repeated testing. The width of the selected area of the back (see Section 5.2.1) is $467.58 \times 0.54 = 252.50$ mm. The horizontal (*x* axis) distance between each landmark is then $252.50/19 = 13.29$ mm which is high compared to the maximum variation

(6.90 mm) measured in the repeated testing. The distance between landmarks is small when the back length is small, but the landmarks will never overlap each other.

The variability of assessing the other clinical parameters from ISIS2 has been carried out. For repeated measurement, the acquiring paired data was followed at most clinics over a period of about 6 months. A total of 62 patients data were used for the intra-rater variability estimation and a total of 39 patients data were used for inter-rater variability estimation.

Table 5.1: Summary of statistics from repeat tests with one set of landmark stickers (intra-rater)

Parameter	**Mean**	**SD**	**Limits of agreement**	
Back length (mm)	0.87	4.44	-7.84	9.57
Pelvic rotation (º)	0.20	1.89	-3.51	3.91
Flexion/extension (º)	-0.23	2.47	-5.08	4.61
Imbalance (mm)	-1.12	5.46	-11.81	9.58
Lateral asymmetry 1 (º)	0.20	1.48	-2.70	3.11
Lateral asymmetry 2 (º)	-0.02	1.60	-3.17	3.12
Max skin angle (º)	-0.12	1.60	-3.24	3.01
Min skin angle (º)	0.20	1.36	-2.47	2.87
Kyphosis (mm)	-0.08	4.18	-8.27	8.10
Lordosis (mm)	-0.15	2.77	-5.57	5.27
Kyphosis (º)	-0.15	3.36	-6.74	6.44
Lordosis (º)	-0.30	5.27	-10.63	10.03
Vol asymmetry L	-0.05	2.05	-4.08	3.98
Vol asymmetry R	0.27	3.43	-6.46	7.00

Table 5.2: Summary of statistics from repeat tests with two sets of landmark stickers (inter-rater)

Parameter	Mean	SD	Limits of agreement	
Back length (mm)	1.59	8.42	-14.91	18.09
Pelvic rotation (º)	-0.28	2.29	-4.78	4.21
Flexion/extension (º)	0.13	2.80	-5.36	5.62
Imbalance (mm)	0.23	7.27	-14.02	14.48
Lateral asymmetry 1 (º)	0.51	4.45	-8.21	9.24
Lateral asymmetry 2 (º)	-1.21	4.47	-9.97	7.54
Max skin angle (º)	0.36	1.90	-3.36	4.08
Min skin angle (º)	0.21	2.14	-3.99	4.40
Kyphosis (mm)	1.18	5.01	-8.64	11.00
Lordosis (mm)	-1.18	4.82	-10.63	8.27
Kyphosis (º)	0.13	4.25	-8.20	8.46
Lordosis (º)	-2.28	6.90	-15.81	11.24
Vol asymmetry L	-0.23	3.59	-7.28	6.81
Vol asymmetry R	0.69	4.91	-8.93	10.32

5.4 Summary

Landmarks have been used to describe the back surface obtained using the ISIS2 system, with 399 landmarks extracted from the back surface automatically. An investigation into the variability in the position of those landmarks has been carried out. The variability in repeated measurements is estimated for intra and inter measurements. The difference in the *x*, *y* and *z* coordinates of the landmark locations for repeated measurements are very close to zero. The precise variation of different coordinates can be seen from the 95% confidence intervals for the mean (landmark 1 to landmark 21) that the *x* coordinates has on average interval between –0.29 and 1.09 mm for intra measurement and between –0.70 and 2.25 mm for inter measurement. For *y* coordinate the range is between –0.58 and 1.14 mm for intra measurement and –2.82 and 2.02 mm for intra measurement. For *z* coordinate the range is between –0.62 and 1.06 mm for intra measurement and –0.9 and 2.33 mm for intra measurement. These narrow intervals indicate precise and reliable estimation. The hypothesis test shows clearly that there is no significant difference between the repeated measurements for intra and inter testing. The Euclidean distance histograms show the length of each landmarks of repeated measurements variation for intra and inter

measurement data where the distributions are almost distributed normally. The Bland-Altman plots show the information about differences versus mean and give the 95% limits of agreement using standard deviation for the population. On average the limits of agreement (landmark 1 to landmark 21) for the *x* coordinate are between –4.74 and 5.55 mm for intra measurement and between –8.36 and 10.08 mm for intra measurement. For *y* coordinate, the range is between 0.25 for intra and –0.38 mm for inter measurements. For *z* coordinate, it is between –6.01 and 6.51 mm for intra measurement and between –14.25 and 13.49 mm for intra measurement. The limits of agreement provide sufficient information to conclude that the data spread is not wide relative to the average human back length and width for most cases. A set of 399 landmarks which are based on these 23 landmarks can be used for Procrustes analysis and EDMA.

6 Procrustes and EDMA for back shape analysis

6.1 Introduction

The main objective of this research is to develop a method which will be able to distinguish deformed backs from normal backs based on full geometrical shape of the back and will be independent of location, rotation and scale effects. The present parameters of ISIS2 are based on lengths and angles, which can be affected by patient stance, breathing and muscle tension. An investigation of Procrustes analysis which would take into account the back shape more fully than lengths and angles was therefore undertaken.

6.2 Riemannian distance

After finding the best match between configurations, it is useful to provide a numerical measure which gives information about shape difference from a reference configuration. The Riemannian distance measurement provides such a numerical value. Riemannian distance gives a measure of the difference between configurations for higher dimensional data using the tangent space of the landmarks.

O'Neill [158] defines Riemannian distance as follows:

> 'For any points p and q of a connected Riemannian manifold M, the Riemannian distance $d(p,q)$ from p to q is the greatest lower bound of $\{L(\alpha) : \alpha \in \Omega(p,q)\}$, where $L(\alpha)$ is the length and $\Omega(p,q)$ is the set of all piecewise smooth curve segments in M from p to q'

After Procrustes analysis, the Riemannian distance is used to estimate distance between the SNS and the individual transformed shapes to differentiate normal backs from deformed backs. For all Procrustes analysis reflection variation was

not under consideration. The Riemannian distance parameter ρ (rho) has a value between 0 and $\pi/2$; the closer this value is to zero, the smaller the difference between the shapes as described by Kendall [48].

6.3 Functions of procOPA, procGPA and riemdist

The statistical software R has capability to interface through user-submitted packages, which allow specialized statistical techniques, graphical devices, as well as import/export capabilities to many external data formats. The shapes package [159] contains functions for statistical analysis of shapes. The functions procOPA, procGPA and riemdist are used for our analysis. The function procOPA takes landmarks of two shapes and it has also scale and reflection logical options that allow if scaling and/or reflection is required. The scaling value is set to TRUE and the reflection is set to FALSE for our analysis. The function matches one shape to another using translation, rotation and possibly scale. The function returns the scale matrix, the centred configuration of the first shape and the Procrustes registered configuration of the second shape. The procGPA function takes a set of shape landmarks and it has also scale and reflection logical options. The scaling value is set to TRUE and the reflection is set to FALSE for our analysis. The function registers landmark configurations into optimal registration using translation, rotation and scaling. The function then returns the Procrustes mean shape, the Procrustes rotated data and other parameters which are not used in this analysis. The riemdist function takes landmarks of two shapes. It calculates the shape distance ρ between two configurations and returns the value. These three functions have been used for our analysis.

6.4 Estimation of standard normal shape using GPA

In this phase we are going to apply GPA to a set of normal backs to obtain or calculate the standard normal shape (SNS). This SNS will then be used as a

standard back for comparison with all other backs. The normal back data set consists of 20 backs. Each back has 399 three dimensional landmarks. The procedure of extracting landmarks has already been described in Chapter 5, Section 5.2. The normal backs are all those available from a small set of volunteers. The back lengths (from the vertebra prominens to the sacrum) range from 406.5 mm to 517.5 mm for these normal backs. The ages of the volunteers range from 13 to 53 years. The landmarks on an individual back are considered a configuration. Figure 6.1 shows the three-dimensional 399 landmarks of 20 configurations where different colours and symbols represent different backs. The axes units for the figure are mm.

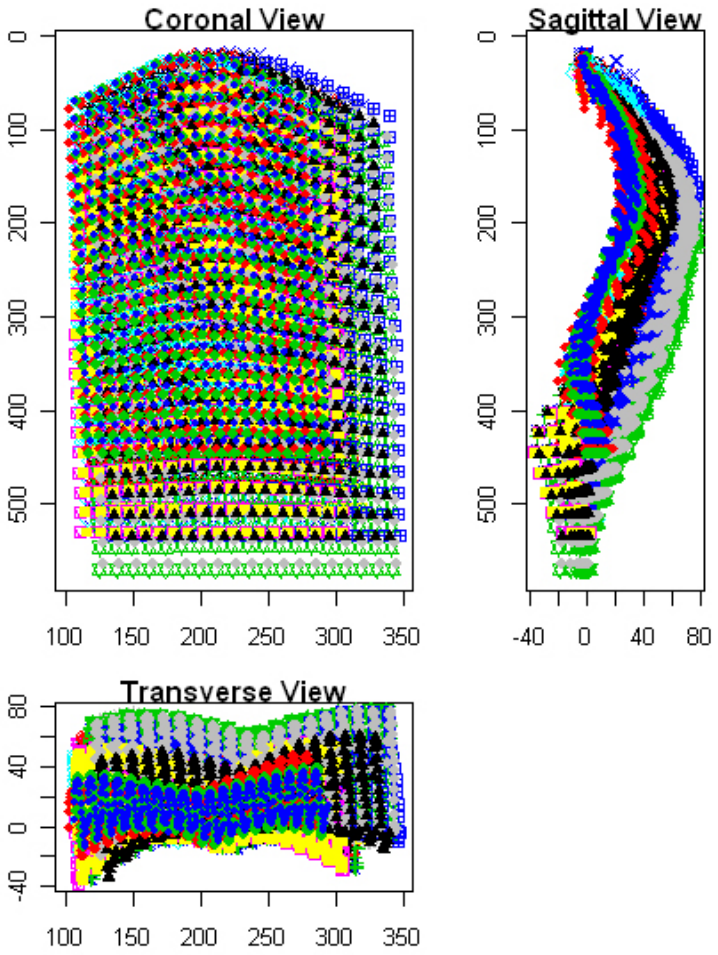

Figure 6.1: Landmarks of 20 normal backs before GPA

These configurations can be written as X_1, X_2, X_3,… ,X_{20} containing the coordinates of the 399 landmarks in three-dimensional space for each of the 20

normal backs. An SNS is estimated by applying GPA to these configurations so that they match as well as possible. This has done using the function procGPA described in Section 6.3. The scaling parameter is set to TRUE because few backs are needed to be expand or reduce to find the best fit among them. The reflection parameter is set to FALSE. The Figure 6.2 shows the three-dimensional 399 landmarks of 20 configurations for full Procrustes rotated, translated and scaled data where different colours and symbols represent different backs. The axes units for the following figure are mm.

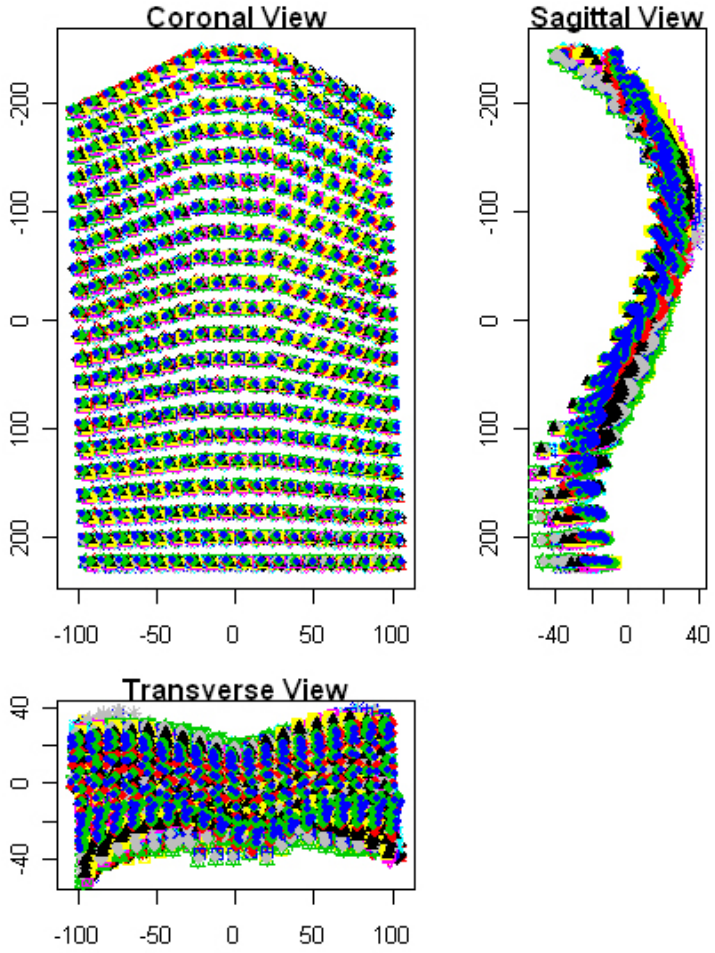

Figure 6.2: Landmarks of 20 normal backs after GPA

The Procrustes mean shape for all normal backs is also estimated and can be assessed from the returned value mshape of the function procGPA. This Procrustes mean shape after GPA is considered to represent the SNS which is then used as a base in differentiating the deformed backs from the normal backs.

The landmarks of the SNS can be seen in Figure 6.3. The axes units for the following figure are mm.

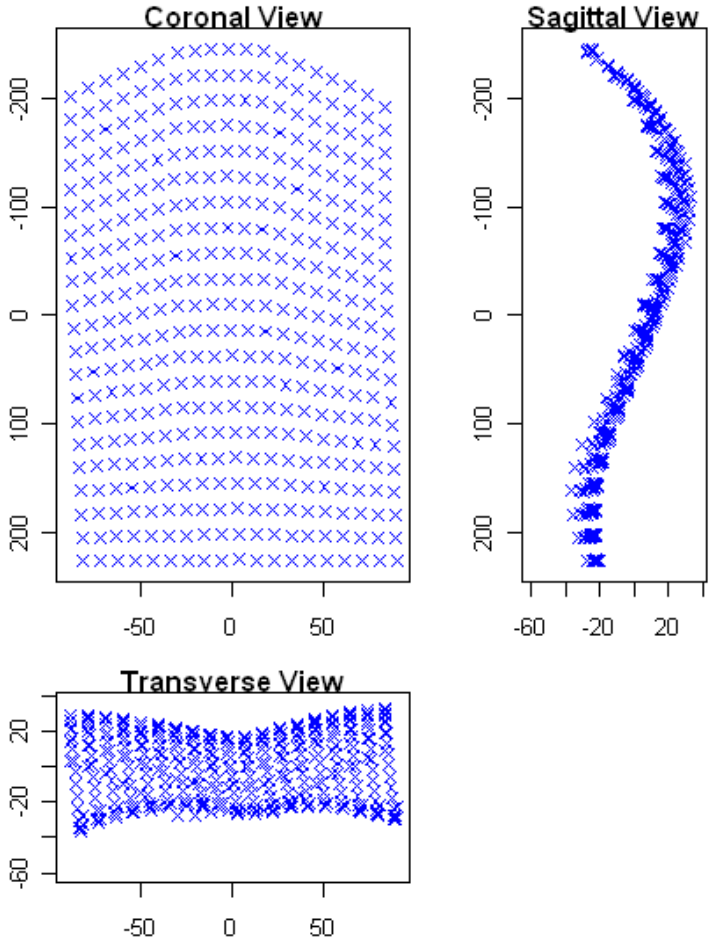

Figure 6.3: Landmarks of SNS after GPA

Only normal backs are used in estimating the SNS and deformed backs are not taken into account. This is because when the numbers of deformed backs are high relative to the number of normal backs, the Procrustes mean shape will be strongly influenced by the shapes of the deformed backs, which is not what is needed.

6.5 Differentiating normal backs from deformed backs using Procrustes analysis

Ordinary Procrustes analysis (OPA) has already been discussed in Section 6.3. After estimating the SNS, OPA has been applied between the SNS and all (normal and deformed) backs using the function procOPA. The function procOPA has been described in Section 6.3. The function returns the Procrustes registered configuration of each back relative to the SNS. The scaling parameter is set to TRUE as individual backs may need to expand or reduce to find the best fit between them and the SNS and individual backs. The Riemannian distance is estimated between the SNS and the individual Procrustes registered configurations using the function riemdist. This function returns the ρ value for each pair of configurations. The summary results can be seen in Table A.9 in Appendix A. In the table, the scale column shows the isotropic scaling parameter applied to an individual backs to expand or reduce relative to the SNS.

The Riemannian distance values are higher for deformed backs than for normal backs in all cases. The mean Riemannian distance for normal backs is 0.037 and 0.101 for deformed backs. This indicates that the average of the normal backs is very different from that of the deformed backs. Box and whisker plots have also been drawn and can be seen in Figure 6.4. The inter quartile range of the Riemannian distance value for normal backs is 0.013 (25% is 0.027 and 75% is 0.04). The inter quartile range for deformed backs is 0.042 (25% is 0.10 and 75% is 0.14). It can be seen clearly from the figure that the data spread for normal backs is very compact which indicates that normal backs are more consistent than deformed backs. There is more variation in the deformed backs as indicated by the wider spread of Riemannian distance values.

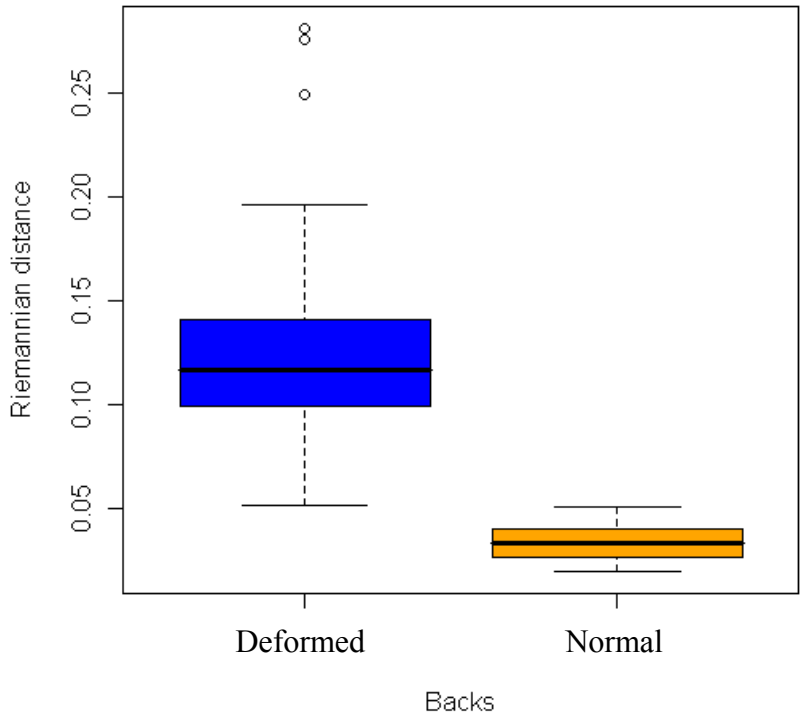

Figure 6.4: Box and whisker plots for Riemannian distance data from 97 deformed backs and 20 normal backs

A *t*-test on the Riemannian differences of normal backs and deformed backs is carried out. This gives information about the difference in the mean between the Riemannian distance of normal and deformed backs. The null hypothesis (H_0) is that there is no difference between the mean of normal and deformed backs. The alternative hypothesis (H_1) is then there is a significant difference between these two means. The level of confidence is $\alpha = 0.05$. The t statistic = 20, df = 114.165 and 95% confidence interval is 0.082 and 0.100 which difference is considered to be extremely statistically significant. The probability that there is no difference between the mean of normal and deformed backs is 0. The *t*-statistic value is high indicating that the two means are extremely statistically significant and the null hypothesis is rejected. A decision can be made from this evidence that there is a significant difference between the Riemannian distance value of SNS to normal backs and SNS to deformed backs. From the box plot and *t*-test above, it is clearly seen that the mean value of Riemannian distance of

the normal backs is significantly lower than that of the deformed backs. As such it can then be concluded that normal backs are differentiable from deformed back using a Riemannian distance measurement.

6.5.1 Estimation of mean form and variance for normal backs

There are 399 landmarks extracted from each back surface data for a set of 20 normal backs. The mean form based on these normal backs is to be estimated. This mean form will be considered as the standard normal form (SNF) which can then be used to locate the areas where most differences occurs on deformed backs compared to the mean normal backs.

As the landmark information is available, the form matrix is constructed for individual normal backs. The essence of the mean form can be captured using the vector of all possible linear distances among landmarks. This can be done even in the presence of the nuisance parameters of translation, rotation and reflection. For our back form analysis, reflection is not under consideration. However, the unfortunate effect of these nuisance parameters becomes apparent when we attempt to estimate the variance. Recall from Section 4.8.1 that the variance and covariance matrix characterizes the perturbation where $\Sigma_K \otimes \Sigma_D$ cannot be estimated directly. A singular version of Σ_K can be estimated, denoted by Σ_K^* and only the eigenvalues of Σ_D. These estimations can be used as tools to evaluate variance in landmarks for normal backs.

Initially, the Euclidean distance between all possible pairs of landmarks are estimated which is known as inter-landmark distances [146]. This data is stored in a 399x399 matrix which is symmetric matrix about the diagonal. This matrix is the form matrix. The form matrix is calculated for each of the 20 normal backs. These form matrices are then used to calculate a mean form and a variance-covariance matrix. The procedure for estimating the mean form and variance-covariance matrix is described in Sections 4.8.3 and 4.8.4. As the matrix size is very large (399x399), the data for just the first 21 landmarks is

presented, the mean form information in Table 6.1 and the variance information in Table 6.2.

Table 6-1: Mean form matrix (mm) of the first 21 landmarks for normal backs

	LM1	LM2	LM3	LM4	LM5	LM6	LM7	LM8	LM9	LM10	LM11	LM12	LM13	LM14	LM15	LM16	LM17	LM18	LM19	LM20	LM21
LM1	0.00																				
LM2	26.66	0.00																			
LM3	52.40	25.77	0.00																		
LM4	76.91	50.38	24.68	0.00																	
LM5	100.40	74.04	48.49	23.89	0.00																
LM6	123.42	97.26	71.91	47.42	23.57	0.00															
LM7	146.06	120.16	95.03	70.70	46.91	23.38	0.00														
LM8	168.45	142.84	117.97	93.83	70.15	46.70	23.35	0.00													
LM9	190.68	165.41	140.84	116.92	93.40	70.06	46.78	23.47	0.00												
LM10	212.90	187.99	163.76	140.09	116.75	93.55	70.38	47.13	23.69	0.00											
LM11	235.26	210.72	186.82	163.42	140.26	117.21	94.14	70.97	47.57	23.89	0.00										
LM12	257.85	233.66	210.07	186.90	163.91	140.99	118.02	94.90	71.53	47.87	23.98	0.00									
LM13	280.67	256.79	233.46	210.48	187.63	164.81	141.91	118.84	95.48	71.82	47.94	23.95	0.00								
LM14	303.69	280.04	256.91	234.08	211.32	188.56	165.70	142.64	119.29	95.62	71.74	47.76	23.81	0.00							
LM15	326.83	303.39	280.42	257.70	235.01	212.30	189.45	166.40	143.05	119.38	95.49	71.52	47.57	23.76	0.00						
LM16	350.04	326.81	304.01	281.41	258.80	236.14	213.33	190.30	166.95	143.28	119.39	95.42	71.47	47.66	23.90	0.00					
LM17	373.34	350.25	327.56	305.04	282.46	259.82	237.02	213.98	190.63	166.95	143.07	119.09	95.15	71.34	47.58	23.69	0.00				
LM18	396.65	373.65	351.02	328.51	305.94	283.29	260.46	237.40	214.03	190.35	166.47	142.50	118.57	94.77	71.01	47.15	23.48	0.00			
LM19	419.96	396.96	374.30	351.76	329.14	306.43	283.56	260.45	237.05	213.36	189.49	165.55	141.65	117.87	94.14	70.35	46.74	23.31	0.00		
LM20	443.25	420.19	397.46	374.83	352.13	329.34	306.40	283.24	259.81	236.12	212.28	188.39	164.54	140.81	117.13	93.45	69.94	46.61	23.34	0.00	
LM21	466.55	443.40	420.56	397.83	375.03	352.16	329.14	305.93	282.48	258.80	235.01	211.18	187.41	163.75	140.15	116.60	93.22	69.99	46.78	23.46	0.00

Table 6-2 : Variance matrix (mm^2) of the first 21 landmarks for normal backs

	LM1	LM2	LM3	LM4	LM5	LM6	LM7	LM8	LM9	LM10	LM11	LM12	LM13	LM14	LM15	LM16	LM17	LM18	LM19	LM20	LM21
LM1	305.20																				
LM2	266.49	237.47																			
LM3	229.45	208.12	186.18																		
LM4	195.93	179.93	163.14	144.65																	
LM5	164.24	152.32	139.74	125.09	109.22																
LM6	133.30	125.40	116.51	105.29	92.73	79.55															
LM7	102.90	98.89	93.45	85.43	75.94	66.01	55.79														
LM8	73.90	72.91	70.40	65.19	58.61	51.73	44.61	36.50													
LM9	47.35	47.91	47.02	43.96	39.86	35.67	31.34	26.16	19.18												
LM10	21.51	23.20	23.58	22.45	20.72	19.05	17.35	15.02	11.49	7.52											
LM11	-4.54	-1.63	0.25	1.40	2.14	2.95	3.77	4.13	3.82	3.29	2.57										
LM12	-30.87	-26.63	-23.19	-19.78	-16.50	-13.13	-9.76	-6.68	-3.77	-0.91	1.71	4.30									
LM13	-57.81	-51.98	-46.39	-40.52	-34.59	-28.65	-22.73	-16.92	-10.99	-5.01	0.77	6.59	12.19								
LM14	-85.74	-77.63	-69.31	-60.64	-51.87	-43.25	-34.73	-26.23	-17.55	-8.80	-0.03	8.79	17.51	26.08							
LM15	-112.95	-103.11	-92.35	-81.15	-69.74	-58.58	-47.50	-36.25	-24.59	-12.78	-0.91	10.96	22.89	34.56	46.45						
LM16	-140.04	-128.39	-115.67	-102.22	-88.27	-74.44	-60.62	-46.46	-31.66	-16.59	-1.63	13.37	28.35	43.03	58.06	73.08					
LM17	-167.26	-153.65	-139.12	-123.43	-107.00	-90.40	-73.71	-56.61	-38.59	-20.28	-2.22	15.96	33.97	51.57	69.60	87.96	106.29				
LM18	-194.47	-178.94	-162.63	-144.50	-125.48	-106.15	-86.70	-66.78	-45.65	-24.17	-2.85	18.57	39.63	60.28	81.23	102.75	124.42	145.99			
LM19	-221.42	-204.48	-186.19	-165.79	-144.15	-122.23	-100.20	-77.44	-53.15	-28.36	-3.79	20.96	45.33	69.08	93.26	118.02	142.82	167.53	192.64		
LM20	-248.69	-230.17	-209.77	-186.90	-162.59	-138.10	-113.48	-87.96	-60.47	-32.30	-4.41	23.61	51.25	78.01	105.44	133.24	160.97	188.63	216.97	244.88	
LM21	-276.50	-256.02	-233.21	-207.52	-180.42	-153.28	-126.04	-97.83	-67.32	-35.97	-4.79	26.38	57.12	86.88	117.47	148.13	178.70	209.30	240.58	271.84	302.49

Each cell in Table 6.1 of the mean form matrix represents a distance in three-dimensional space that does not require a coordinate system. For example, the cell that contains the number 26.6 (Row LM2, Column LM1) in the mean form matrix of the normal backs represents the distance between landmarks 1 and 2. This distance is calculated directly from the landmark coordinate data. This mean form is the SNF and will be used for locating the position of deformities for backs. A graphical representation of the SNF can be seen in Figure 6.5. The axes units are in mm.

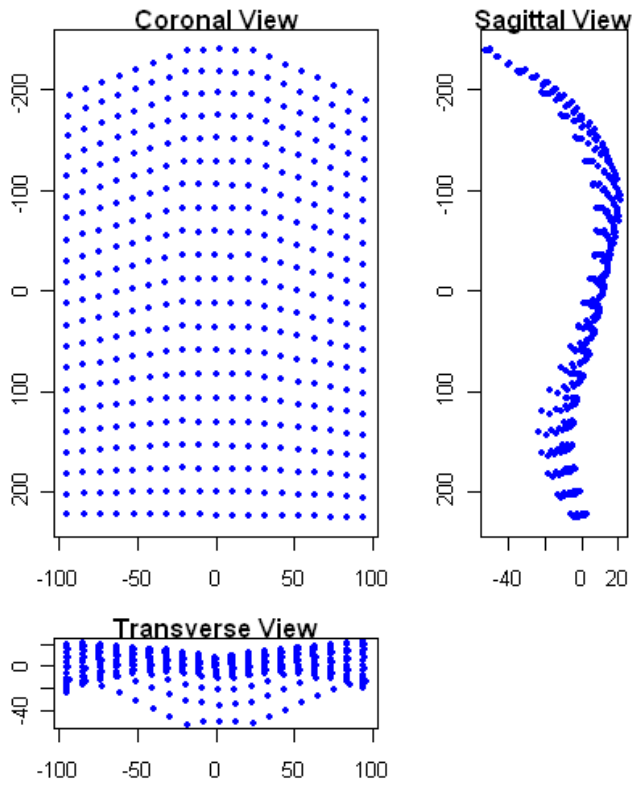

Figure 6.5: Landmarks of mean form (mm) considered as SNF

6.6 Form difference using EDMA

Suppose the forms of two objects, *A* and *B*, each with *K* landmarks are to be compared. Following the ideas presented above, the forms of these two objects correspond to two points in an *L*-dimensional Euclidean space. If the forms are identical, these two points are the same. Two identical forms must have the

same values for each element of the matrix, and correspond to the same point in the form space. If forms differ by their size only, the two points lie on a ray that passes through the origin. If neither of these conditions are true, then it can be concluded that the forms are different. There are several ways to describe this difference. An obvious description is the vector difference *FM(B)-FM(A)* where subtraction is done element-wise (i.e., for each individual linear distance). This representation defines the absolute difference between forms. Alternatively, the changed morphology relative to the initial morphology can be studied. To do this, Richtsmeier and Lele proposed the use of the form difference matrix (*FDM)* [54, 150] as following

$$FDM(B,A) = \frac{FM_{ij}(B)}{FM_{ij}(A)} \text{ where } i, j = 1,2,\cdots,K \tag{4.15}$$

There the ratios of corresponding linear distances from the two forms are calculated.

*FDM*s contain all the relevant information (as represented by the landmarks collected) regarding morphological distances between two forms (or sample of forms). Differences of form can reflect a simple difference in scaling of two forms (i.e. only in size), or a combination of difference in size and shape. Again, two forms *FM(A)* and *FM(B)* have the same shape if the multiplication of *FM(A)* with a unique positive scalar equals *FM(B)* which means that all elements of *FDM* are equal.

6.6.1 Estimating of form difference between deformed backs and SNF

Landmarks are extracted from individual deformed backs, and each deformed back is used to estimate the form difference relative to the SNF. A deformed back can be seen in Figure 6.6 and extracted landmarks of the deformed back can be seen in Figure 6.7. The axes units of Figure 6.7 are in mm.

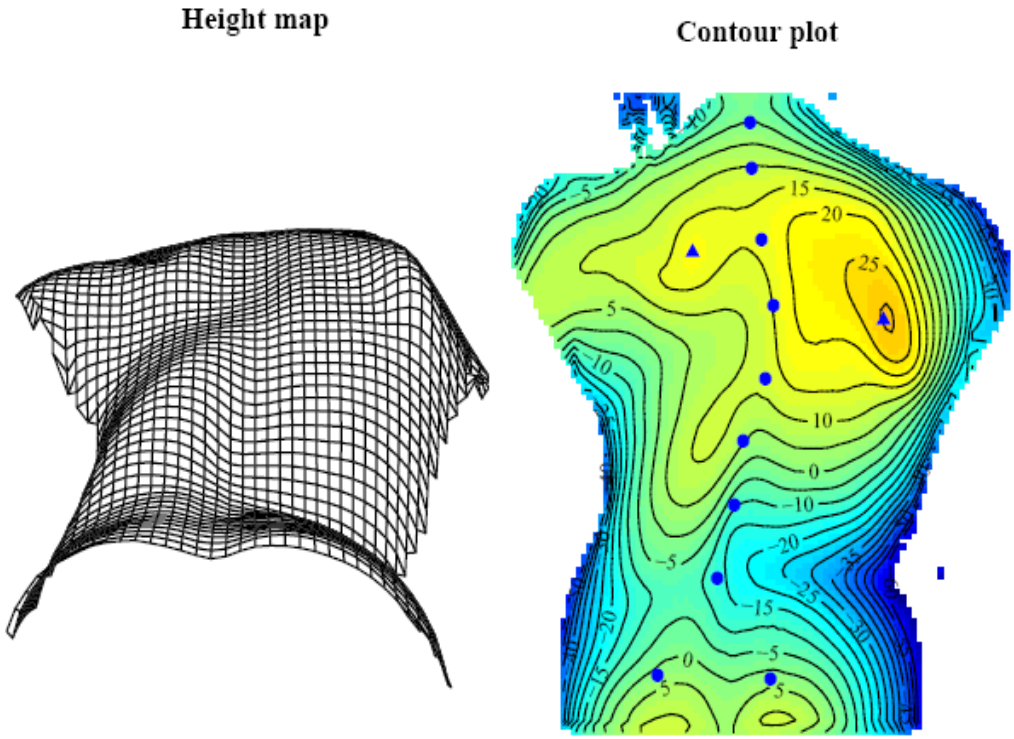

Figure 6.6: Height map and contour plot of a deformed back

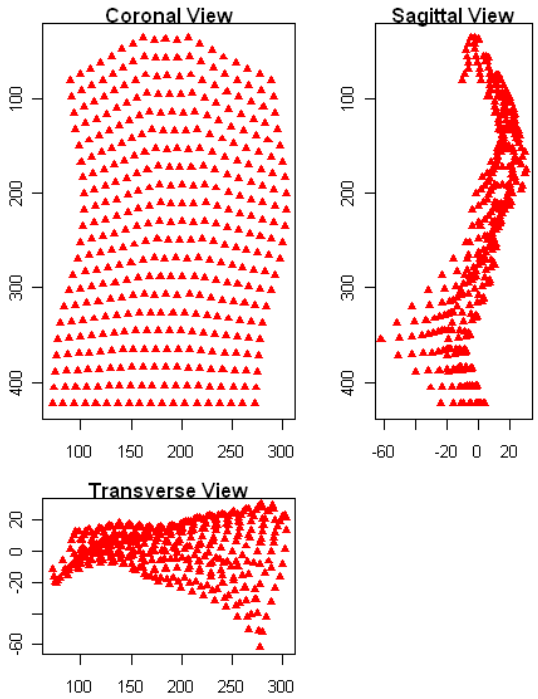

Figure 6.7: Visualizing landmarks the deformed back shown in Figure 6.6.

Initially, the Euclidean distances between all possible pairs of landmarks are estimated for a deformed back and this matrix is considered to be deformed back FM. The Euclidean distances between all possible pairs of landmarks are then estimated for the SNF and this matrix is considered to be SNF FM. The FDM is estimated using the equation (4.5) where the deformed back FM is used as numerator and the SNF FM is used as denominator. The median value for each landmark is estimated considering the whole FDM matrix. The median value is then subtracted from the FDM. The sum of columns to the absolute FDM is estimated [160]. This matrix is considered to be degree of difference (DOF).

The location of differences between deformed back and the SNF under study, the term DOF is used to describe landmarks whose relative ranking is high in terms of the contribution to the difference in form. This value gives information about the deformity; a high value indicates higher deformity at the location of that landmark. This analysis has been applied to 97 deformed backs. Now it is time to present analytical results in a meaningful way so that the summary of the analysis can be interpreted more easily.

A method of displaying influential landmarks is proposed by Cole and Richtsmeier [161]. The method involves the use of a two dimensional scatter plot to summarize, explore and interpret the FDM. In our case, as the number of landmarks is 399, it is very difficult to display and interpret the DOF using this technique. To solve this problem, a colour representation technique has been used to display the deformity between individual backs and the SNF.

6.6.2 Visualizing the degree of difference

Colour scales are an effective and commonly used method for visualizing scalar data. Colour scales are well suited for giving an overall impression of the distribution of the scalar field, although exact quantitative information cannot be perceived accurately. To demonstrate the process of creating the colour scales, Blue-Cyan-Green-Yellow-Red scale is used in which blue represents low values, green represents middle values and red represents high values.

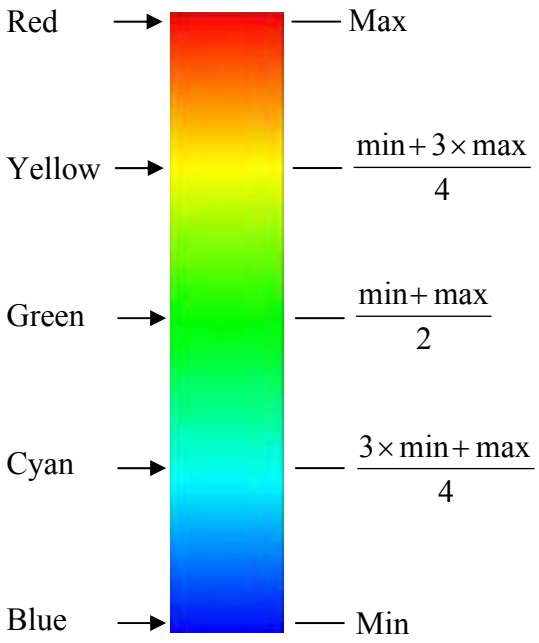

Figure 6.8: Blue-Cyan-Green-Yellow-Red colour scale

Cyan and yellow are used to introduce more colour variations that make it a four-segment scale: Blue-Cyan-Green-Yellow-Red. This scale is illustrated in the normalised RGB space shown in Figure 6.8.

A simple method of mapping the colour scale to the degree of difference is to partition the data using a fixed interval. Each class occupies an equal interval along the number line as shown in Figure 6.8. Let $Z_{\min}$ and $Z_{\max}$ be the minimum and maximum data values, and *s* be the number of classes, then the class interval (I_{equal}) is calculated by equation (6.1):

$$I_{equal} = \frac{Z_{\max} - Z_{mix}}{s} \tag{6.1}$$

To define the colour map, the first and last colours in the scale are assigned to the first and last classes respectively, while all other classes are distributed linearly over the rest of the colours (Figure 6.9).

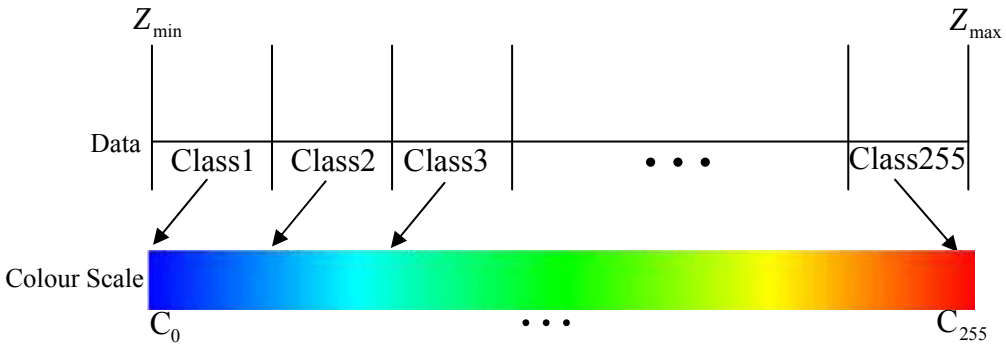

Figure 6.9: Equal interval classification and colour mapping

Figure 6.9 shows colour mapping based on an equal interval classification which is applied for visualizing the DOF differences between a deformed back and the SNF. A typical result can be seen form in Figure 6.10.

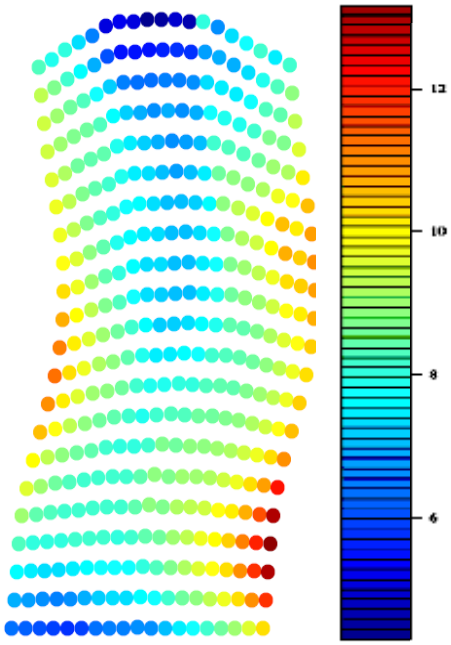

Figure 6.10: Visualizing the deformation location of the deformed back relative to the SNF

In Figure 6.9, the degree of difference for 399 landmarks relative to the SNF is displayed for the deformed back shown in Figure 6.10. The DOF is showed on

the original landmarks locations. There is no unit of this measure as this is the ratio of two forms. Figure 6.9 shows that the vertebrae region of the deformed back is blue in colour indicating that this region is not deformed. Again, the red colour of the right bottom region indicates high deformity of the deformed back from SNF.

6.7 Summary

Analysis for locating the deformation position on back surface has been carried out using R. Initially the Euclidean distance between all possible pairs of landmarks is estimated which is called the inter-landmark distance matrix. The inter-landmark distance matrix is calculated for a set of 20 normal backs. These inter-landmark distance matrices are then used to estimate a mean form and a variance-covariance matrix. The mean form is called the SNF. The inter-landmark distance matrix is estimated for all deformed backs. The form difference matrix is estimated by the division of individual deformed backs by the SNF. The median value is taken out and the sum of divergences is estimated for each landmark considering the whole form difference matrix. These values give information about the degree of difference of a deformed back relative to the SNF. Landmarks with the greatest degree of differences will have higher values. A graphical representation is then used to display this information. This shows the location of deformation between the SNF and individual deformed backs. A set of 97 deformed backs has been analysed using EDMA.

6.8 Summary

Analysis of the three-dimensional landmarks of the backs in patients with normal and deformed backs has been carried out using R. The back surfaces were measured using ISIS2, a structured light surface topography system, in a spinal deformity clinic. Some bony landmarks on the backs are indicated by small coloured paper stickers and these are used to determine the placement of the landmarks. A total of 399 landmarks were extracted from the back surface,

21 down the back for 19 columns parallel to spine, giving a grid of 21 x 19 landmarks distributed over most of the back surface. An SNS is then estimated from all the normal backs. Procrustes analysis is then applied between this SNS and all backs to produce information about rotation, scaling and translation for optimal fitting of the backs. The Riemannian distance parameter between each back and the SNS is then calculated to give a measure of the overall differences. The Riemannian distance values are higher for deformed backs than for normal backs. The box-and-whisker plots of the Riemannian distances for the normal backs and deformed backs show that the data spread for normal backs is very compact compared to that for the deformed backs. The data spread for deformed backs is much wider because of the range and degree of deformities that can occur. A *t*-test is then applied to the Riemannian distance values for normal backs and deformed backs. From results of this, it can be concluded that deformed backs are distinguishable from the normal backs.

7 Discussions

7.1 Discussion on landmark variation

Statistical study of shape analysis starts with the shape information which can be represented in different ways. There are different shape descriptors. Landmarks have been chosen as the shape descriptors for this work, because of its simplicity and ease of use for the stored back surface information obtained using ISIS2. Initially, a set of 24 landmarks were extracted based on the anatomical and mathematically derived locations on back surface. The number of landmarks is not a fixed number and it can be increased or decreased depending on the objective of the analysis. It was found that these 24 landmarks do not provide maximum information as required for our analysis. The number of landmarks was then increased to 399, distributed over the back surface and that provides better information. The number of landmarks can be further increased, but the computational time and memory space required will then increase. The number provide of landmarks has been chosen to necessary information about the back and yet still be optimal for computational time and memory space.

To use these 399 landmarks, the first thing is to realize how reliable those landmarks are for the analysis and how much variation can take place for repeated measurements. It can be found by estimating the variability and decide whether the variability is reasonable to use these landmarks for further analysis or any transformation is needed to minimize variations. As 399 landmarks are based on the first 21 landmarks where these 21 landmarks are extracted from the vertebra prominens to the sacrum (see Section 5.2.1), it is important to estimate the variability in these 21 landmarks. Recall that landmark number 21 in the 399 landmarks is based on the locations of dimples of Venus and these two points are also included for estimating variability. A total of 23 landmarks are used for estimating variability.

A series of parametric statistical tests has been carried out to estimate the variability. For hypothesis testing it is taken an account of how the uncertainties in measurements that affect other parameters. A conclusion has been derived from the analytical results that there is no significant difference in the locations of the landmarks between paired measurements (see Section 5.3.3). As all the cases the value is less than the probability that lies in 95% confidence interval (can be seen from Table A.3, A.4 and A.5 in Appendix A) or acceptance region ensures that there is no significant evidence that the null hypothesis is wrong (fail to reject). Euclidean distances of 23 landmarks between repeated measurements are estimated and histogram is plotted. It can be concluded from the results that the error distribution of the *x*, *y* and *z* coordinates are not uniform and it can be assumed that the error for individual landmarks will like an ellipsoid. The Bland-Altman method for repeated measurements is applied to the *x*, *y* and *z* coordinates of 23 landmarks. This method gives 95% limits of agreement based on standard deviation of the mean. The summary can be seen from Table A.6, A.7 and A.8 in Appendix A. The difference of mean for repeated measurements is very close to zero in most cases.

After applying different statistical methods to estimate the variability for the *x*, *y* and *z* coordinates of these 23 landmarks, it has been found that the maximum variation is lower than the distance between landmarks. The variations of *x*, *y* and *z* coordinates for 23 landmarks are small relative to the average back length and width (selected for landmark distribution). It has also been found that these landmarks will not overlap each other. These landmark variations will not have effect to use further for other analysis.

7.2 Discussion of Procrustes analysis

The objective of the analysis is to differentiate between normal and deformed backs taking the full geometrical distribution of the back surface into account rather than extracting specific lengths and angles. A set of 20 normal backs has been analysed to estimate the SNS. In total 117 backs (20 normal backs and 97

deformed backs) are then translated, rotated and scaled according to the SNS to find the best fit for each. The Riemannian distances between the SNS and all backs are then calculated; the results are presented in box and whisker plots in Figure 6.4 and numerically in Table A.9 in Appendix A. The highest Riemannian difference value for normal backs is 0.051 (NormalBack 20, Riemannian distance = 0.051, Scale = 1.143) and the lowest Riemannian difference value for deformed backs is 0.052 (DeformedBack 24, Riemannian distance = 0.052, scale = 0.902). The difference between the highest value for a normal back (NormalBack 20) and the lowest for a deformed back (DeformedBack 24) is small. However, it can be seen from Figure 6.4 that the Riemannian distance values for the deformed backs relative to the SNS are generally greater than the values for normal backs. The Riemannian distance value of DeformBack 82 (Riemannian distance = 0.281 and scale =1.116) is the highest among all backs. The landmarks from the three backs, the SNS, NormalBack 20 and DeformedBack 82 landmarks after Procrustes analysis are plotted and can be seen in Figure 7.1. The axes units are in mm.

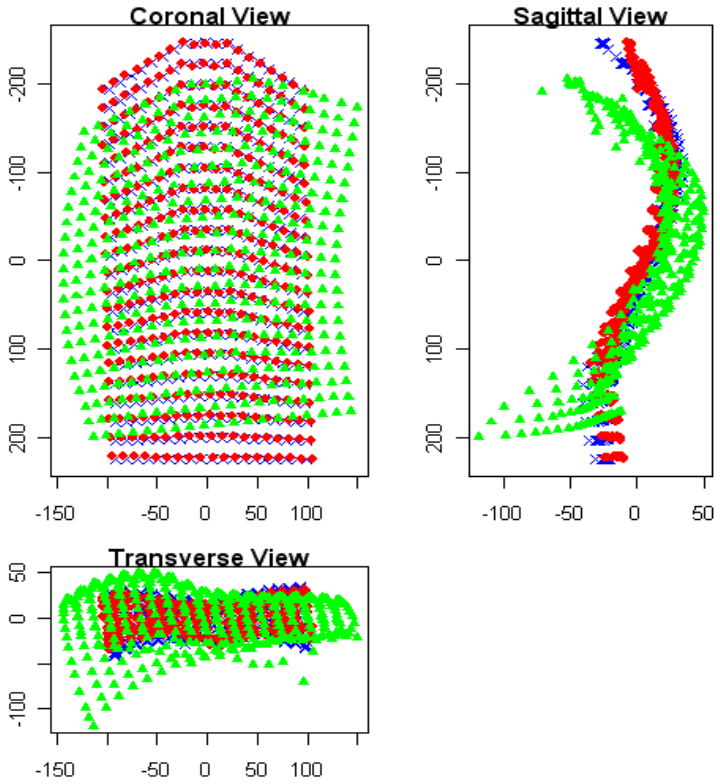

Figure 7.1: Three dimensional landmarks of SNS (blue cross), NormalBack 20 (red circle) and Deformedback 82 (green triangle)

The normal backs were collected from male and female volunteers whose ages ranged between 13 and 53 years. The deformed backs were collected from male and female patients whose ages ranged between 5.89 and 41.38 years. Procrustes analysis uses isotropic scaling to find the best match for all configurations. In Table A.9 in Appendix A, it can be seen that some backs are reduced in size in the Procrustes processing (scale<1) and other backs are expanded (scale>1) for finding the best match with the SNS. Among twenty normal backs, eleven backs are reduced and nine backs are expanded. Most of the reduced normal backs are backs from young adult or adult volunteers who have reached their full height. On the other hand, the expanded normal backs were collected from the young patients who are not as tall (or at least whose back length is smaller).

In Table A.9 in Appendix A, the Riemannian distance values of NormalBack 1 and NormalBack 3 are very close. These two backs come from the same volunteer but the photographs were taken some hours apart. Again, DeformBack 4 and DeformBack 6 are the backs of the same patient but the second photograph was taken after one year. The Riemannian distance value then displays the change in the back over this period.

Procrustes analysis uses scaling which is a linear transformation that increases or reduces the configuration by a scale factor. This scale factor is the same in all directions of the configuration, which is known as isotropic scaling. Isotropic scaling affects size and it has no effect on shape [162]. The human back does not grow uniformly along the different axes. To find the best match between back shapes, anisotropic scaling under Gaussian error distribution can be a good idea. This can be investigated in future research.

EDMA has been used to locate the position of the deformity on back surface. The process starts with estimating a mean form from a set of normal backs. EDMA uses multidimensional scaling on the matrix of Euclidean inter-landmark distances that helps to estimate mean form [163]. This scaling procedure is

different from Procrustes isotropic scaling. A multidimensional scaling algorithm starts with a matrix of item–item similarities, and then assigns a location to each item in *K*-dimensional space rather than assigning a scaling factor to *K*-dimensional space.

Lele [146] provided evidence of error associated with Procrustes estimation of shape and form. According to him, the Procrustes estimator of form is inconsistent. He has also raised a question about the consistency of the Procrustes estimator of shape. This is because the Procrustes method when applied under the Gaussian perturbation model used by Goodall [51] does not eliminate the nuisance parameters [54, 146, 164]. Subsequently, Kent and Mardia [165] proved that the Procrustes estimator of shape or form is consistent under various assumptions. In particular, they have proved that the Procrustes estimator of shape is consistent under the assumption of an isotropic error distribution. Rohlf's [166, 167] work suggesting that the statistical geometry of EDMA can introduce structure such as neither correlation which does not exist nor statistical power of the EDMA procedures depends greatly on the shape differences.

7.3 Discussion on EDMA

EDMA has been used to locate the position of the deformity on back surface. The process starts with estimating a mean form from a set of normal backs. EDMA uses multidimensional scaling on the matrix of Euclidean inter-landmark distances that helps to estimate mean form [163]. This scaling procedure is different from Procrustes isotropic scaling. A multidimensional scaling algorithm starts with a matrix of item–item similarities, and then assigns a location to each item in *K*-dimensional space rather than assigning a scaling factor to *K*-dimensional space.

Lele [146] provided evidence of error associated with Procrustes estimation of shape and form. According to him, the Procrustes estimator of form is

inconsistent. He has also raised a question about the consistency of the Procrustes estimator of shape. This is because the Procrustes method when applied under the Gaussian perturbation model used by Goodall [51] does not eliminate the nuisance parameters [54, 146, 164]. Subsequently, Kent and Mardia [165] proved that the Procrustes estimator of shape or form is consistent under various assumptions. In particular, they have proved that the Procrustes estimator of shape is consistent under the assumption of an isotropic error distribution. Rohlf's [166, 167] work suggesting that the statistical geometry of EDMA can introduce structure such as neither correlation which does not exist nor statistical power of the EDMA procedures depends greatly on the shape differences.

8 Conclusions and future work

8.1 Conclusions

A literature survey covering back deformity and statistical shape analysis has been carried out. The back deformity literature survey gives information about different reasons, types and possible treatment of human back deformities. ISIS2 provides topological surface information for a better understanding of the back surface. The back surface data that have been analyzed for this research are obtained from ISIS2. There are significance differences in deformed backs compared to normal backs. Landmarks are extracted from each individual back surface. The variability in landmarks for repeated measurements is estimated using different statistical techniques. The results show that the variability in landmark locations is not significant and therefore it is acceptable to use these landmarks for further analysis. The landmarks are therefore used for shape analysis. There are different methods of shape analysis. Procrustes shape analysis and Riemannian distance analysis have been used to quantify the three dimensional shape of human back. EDMA has been used to estimate the degree of deformity at the location of each landmark.

A set of 20 normal backs and 97 deformed backs has been used for our analysis. A total of 399 landmarks containing three-dimensional coordinate values were extracted from each back surface, 21 down to spine plus 21 down 18 columns parallel to the spine distributed over most of the back surface, 9 to left and 9 to right.

An estimation of variability in landmarks for repeated intra and inter measurements has been carried out. Landmarks on the spine and landmarks on the dimples of Venus are used for this estimation to ensure whether it is reasonable to use these landmarks for further analysis. Hypothesis testing is applied to the coordinate locations of these landmarks data and a conclusion is drawn that there is no significant difference in these coordinate locations. The

distance is estimated between paired measurements and Euclidean distance histograms are plotted. The histograms show the length of each landmarks of repeated measurements variation for intra and inter measurement data. Bland-Altman plots are also used to estimate the 95% limits of agreement. The limits of agreement provide sufficient information to conclude that the data spread is not wide relative to the average human back length and width for most cases. The analytic results of variability indicate that there is no difference between the repeated measurements and so the landmarks can be used for further analysis (for example, Procrustes analysis, EDMA etc).

Procrustes analysis has been applied to a number of normal and deformed backs. A mean Procrustes shape called the standard normal shape (SNS) is estimated using GPA from all the normal backs. OPA is then used between this SNS and all backs to produce information about rotation, scaling and translation for optimal fitting of the backs. The Riemannian distance parameter between each back and the SNS is then calculated to give a measure of the overall differences. The Riemannian distance values for the normal backs are significantly lower than those for the deformed backs. This suggests that the Riemannian distance parameter may be suitable for differentiating between normal and deformed backs. The box-and-whisker plot of the Riemannian distances for the normal backs and deformed backs show that the data spread for normal backs is very compact compared to that for the deformed backs. From the above scenario, it can be concluded that deformed backs are distinguishable from the normal backs. A numerical value is assessed for individual back that is based on the entire geometry of the back surface. This numerical value is obtained which indicates whether the assessed back is deformed or normal depending on the weight of the value, either high or low.

EDMA has been used to estimate the degree of deformity and visualize the position of the deformity. Initially a mean form called the standard normal form (SNF) is estimated from the set of 20 normal backs. Form difference is estimated between the SNF and individual deformed backs. The degree of

deformity is then estimated for individual landmarks and the results are plotted in colour to visualize the location of deformity. The results showed that EDMA can help to estimate and visualize the position of the deformity. The area with higher values indicates the high degree of deformity relative to the SNF while the lower value indicates low deformity.

8.2 Recommendations for future work

Many suggestions and recommendations for future work can be outlined. A procedure for locating anatomical landmarks on the back surface can be automated from back surface information without human intervention. A landmark detection procedure can be developed which will select most of the back surface for distributing landmarks and will be independent of back length. Procrustes analysis uses isotropic scaling for finding the best match among configurations. As different people have different ratios of length and width, an anisotropic scaling can be used for Procrustes analysis where the scaling factor for the different coordinates will be different. The entire surface which is selected for distributing landmarks can be used for EDMA rather than few landmarks which will provide more precise information of the degree of deformation. User friendly software can be developed which will be able to animate three-dimensional back surface with many features (flexible rotation to any direction, option to select landmarks area, display multiple backs and analysis results etc).

9 Appendix A

Table A. 1: Calculation of 95% range of *x*, *y* and *z* coordinates for 23 intra data

intra data												
Landmark	*x*				*y*				*z*			
	$\bar{x}$	Estimated 95% range		Percent lie in range	$\bar{y}$	Estimated 95% range		Percent lie in range	$\bar{z}$	Estimated 95% range		Percent lie in range
1	0	0	0	100%	0	0	0	100%	0	0	0	95%
2	0.04	-0.75	0.75	93.33%	0.07	-1.53	1.83	95%	0.28	-2.54	2.97	93.33%
3	0.08	-1.5	1.5	93.33%	0.13	-2.97	3.23	93.33%	0.25	-3.96	5.25	96.67%
4	0.12	-2.25	2.25	93.33%	0.17	-4.3	5.17	93.33%	0.32	-4.86	6.29	98.33%
5	0.15	-3	3	93.33%	0.2	-5.48	8.09	93.33%	0.4	-7.07	7.81	95%
6	0.19	-3.75	3.75	93.33%	0.23	-6.45	11.18	95%	0.28	-8.39	9.04	93.33%
7	0.23	-4.5	4.5	93.33%	0.26	-7.16	14.17	96.67%	0.29	-10.02	9.81	93.33%
8	0.27	-5.25	5.25	93.33%	0.29	-7.54	16.78	96.67%	0.18	-10.46	10.65	95%
9	0.31	-6	6	93.33%	0.31	-7.65	18.75	96.67%	0.07	-11.41	10.77	91.67%
10	0.34	-6.75	6.75	93.33%	0.34	-7.61	19.79	96.67%	0	-13.2	10.59	91.67%
11	0.38	-7.5	7.5	93.33%	0.36	-7.54	19.78	96.67%	-0.02	-14.01	12.23	91.67%
12	0.42	-8.25	8.25	93.33%	0.38	-7.52	18.89	93.33%	0.02	-14.75	13.15	90%
13	0.46	-9	9	93.33%	0.41	-8.6	17.27	93.33%	0.06	-14.63	14.77	91.67%
14	0.5	-9.75	9.75	93.33%	0.44	-9.81	15.1	91.67%	0.06	-14.77	14.66	95%
15	0.54	-10.5	10.5	93.33%	0.45	-11.04	12.56	91.67%	0.2	-12.86	13.23	95%
16	0.57	-11.25	11.25	93.33%	0.41	-12.26	9.82	91.67%	0.31	-11.31	12.18	95%
17	0.61	-12	12	93.33%	0.33	-13.4	10.25	93.33%	0.39	-9.27	11.19	95%
18	0.65	-12.75	12.75	93.33%	0.24	-14.45	10.98	95%	0.47	-6.15	9.69	91.67%
19	0.69	-13.5	13.5	93.33%	0.16	-15.39	11.66	93.33%	0.49	-2.74	5.22	95%
20	0.73	-14.25	14.25	93.33%	0.09	-16.21	12.23	93.33%	0.3	-1.18	2.9	96.67%
21	0.77	-15	15	93.33%	0.04	-16.9	12.67	95%	0.04	-1.12	2.54	95%
22	0.6	-15.89	13.31	93.33%	-0.14	-18.18	13.1	95%	0.01	-1.23	2.22	95%
23	0.61	-14.89	12.32	91.67%	-0.02	-17.23	14.04	96.67%	0.01	-1.22	2.32	96.67%

Table A. 2: Calculation of 95% range of *x*, *y* and *z* coordinates for 23 inter data

inter data												
Landmark	*x*				*y*				*z*			
	$\bar{x}$	Estimated 95% range		Percent lie in range	$\bar{y}$	Estimated 95% range		Percent lie in range	$\bar{z}$	Estimated 95% range		Percent lie in range
1	0	0	0	100%	0	0	0	100%	0	0	0	94.59%
2	0.09	-0.75	1.05	97.3%	0.01	-4.67	3.17	94.59%	0.15	-3.59	3.05	94.59%
3	0.17	-1.5	2.1	97.3%	-0.26	-7.88	4.13	97.3%	0.48	-4.3	4.83	100%
4	0.26	-2.25	3.15	97.3%	-0.67	-9.29	4.44	89.19%	0.66	-4.63	6.5	100%
5	0.35	-3	4.2	97.3%	-1.06	-11.88	4.79	91.89%	0.85	-6.22	7.16	100%
6	0.43	-3.75	5.25	97.3%	-1.28	-14.72	6.8	94.59%	0.73	-6.81	8.39	100%
7	0.52	-4.5	6.3	97.3%	-1.3	-16.62	8.67	91.89%	0.7	-7.88	9.53	100%
8	0.61	-5.25	7.35	97.3%	-1.12	-16.98	10.1	91.89%	0.76	-8.87	11.61	97.3%
9	0.69	-6	8.4	97.3%	-0.78	-16.48	11.01	97.3%	0.64	-9.7	13.06	97.3%
10	0.78	-6.75	9.45	97.3%	-0.42	-16.39	12.34	97.3%	0.64	-10.24	14.04	97.3%
11	0.86	-7.5	10.5	97.3%	-0.16	-17.69	15.09	97.3%	0.59	-10.89	15.38	94.59%
12	0.95	-8.25	11.55	97.3%	0.01	-17.56	16.37	91.89%	0.73	-10.72	17.04	94.59%
13	1.04	-9	12.6	97.3%	0.12	-18.89	18.05	94.59%	1.01	-10.68	19.12	94.59%
14	1.12	-9.75	13.65	97.3%	0.22	-20.65	21.13	94.59%	1.22	-11.46	20.14	94.59%
15	1.21	-10.5	14.7	97.3%	0.27	-22.72	23.86	94.59%	1.46	-11.81	22.09	94.59%
16	1.3	-11.25	15.75	97.3%	0.23	-25.02	26.07	94.59%	1.41	-12.08	21.93	94.59%
17	1.38	-12	16.8	97.3%	0.09	-27.37	27.59	94.59%	0.97	-10.91	19.74	97.3%
18	1.47	-12.75	17.85	97.3%	-0.12	-29.48	28.22	94.59%	0.74	-6.82	14.41	97.3%
19	1.56	-13.5	18.9	97.3%	-0.36	-31.06	27.81	94.59%	0.41	-5.2	9.06	97.3%
20	1.64	-14.25	19.95	97.3%	-0.61	-31.83	26.19	94.59%	0.25	-3.13	4.15	100%
21	1.73	-15	21	97.3%	-0.83	-31.56	23.24	94.59%	-0.08	-2.46	1.44	94.59
23	1.74	-14.91	22.13	97.3%	-0.03	-18.14	37.08	97.3%	0.15	-2.35	2.66	92.0%
22	3.28	-18.55	20.64	97.3%	-0.78	-21.43	19.52	92.0%	0.15	-2.34	2.65	92.0%
23	1.74	-14.91	22.13	97.3%	-0.03	-18.14	37.08	97.3%	0.15	-2.35	2.66	92.0%

Table A. 3: Paired sample *t*-test for *x* coordinate

Land mark	intra							inter						
	$\bar{x}$	SD	SE	*p* - value	*t* - value	95% confidence interval		$\bar{x}$	SD	SE	*p* - value	*t* - value	95% confidence interval	
1	0	0	0	NA	NA	NA	NA	0	0	0	NA	NA	NA	NA
2	0.04	0.26	0.03	0.25	1.16	-0.03	0.1	0.09	0.46	0.08	0.26	1.14	-0.07	0.24
3	0.08	0.51	0.07	0.25	1.16	-0.06	0.21	0.17	0.92	0.15	0.26	1.14	-0.13	0.48
4	0.12	0.77	0.1	0.25	1.16	-0.08	0.31	0.26	1.38	0.23	0.26	1.14	-0.2	0.72
5	0.15	1.02	0.13	0.25	1.16	-0.11	0.42	0.35	1.84	0.3	0.26	1.14	-0.27	0.96
6	0.19	1.28	0.17	0.25	1.16	-0.14	0.52	0.43	2.31	0.38	0.26	1.14	-0.34	1.2
7	0.23	1.54	0.2	0.25	1.16	-0.17	0.63	0.52	2.77	0.45	0.26	1.14	-0.4	1.44
8	0.27	1.79	0.23	0.25	1.16	-0.19	0.73	0.61	3.23	0.53	0.26	1.14	-0.47	1.68
9	0.31	2.05	0.26	0.25	1.16	-0.22	0.84	0.69	3.69	0.61	0.26	1.14	-0.54	1.92
10	0.34	2.3	0.3	0.25	1.16	-0.25	0.94	0.78	4.15	0.68	0.26	1.14	-0.61	2.16
11	0.38	2.56	0.33	0.25	1.16	-0.28	1.04	0.86	4.61	0.76	0.26	1.14	-0.67	2.4
12	0.42	2.82	0.36	0.25	1.16	-0.31	1.15	0.95	5.07	0.83	0.26	1.14	-0.74	2.64
13	0.46	3.07	0.4	0.25	1.16	-0.33	1.25	1.04	5.53	0.91	0.26	1.14	-0.81	2.88
14	0.5	3.33	0.43	0.25	1.16	-0.36	1.36	1.12	5.99	0.99	0.26	1.14	-0.87	3.12
15	0.54	3.58	0.46	0.25	1.16	-0.39	1.46	1.21	6.46	1.06	0.26	1.14	-0.94	3.36
16	0.57	3.84	0.5	0.25	1.16	-0.42	1.57	1.3	6.92	1.14	0.26	1.14	-1.01	3.6
17	0.61	4.1	0.53	0.25	1.16	-0.44	1.67	1.38	7.38	1.21	0.26	1.14	-1.08	3.84
18	0.65	4.35	0.56	0.25	1.16	-0.47	1.78	1.47	7.84	1.29	0.26	1.14	-1.14	4.08
19	0.69	4.61	0.59	0.25	1.16	-0.5	1.88	1.56	8.3	1.36	0.26	1.14	-1.21	4.32
20	0.73	4.86	0.63	0.25	1.16	-0.53	1.98	1.64	8.76	1.44	0.26	1.14	-1.28	4.56
21	0.77	5.12	0.66	0.25	1.16	-0.56	2.09	1.73	9.22	1.52	0.26	1.14	-1.34	4.8
22	0.6	4.93	0.64	0.35	0.94	-0.68	1.87	3.28	10.34	1.7	0.06	1.93	-0.17	6.73
23	0.61	4.8	0.62	0.33	0.98	-0.63	1.85	1.74	9.19	1.51	0.26	1.16	-1.32	4.81

$\bar{x}$: mean within paired difference (mm), SD: standard deviation, SE: standard error

Table A. 4: Paired sample *t*-test for *y* coordinate

Land Mark	Intra							inter						
	$\bar{y}$	SD	SE	*p* - value	*t* - value	95% confidence interval		$\bar{y}$	SD	SE	*p* - value	*t* - value	95% confidence interval	
1	0	0	0	NA	NA	NA	NA	0	0	0	NA	NA	NA	NA
2	0.07	0.61	0.08	0.36	0.91	-0.09	0.23	0.01	1.52	0.25	0.96	0.05	-0.49	0.52
3	0.13	1.12	0.14	0.38	0.88	-0.16	0.42	-0.26	2.48	0.41	0.53	-0.64	-1.09	0.56
4	0.17	1.57	0.2	0.41	0.82	-0.24	0.57	-0.67	3.33	0.55	0.23	-1.23	-1.78	0.44
5	0.2	2	0.26	0.45	0.76	-0.32	0.71	-1.06	4.25	0.7	0.14	-1.51	-2.47	0.36
6	0.23	2.4	0.31	0.47	0.73	-0.4	0.85	-1.28	5.19	0.85	0.14	-1.49	-3.01	0.46
7	0.26	2.76	0.36	0.47	0.72	-0.45	0.97	-1.3	6.1	1.00	0.21	-1.29	-3.33	0.74
8	0.29	3.07	0.4	0.47	0.73	-0.5	1.08	-1.12	6.83	1.12	0.33	-1.00	-3.39	1.16
9	0.31	3.33	0.43	0.47	0.73	-0.54	1.17	-0.78	7.26	1.19	0.52	-0.66	-3.2	1.64
10	0.34	3.51	0.45	0.45	0.75	-0.57	1.25	-0.42	7.54	1.24	0.73	-0.34	-2.94	2.09
11	0.36	3.61	0.47	0.44	0.78	-0.57	1.3	-0.16	7.78	1.28	0.9	-0.12	-2.75	2.44
12	0.38	3.68	0.47	0.42	0.8	-0.57	1.33	0.01	8.04	1.32	1.00	0.00	-2.68	2.69
13	0.41	3.71	0.48	0.4	0.85	-0.55	1.36	0.12	8.35	1.37	0.93	0.09	-2.66	2.91
14	0.44	3.75	0.48	0.37	0.91	-0.53	1.41	0.22	8.7	1.43	0.88	0.16	-2.68	3.12
15	0.45	3.84	0.5	0.37	0.91	-0.54	1.44	0.27	9.07	1.49	0.86	0.18	-2.75	3.3
16	0.41	3.96	0.51	0.42	0.81	-0.61	1.44	0.23	9.4	1.54	0.88	0.15	-2.9	3.36
17	0.33	4.12	0.53	0.54	0.62	-0.73	1.39	0.09	9.66	1.59	0.95	0.06	-3.13	3.32
18	0.24	4.33	0.56	0.67	0.42	-0.88	1.36	-0.12	9.88	1.62	0.94	-0.07	-3.41	3.18
19	0.16	4.56	0.59	0.79	0.27	-1.02	1.33	-0.36	10.04	1.65	0.83	-0.22	-3.71	2.98
20	0.09	4.79	0.62	0.88	0.15	-1.14	1.33	-0.61	10.1	1.66	0.72	-0.37	-3.98	2.76
21	0.04	5.02	0.65	0.95	0.07	-1.25	1.34	-0.83	10.08	1.66	0.62	-0.5	-4.2	2.53
22	-0.14	5.27	0.68	0.84	-0.2	-1.5	1.22	-0.78	9.69	1.59	0.63	-0.49	-4.01	2.45
23	-0.02	5.3	0.68	0.98	-0.03	-1.39	1.35	-0.03	10.85	1.78	0.99	-0.01	-3.64	3.59

$\bar{y}$: mean within paired difference (mm), SD: standard deviation, SE: standard error

Table A. 5: Paired sample *t*-test for *z* coordinate

Land mark	Intra							inter						
	$\bar{z}$	SD	SE	*p* - value	*t* - value	95% confidence interval		$\bar{z}$	SD	SE	*p* - value	*t* - value	95% confidence interval	
1	0	0	0	NA	NA	NA	NA	0	0	0	NA	NA	NA	NA
2	0.28	1.22	0.16	0.08	1.79	-0.03	0.6	0.15	1.63	0.27	0.58	0.56	-0.39	0.69
3	0.25	1.99	0.26	0.34	0.96	-0.27	0.76	0.48	2.46	0.4	0.24	1.18	-0.34	1.3
4	0.32	2.6	0.34	0.34	0.95	-0.35	0.99	0.66	3.12	0.51	0.21	1.28	-0.39	1.7
5	0.4	3.24	0.42	0.35	0.95	-0.44	1.23	0.85	3.79	0.62	0.18	1.36	-0.42	2.11
6	0.28	3.65	0.47	0.55	0.6	-0.66	1.23	0.73	4.12	0.68	0.29	1.08	-0.64	2.11
7	0.29	4.08	0.53	0.59	0.55	-0.77	1.34	0.7	4.59	0.76	0.36	0.92	-0.84	2.23
8	0.18	4.23	0.55	0.74	0.34	-0.91	1.28	0.76	5.31	0.87	0.39	0.87	-1.02	2.53
9	0.07	4.43	0.57	0.91	0.12	-1.08	1.21	0.64	5.71	0.94	0.5	0.68	-1.26	2.55
10	0.00	4.72	0.61	1.00	0.00	-1.22	1.22	0.64	6.28	1.03	0.54	0.62	-1.46	2.73
11	-0.02	4.89	0.63	0.97	-0.04	-1.29	1.24	0.59	6.78	1.11	0.6	0.53	-1.67	2.85
12	0.02	4.89	0.63	0.98	0.03	-1.24	1.28	0.73	7.03	1.16	0.53	0.63	-1.62	3.07
13	0.06	4.72	0.61	0.92	0.1	-1.16	1.28	1.01	7.46	1.23	0.41	0.83	-1.47	3.5
14	0.06	4.37	0.56	0.92	0.1	-1.07	1.19	1.22	7.44	1.22	0.32	1.00	-1.25	3.7
15	0.2	3.94	0.51	0.69	0.39	-0.82	1.22	1.46	7.42	1.22	0.24	1.19	-1.02	3.93
16	0.31	3.46	0.45	0.49	0.7	-0.58	1.2	1.41	6.91	1.14	0.22	1.24	-0.9	3.71
17	0.39	2.95	0.38	0.31	1.02	-0.37	1.15	0.97	5.96	0.98	0.33	1.00	-1.01	2.96
18	0.47	2.49	0.32	0.15	1.46	-0.18	1.11	0.74	4.62	0.76	0.34	0.97	-0.8	2.28
19	0.49	1.73	0.22	0.1	1.68	0.05	0.94	0.41	3.29	0.54	0.45	0.76	-0.68	1.51
20	0.3	0.96	0.12	0.16	1.44	0.05	0.55	0.25	2.01	0.33	0.46	0.74	-0.42	0.92
21	0.04	0.7	0.09	0.63	0.49	-0.14	0.22	-0.08	0.96	0.16	0.61	-0.51	-0.4	0.24
22	0.01	0.79	0.1	0.92	0.1	-0.19	0.22	0.04	1.44	0.24	0.86	0.18	-0.44	0.52
23	0.01	0.79	0.1	0.9	0.12	-0.19	0.22	0.04	1.44	0.24	0.86	0.18	-0.44	0.52

$\bar{z}$: mean within paired difference (mm), SD: standard deviation, SE: standard error

Table A. 6: Bland-Altman difference plot summary of *x* coordinate

Land mark	intra				Inter			
	x		Limits of agreement		*x*		Limits of agreement	
	$\bar{x}$	SD	L	U	$\bar{x}$	SD	L	U
1	0.00	0.00	0.00	0.00	0.00	0.00	0.00	0.00
2	0.04	0.26	-0.47	0.55	0.09	0.46	-0.84	1.01
3	0.08	0.51	-0.95	1.10	0.17	0.92	-1.67	2.02
4	0.12	0.77	-1.42	1.65	0.26	1.38	-2.51	3.03
5	0.15	1.02	-1.89	2.20	0.35	1.84	-3.34	4.03
6	0.19	1.28	-2.37	2.75	0.43	2.31	-4.18	5.04
7	0.23	1.54	-2.84	3.30	0.52	2.77	-5.01	6.05
8	0.27	1.79	-3.32	3.85	0.61	3.23	-5.85	7.06
9	0.31	2.05	-3.79	4.40	0.69	3.69	-6.69	8.07
10	0.34	2.30	-4.26	4.95	0.78	4.15	-7.52	9.08
11	0.38	2.56	-4.74	5.50	0.86	4.61	-8.36	10.09
12	0.42	2.82	-5.21	6.05	0.95	5.07	-9.19	11.10
13	0.46	3.07	-5.68	6.60	1.04	5.53	-10.03	12.10
14	0.50	3.33	-6.16	7.15	1.12	5.99	-10.86	13.11
15	0.54	3.58	-6.63	7.70	1.21	6.46	-11.70	14.12
16	0.57	3.84	-7.11	8.26	1.30	6.92	-12.54	15.13
17	0.61	4.10	-7.58	8.81	1.38	7.38	-13.37	16.14
18	0.65	4.35	-8.05	9.36	1.47	7.84	-14.21	17.15
19	0.69	4.61	-8.53	9.91	1.56	8.30	-15.04	18.16
20	0.73	4.86	-9.00	10.46	1.64	8.76	-15.88	19.16
21	0.77	5.12	-9.47	11.01	1.73	9.22	-16.71	20.17
22	0.60	4.93	-9.26	10.46	3.28	10.34	-17.40	23.96
23	0.61	4.80	-8.99	10.21	1.74	9.19	-16.63	20.12

$\bar{x}$: mean within paired difference (mm), L= Lower, U= Upper

Table A. 7: Bland-Altman difference plot summary of *y* coordinate

Land mark	intra				Inter			
	y		Limits of agreement		*y*		Limits of agreement	
	$\bar{y}$	SD	L	U	$\bar{y}$	SD	L	U
1	0.00	0.00	0.00	0.00	0.00	0.00	0.00	0.00
2	0.07	0.61	-1.15	1.30	0.01	1.52	-3.02	3.05
3	0.13	1.12	-2.11	2.36	-0.26	2.48	-5.21	4.69
4	0.17	1.57	-2.98	3.31	-0.67	3.33	-7.32	5.98
5	0.20	2.00	-3.81	4.20	-1.06	4.25	-9.55	7.43
6	0.23	2.40	-4.58	5.03	-1.28	5.19	-11.66	9.11
7	0.26	2.76	-5.25	5.77	-1.30	6.10	-13.50	10.91
8	0.29	3.07	-5.85	6.42	-1.12	6.83	-14.77	12.54
9	0.31	3.33	-6.34	6.97	-0.78	7.26	-15.30	13.74
10	0.34	3.51	-6.67	7.35	-0.42	7.54	-15.49	14.65
11	0.36	3.61	-6.87	7.59	-0.16	7.78	-15.72	15.41
12	0.38	3.68	-6.97	7.73	0.01	8.04	-16.08	16.09
13	0.41	3.71	-7.02	7.83	0.12	8.35	-16.58	16.83
14	0.44	3.75	-7.07	7.95	0.22	8.70	-17.18	17.63
15	0.45	3.84	-7.22	8.13	0.27	9.07	-17.87	18.41
16	0.41	3.96	-7.50	8.33	0.23	9.40	-18.56	19.02
17	0.33	4.12	-7.91	8.57	0.09	9.66	-19.23	19.42
18	0.24	4.33	-8.43	8.90	-0.12	9.88	-19.88	19.64
19	0.16	4.56	-8.97	9.28	-0.36	10.04	-20.44	19.71
20	0.09	4.79	-9.49	9.67	-0.61	10.10	-20.82	19.60
21	0.04	5.02	-9.99	10.07	-0.83	10.08	-21.00	19.33
22	-0.14	5.27	-10.67	10.39	-0.78	9.69	-20.17	18.60
23	-0.02	5.30	-10.62	10.59	-0.03	10.85	-21.73	21.68

$\bar{y}$: mean within paired difference (mm), L= Lower, U= Upper

Table A. 8: Bland-Altman difference plot summary of *z* coordinate

Land mark	intra				Inter			
	z		Limits of agreement		*z*		Limits of agreement	
	$\bar{z}$	SD	L	U	$\bar{z}$	SD	L	U
1	0.00	0.00	0.00	0.00	0.00	0.00	0.00	0.00
2	0.28	1.22	-2.16	2.73	0.15	1.63	-3.10	3.40
3	0.25	1.99	-3.73	4.22	0.48	2.46	-4.45	5.40
4	0.32	2.60	-4.88	5.52	0.66	3.12	-5.59	6.90
5	0.40	3.24	-6.08	6.87	0.85	3.79	-6.72	8.42
6	0.28	3.65	-7.03	7.59	0.73	4.12	-7.52	8.98
7	0.29	4.08	-7.87	8.44	0.70	4.59	-8.49	9.88
8	0.18	4.23	-8.28	8.65	0.76	5.31	-9.87	11.38
9	0.07	4.43	-8.79	8.93	0.64	5.71	-10.79	12.07
10	0.00	4.72	-9.43	9.44	0.64	6.28	-11.92	13.19
11	-0.02	4.89	-9.81	9.76	0.59	6.78	-12.97	14.15
12	0.02	4.89	-9.76	9.80	0.73	7.03	-13.33	14.79
13	0.06	4.72	-9.39	9.51	1.01	7.46	-13.90	15.93
14	0.06	4.37	-8.69	8.81	1.22	7.44	-13.65	16.09
15	0.20	3.94	-7.68	8.08	1.46	7.42	-13.38	16.29
16	0.31	3.46	-6.60	7.23	1.41	6.91	-12.42	15.24
17	0.39	2.95	-5.51	6.29	0.97	5.96	-10.94	12.88
18	0.47	2.49	-4.51	5.44	0.74	4.62	-8.50	9.98
19	0.49	1.73	-2.96	3.95	0.41	3.29	-6.16	6.99
20	0.30	0.96	-1.62	2.22	0.25	2.01	-3.78	4.27
21	0.04	0.70	-1.35	1.43	-0.08	0.96	-2.00	1.84
22	0.01	0.79	-1.57	1.59	0.04	1.44	-2.83	2.92
23	0.01	0.79	-1.58	1.60	0.04	1.44	-2.83	2.92

$\bar{z}$: mean within paired difference (mm), L= Lower, U= Upper

Table A. 9: Summary of Procrustes analysis for backs

Backs	Riemannian Distance	Scale
NormalBack 1	0.024	0.965
NormalBack 2	0.02	1.046
NormalBack 3	0.025	0.97
NormalBack 4	0.034	0.933
NormalBack 5	0.038	0.991
NormalBack 6	0.023	1.023
NormalBack 7	0.04	1.01
NormalBack 8	0.033	0.935
NormalBack 9	0.031	1.046
NormalBack 10	0.034	1.039
NormalBack 11	0.043	0.901
NormalBack 12	0.028	0.923
NormalBack 13	0.028	1.146
NormalBack 14	0.033	0.983
NormalBack 15	0.041	0.987
NormalBack 16	0.038	0.905
NormalBack 17	0.021	0.947
NormalBack 18	0.045	1.141
NormalBack 19	0.048	1.109
NormalBack 20	0.051	1.143
DeformBack 1	0.074	0.943
DeformBack 2	0.128	1.019
DeformBack 3	0.082	1.008
DeformBack 4	0.129	0.89
DeformBack 5	0.086	0.989
DeformBack 6	0.137	1.276
DeformBack 7	0.176	1.031
DeformBack 8	0.11	0.998
DeformBack 9	0.129	1.043
DeformBack 10	0.116	1.06
DeformBack 11	0.083	1.485
DeformBack 12	0.173	1.304
DeformBack 13	0.118	0.993
DeformBack 14	0.076	1.13
DeformBack 15	0.147	1.063
DeformBack 16	0.165	1.31
DeformBack 17	0.119	1.132
DeformBack 18	0.148	1.2
DeformBack 19	0.084	0.98
DeformBack 20	0.093	1.041
DeformBack 21	0.153	1.525
DeformBack 22	0.176	0.991
DeformBack 23	0.146	1.032

DeformBack 24	0.052	0.902
DeformBack 25	0.069	1.125
DeformBack 26	0.109	1.215
DeformBack 27	0.077	1.108
DeformBack 28	0.137	0.93
DeformBack 29	0.145	0.966
DeformBack 30	0.152	1.21
DeformBack 31	0.196	1.228
DeformBack 32	0.19	1.551
DeformBack 33	0.105	1.172
DeformBack 34	0.105	1.051
DeformBack 35	0.104	1.045
DeformBack 36	0.167	1.057
DeformBack 37	0.098	0.907
DeformBack 38	0.099	0.965
DeformBack 39	0.139	1.151
DeformBack 40	0.124	0.943
DeformBack 41	0.105	1.014
DeformBack 42	0.09	0.98
DeformBack 43	0.091	0.933
DeformBack 44	0.089	0.983
DeformBack 45	0.115	0.995
DeformBack 46	0.074	0.943
DeformBack 47	0.137	0.974
DeformBack 48	0.112	1.012
DeformBack 49	0.091	1.084
DeformBack 50	0.088	1.011
DeformBack 51	0.09	1.372
DeformBack 52	0.128	1.019
DeformBack 53	0.082	1.008
DeformBack 54	0.09	0.967
DeformBack 55	0.092	0.934
DeformBack 56	0.129	0.89
DeformBack 57	0.086	0.989
DeformBack 58	0.117	0.945
DeformBack 59	0.154	1.036
DeformBack 60	0.084	0.966
DeformBack 61	0.137	1.276
DeformBack 62	0.13	1.032
DeformBack 63	0.115	1.011
DeformBack 64	0.249	1.083
DeformBack 65	0.191	1.403
DeformBack 66	0.109	1.023
DeformBack 67	0.133	1.026
DeformBack 68	0.13	1.058
DeformBack 69	0.176	1.031
DeformBack 70	0.11	0.998

DeformBack 71	0.128	0.968
DeformBack 72	0.187	1.635
DeformBack 73	0.141	0.974
DeformBack 74	0.276	1.569
DeformBack 75	0.1	1.15
DeformBack 76	0.129	0.989
DeformBack 77	0.129	1.043
DeformBack 78	0.103	1.314
DeformBack 79	0.117	1.03
DeformBack 80	0.115	1.003
DeformBack 81	0.15	1.138
DeformBack 82	0.281	1.116
DeformBack 83	0.174	1.217
DeformBack 84	0.118	1.016
DeformBack 85	0.108	1.005
DeformBack 86	0.113	1.065
DeformBack 87	0.104	1.049
DeformBack 88	0.102	0.841
DeformBack 89	0.142	1.187
DeformBack 90	0.116	1.06
DeformBack 91	0.083	1.485
DeformBack 92	0.173	1.304
DeformBack 93	0.118	0.993
DeformBack 94	0.113	0.978
DeformBack 95	0.109	1.16
DeformBack 96	0.126	0.952
DeformBack 97	0.133	1.382

10 References

[1] T. J. Errico, B. S. Lonner, and A. W. Moulton, *Surgical Management of Spinal Deformities*. London: Elsevier's Health Science, 2008.

[2] A. Turner-Smith, "A television/computer three-dimensional surface shape measurement system," *Journal of Biomechanics,* vol. 21, pp. 515–529, 1988.

[3] A. Turner-Smith, J. Harris, G. Houghton, and R. Jefferson, "A method for analysis of back shape in scoliosis," *Journal of Biomechanics,* vol. 21, pp. 497-509, 1988.

[4] T. Theologis, A. Turner-Smith, and J. Fairbank, "Quantification of the cosmetic defect of adolescent idiopathic scoliosis - the influence of treatment," in *International symposium on 3D scoliotic deformities*, J. Dansereau, Ed. Stuttgart: Gustav Fischer Verlag, 1992, pp. 444–448.

[5] F. Berryman, P. Pynsent, J. Fairbank, and S. Disney, "A new system for measuring three-dimensional back shape in scoliosis," *European Spine Journal,* vol. 17, pp. 663-672, 2008.

[6] A. Wojcik, M. Mehta, and G. Philips, "Surface imaging of body and spinal shape by the Quantec system," *Journal of Bone and Joint Surgery,* vol. 76-B, p. 15, 1994.

[7] A. Aliverti, G. Ferrigno, F. Rotelli, and G. C. Santambrogio, "Back surface analysis by laser beam scanning and stereo-photogrammetry," in *Three Dimensional Analysis of Spinal Deformities*, M. D. Amico, A. Merolli, and G. C. Santambrogio, Eds. Amsterdam, Netherlands: IOS Press, 1995, pp. 51-56.

[8] H. Weiss, K. Lohschmidt, and N. El Obeidi, "Trunk deformity in relation to breathing - a comparative analysis with the Formetric system," in *Research into Spinal Deformities 1*, J. Sevastik and K. Diab, Eds. Amsterdam: IOS Press, 1997.

[9] B. Drerup and E. Hierholzer, "Evaluation of frontal radiographs of scoliotic spines—Part II. Relations between lateral deviation, lateral tilt and axial rotation of vertebrae," *Journal of Biomechanics,* vol. 25, pp. 1443-1450, 1992.

[10] B. Drerup and E. Hierholzer, "Description of scoliotic deformity by modulated sinusoidal functions," in *Three dimensional analysis of spinal deformities*, M. D'Amico, A. Merolli, and G. C. Santambrogio, Eds. Netherlands: IOS Press, 1995.

[11] B. Drerup and E. Hierholzer, "Back shape measurement using video rasterstereography and three-dimensional reconstruction of spinal shape," *Clinical Biomechanics,* vol. 9, pp. 28-36, 1994.

[12] WrongDiagnosis.com, "Causes of Types of Back symptoms," Health Grades Inc, URL http://www.wrongdiagnosis.com/sym/back_symptoms.htm, 2010.

[13] Primal Pictures Ltd, "Anatomical Language, URL http://www.anatomy.tv/StudyGuides/StudyGuide.aspx?guideid=9&NextID=0&customer=primal," 2007.

[14] S. G. Marketos and P. K. Skiadas, "Galen: A pioneer of spine research," *Spine,* vol. 24, pp. 2358-2362, 1999.

[15] "Scoliosis and Spinal Deformities," The Children's Hospital Orthopedic Surgical Foundation, URL http://www.youngwomenshealth.org/scoliosis-article.html, 2009.

[16] J. D. Hsu, J. W. Michael, and J. R. Fisk, *AAOS Atlas of Orthoses and Assistive Devices*, Fourth edition ed.: Mosby, 2008.

[17] M. J. McMaster, "Infantile idiopathic scoliosis: can it be prevented ?," *The Journal of Bone and Joint Surgery,* vol. 65-B, pp. 612-617, 1983.

[18] C. M. Robinson and M. J. McMaster, "Juvenile idiopathic scoliosis. Curve patterns and prognosis in one hundred and nine patients," *J Bone Joint Surg Am,* vol. 78, pp. 1140-1148, 1996.

[19] "Adolescent Idiopathic Scoliosis," North American Spine Society, 2009.

[20] J. Bettany, D. Harrison, M. Edgar, A. Ransford, P. Webb, and T. Morley, "The effect of anterior instrumentation on back shape in adolescent idiopathic scoliosis: preliminary results," in *Surface Topography and Spinal Deformity*, A. Alberti, B. Drerup, and E. Hierholzer, Eds. Stuttgart: Gustav Fischer Verlag, 1992.

[21] R. F. Heary and T. J. Albert, *Spinal Deformities*: Thieme Medical Publishers, 2007.

[22] W. Bunnell, "An objective criterion for scoliosis screening," *Journal of Bone and Joint Surgery,* vol. 66-A, pp. 1381-1387, 1984.

[23] W. Bunnell, "Outcome of spinal screening," *Spine,* vol. 18, pp. 1572-1580, 1993.

[24] T. Thulbourne and R. Gillespie, "The rib hump in idiopathic scoliosis," *Journal of Bone and Joint Surgery,* vol. 58-B, pp. 64–71, 1976.

[25] W. Pun, K. Luk, W. Lee, and J. Leong, "A simple method to estimate the rib hump in scoliosis," *Spine,* vol. 12, pp. 342–345, 1987.

[26] I. Adair, M. VanWijk, and G. Armstrong, "Moiré topography in scoliosis screening," *Clinical Orthopaedics,* vol. 129, pp. 165–171, 1977.

[27] M. Sahlstrand, "The clinical value of moiré topography in the management of scoliosis," *Spine,* vol. 11, pp. 409–417, 1986.

[28] W. Frobin and E. Hierholzer, "Video rasterstereography: a method for on-line measurement of body surfaces," *Photogrammetric Engineering and Remote Sensing,* vol. 57, pp. 1341–1345, 1991.

[29] L. Hackenburg, E. Hierholzer, and U. Liljenqvist, "Accuracy of rasterstereography versus radiography in idiopathic scoliosis after anterior correction and fusion," in *Research into Spinal Deformities 4*, T. Grivas, Ed. Amsterdam: IOS Press, 2002, pp. 241–245.

[30] D. L. Hill, D. C. Berg, V. J. Raso, E. Lou, N. G. Durdle, J. K. Mahood, and M. J. Moreau, "Evaluation of a laser scanner for surface topography," *Studies in Health Technology and Informatics,* vol. 88, pp. 90-94, 2002.

[31] S. Treuillet, Y. Lucas, G. Crepin, B. Peuchot, and J. C. Pichaud, "SYDESCO: A Laser-Video Scanner for 3D Scoliosis Evaluations," in *Research into Spinal Deformities 3*, Alan Tanguy and B. Peuchot, Eds. Amsterdam, The Netherlands: IOS Press, 2002, pp. 70-75.

[32] J. Climent, A. Reig, J. Sánchez, and C. Roda, "Construction and validation of a specific quality of life instrument for adolescents with spine deformities," *Spine,* vol. 20, pp. 2006-2011, 1995.

[33] J. Thometz, R. Lamdan, X. Liu, and R. Lyon, "Relationship between Quantec measurement and Cobb angle in patients with idiopathic scoliosis," *Journal of Pediatric Orthopaedics,* vol. 20, pp. 512–516, July-August 2000.

[34] A. Schmitz, U. Jaeger, R. Koenig, J. Kandyba, U. Wagner, J. Giesecke, and O. Schmitt, "A new MRI technique for imaging scoliosis in the sagittal plane," *Eur Spine J,* vol. 10, pp. 114–117, 2001.

[35] N. Wright, "Imaging in scoliosis," *Arch Dis Child,* vol. 82, pp. 38–40, 2000.

[36] J. Dubousset, G. Charpak, I. Dorion, W. Skalli, F. Lavaste, J. Deguise, G. Kalifa, and S. Ferey, "A new 2D and 3D imaging approach to musculoskeletal physiology and pathology with low-dose radiation and the standing position: The EOS system," *Bulletin de l'Academie nationale de medecine,* vol. 189, pp. 287–297, 2005.

[37] R. Burwell, R. Aujla, A. Cole, A. Kirkby, R. Pratt, J. Webb, and A. Moulton, "Preliminary study of a new real-time ultrasound method for measuring spinal and rib rotation in preoperative patients with adolescent idiopathic scoliosis," in *Research into Spinal Deformities 4*, T. Grivas, Ed. Amsterdam: IOS Press, 2002, pp. 262–266.

[38] J. Cobb, "Outline for the study of scoliosis," *American Academy of Orthopedic Surgeons Instructional Course Lectures,* vol. 5, pp. 261–275, 1948.

[39] "Cobb angle," Scoliosis Treatment4u, URL http://www.scoliosistreatment4u.com/, 2010.

[40] D. Hoffman, J. Lonstein, M. Morin, W. Visscher, B. Harris, and J. Boice, "Breast cancer in women with scoliosis exposed to multiple diagnostic X-rays," *Journal of National Cancer Institute,* vol. 81, pp. 1307–1312, 1989.

[41] M. Morin Doody, J. Lonstein, M. Stovall, D. Hacker, N. Luckyanov, and C. Land, "Breast cancer mortality after diagnostic radiography: findings from the U.S. Scoliosis Cohort Study," *Spine,* vol. 25, pp. 2052–2063, 2000.

[42] A. Berrington de González and S. Darby, "Risk of cancer from diagnostic X-rays: estimates for the UK and 14 other countries," *The Lancet,* vol. 363, pp. 345-351, 2004.

[43] I. L. Dryden and K. V. Mardia, *Statistical Shape Analysis*: John Wiley & Sons, Chichester, 1998.

[44] D. G. Kendall, "The diffusion of shape," *Advances in Applied Probability,* vol. 9, pp. 428–430, 1977.

[45] F. L. Bookstein, *The measurement of biological shape and shape space change* vol. 24. New York: Springer-Verlag, 1978.

[46] F. L. Bookstein, "Landmark methods for forms without landmarks: Morphometrics of group differences in outline shape," *Medical Image Analysis,* vol. 1, pp. 225-243, 1997.

[47] D. G. Kendall, D. Barden, T. K. Carne, and H. Le, *Shape and Shape Theory*. Wiley, Chichester, 1999.

[48] D. G. Kendall, "Shape manifolds, Procrustean metrics and complex projective spaces," *Bulletin of the London Mathematical Society,* vol. 16, pp. 81-121, 1984.

[49] S. Lele and J. Richtsmeier, *An Invariant Approach to Statistical Analysis of Shapes*, First ed. London: Chapman and Hall-CRC Press, 2001.

[50] F. L. Bookstein, "Features of deformation grids: an approach via singularity theory," in *Proceedings of the Fourteenth Annual Symposium on Computational Geometry*, Minnesota, 1998, pp. 214-221.

[51] C. Goodall, "Procrustes methods in the statistical analysis of shape," *Journal Royal Statistical Society, Series B-Methodological,* vol. 53, pp. 285-339, 1991.

[52] R. Ball, C. Shu, P. Xi, M. Rioux, Y. Luximon, and J. Molenbroek, "A comparison between Chinese and Caucasian head shapes," *Applied Ergonomics,* vol. 41, pp. 832-839, 2010.

[53] T. Druml, R. Telalbasic, and I. Curik, "Body shape analysis of Bosnian mountain horses using Procrustes statistics," *Italian Journal of Animal Science,* vol. 8, pp. 131-133, 2009.

[54] S. Lele and J. Richtsmeier, "Euclidean distance matrix analysis: a coordinate-free approach for comparing biological shapes using landmark data," *American Journal of Physical Anthropology,* vol. 86, pp. 415-427, 1991.

[55] B. Corner and J. Richtsmeier, "Cranial growth in the squirrel monkey (Saimiri sciureus): a quantitative analysis using three dimensional coordinate data," *American Journal of Physical Anthropology,* vol. 87, pp. 67-81, 1992.

[56] J. Richtsmeier, J. Cheverud, S. Danahey, B. Corner, and S. Lele, "Sexual dimorphism of ontogeny in the crab-eating macaque (Macaca fascicularis)," *Journal of Human Evolution,* vol. 25, pp. 1-30, 1993.

[57] H. Gray, "Anatomy of the human body," in *Online Edition*: Published May 2000 by Bartleby URL http://www.bartleby.com/107, 1918.

[58] B. Arai and C. Read, "Modeling the Human Spine," URL www.conleyread.net/en_us/docs/231_ConleyRead_ProjectFinalPresentation_BenjaminArai.ppt, 2005.

[59] G. D. Cramer and S. A. Darby, *Basic and clinical anatomy of the spine, spinal cord, and ANS*, 2nd ed.: Elsevier Health Sciences, 2005.

[60] J. Mahood, M. Moreau, D. Hill, and V. Raso, "Perceptions of cosmetic deformity in scoliosis," in *Three Dimensional Analysis of Spinal Deformities*, M. D'Amico, A. Merolli, and G. C. Santambrogio, Eds. Amsterdam, Netherlands: IOS Press, 1995, pp. 239-242.

[61] Photobucket, "Scoliosis photos," URL http://photobucket.com/images/scoliosis/, Accessed 02 March, 2011.

[62] W. Bunnell, "The natural history of idiopathic scoliosis," *Clinical Orthopaedics,* vol. 229, pp. 20–25, 1988.

[63] S. Weinstein, "Adolescent idiopathic scoliosis." vol. 2000: University of Iowa, 1998.

[64] S. Weinstein, "Natural History," *Spine,* vol. 24, pp. 2592–2600, 1999.

[65] M. Richardson, "Approaches to differential diagnosis in musculoskeletal imaging - scoliosis." vol. 2000: www.rad.washington.edu/mskbook/scoliosis.html, 1999.

[66] I. Stokes, "Three-dimensional terminology of spinal deformity: A report presented to the scoliosis research society by the scoliosis research society working group on 3-D terminology of spinal deformity," *Spine,* vol. 19, pp. 236–248, 1994.

[67] G. Houghton, A. McInerney, and A. Tew, "Brace compliance in adolescent idiopathic scoliosis," *Journal of Bone and Joint Surgery,* vol. 69-B, p. 852, 1987.

[68] R. Winter and J. Lonstein, "To brace or not to brace:the true value of school screening," *Spine,* vol. 22, pp. 1283–1284, 1997.

[69] A. Nachemson and L. Peterson, "Effectiveness of treatment with a brace in girls who have adolescent idiopathic scoliosis. A prospective, controlled study based on data from the Brace Study of the Scoliosis Research Society.," *J Bone Joint Surg,* vol. 77A, pp. 815–822, 1995.

[70] C. Goldberg, D. Moore, E. Fogarty, and F. Dowling, "Adolescent idiopathic scoliosis - the effect of brace treatment on the incidence of surgery," *Spine,* vol. 26, pp. 42–47, 2001.

[71] C. Goldberg, D. Moore, E. Fogarty, and F. Dowling, "Adolescent idiopathic scoliosis: is the search for aetiology constrained by orthosis," in *Research into Spinal Deformities 3*, A. Tanguy and B. Peuchot, Eds. Amsterdam: IOS Press, 2002, pp. 222–225.

[72] J. R. Cobb, "Outline for the study of scoliosis," *In Instructional Course Lectures, The American Academy of Orthopaedic Surgeons,* vol. 5, pp. 261-275, 1948.

[73] I. Stokes and M. Moreland, "Concordance of back surface asymmetry and spine shape in idiopathic scoliosis," *Spine,* vol. 14, pp. 73–78, Jan 1989.

[74] D. Carman, R. Browne, and J. Birch, "Measurement of scoliosis and kyphosis radiographs," *Journal of Bone and Joint Surgery,* vol. 72-A, pp. 328–333, 1990.

[75] J. Mahood, M. Moreau, D. Hill, and V. Raso, "Perceptions of cosmetic deformity in scoliosis," in *Three dimensional analysis of spinal deformities*, M. D'Amico, A. Merolli, and G. Santambrogio, Eds. Amsterdam: IOS Press, 1995.

[76] R. Burwell, J. Patterson, J. Webb, and A. Wojcik, "School screening for scoliosis - the multiple ATI system of back shape appraisal using the scoliometer with observations on the sagittal declive angle," in *5th International Symposium on Surface Topography and Body Deformity 1988*, Neugebauer and Windischbauer, Eds., 1988.

[77] L. Amendt, K. Ause-Ellias, J. Eybers, C. Wadsworth, D. Nielsen, and S. Weinstein, "Validity and reliability testing of the Scoliometer," *Physical Therapy,* vol. 70, pp. 108–17, 1990.

[78] D. Pearsall, J. Reid, and D. Hedden, "Comparison of three noninvasive methods for measuring scoliosis," *Physical Therapy,* vol. 72, pp. 648–657, 1992.

[79] T. Karachalios, J. Sofianos, N. Roidis, G. Sapkas, D. Korres, and K. Nikolopoulos, "Ten year follow-up evaluation of a school screening program for scoliosis," *Spine,* vol. 24, pp. 2318–2324, 1999.

[80] P. Côté, B. Kreitz, and J. Martel, "A study of the diagnostic accuracy and reliability of the scoliometer and Adam's forward bend test," *Spine,* vol. 23, pp. 796–802, 1998.

[81] L. Galatz, P. Sturm, S. Bomze, and S. Simmens, "Interobserver reliability of scoliometer measurements of rotational deformity in adolescent idiopathic scoliosis," in *Research into Spinal Deformities 2. Proc. IRSSD 98.*, I. Stokes, Ed. Amsterdam: IOS Press, 1999.

[82] R. Burwell, N. James, F. Johnson, J. Webb, and Y. Wilson, "Standardised trunk asymmetry scores. A study of back contour in healthy school children.," *Journal of Bone and Joint Surgery,* vol. 65-B, pp. 452–463, 1983.

[83] J. Pearson, "Automated visual measurement of body shape in scoliosis," in *Coherent and Electro-Optics Research Group* Liverpool: PhD thesis from Liverpool John Moores University, 1996.

[84] M. Ruggerone and J. Austin, "Moiré topography in scoliosis. Correlations with vertebral lateral curvature as determined by radiography," *Physical Therapy,* vol. 66, pp. 1072–1077, 1986.

[85] N. Suzuki, T. Ono, M. Tezuko, and S. Kamiishi, "Moiré topography and back shape analysis - clinical applications," in *International Symposium on 3D Scoliotic Deformities*, J. Dansereau, Ed. Montreal: Gustav Fischer Verlag, 1992.

[86] G. Windischbauer and H. Neugebauer, "Digital 3D moiré - topography," in *Three dimensional analysis of spinal deformities*, M. D'Amico, A. Merolli, and G. Santambrogio, Eds. Amsterdam: IOS Press, 1995.

[87] H. Takasaki, "Moiré Topography," *Applied Optics,* vol. 9, pp. 1467-1472, 1970.

[88] Y. Harada, Y. Takemitsu, and M. Imai, "The role of contour line photography using the light cutting method and Moire photography in school screening for scoliosis," in *Moire fringe topography and spinal deformity. Proceedings of an International Conference*, New York, 1981, pp. 113-121.

[89] T. Kotwicki, E. Kinel, W. Stryla, and A. Szulc, "Discrepancy in clinical versus radiological parameters describing deformity due to brace treatment for moderate idiopathic scoliosis," *Scoliosis,* vol. 2, pp. 1-8, 2007.

[90] T. Grivas, G. Karras, J. Katrabasas, and N. Papavasiliou, "Study of posterior trunk surface changes by age and sex using moiré topography," in *Research into Spinal Deformities 1*, J. Sevastik and K. Diab, Eds. Amsterdam: IOS Press, 1997, pp. 331–334.

[91] M. Pirga, A. Kozlowska, and M. Kujawinska, "Generalization of the scaling problem for the automatic moiré and fringe projection shape measurement systems," in *Fringe 93, 2nd International Workshop on automatic processing of fringe patterns*, W. Juptner and W. Osten, Eds.: Akademie Verlag, 1993.

[92] W. Frobin and E. Hierholzer, "Automatic measurement of body surfaces using rasterstereography. I - Image scan and control point measurement," *Photogrammetric Engineering and Remote Sensing,* vol. 49, pp. 377-384, 1983.

[93] A. Moran and R. Lipczynski, "Automatic digitization and analysis of moiré topograms on a personal computer for clinical use," *Medical Engineering and Physics,* vol. 16, pp. 259–264, 1994.

[94] G. Windischbauer and J. Schedle, "Moire-topographical evaluation of the back shape deformities by basic programmable computer," in *Moiré Fringe Topography and Spinal Deformity*, Stuttgart, West Germany, 1983, pp. 227-232.

[95] D. Groves and P. Curran, "An accurate, fast and cost effective method for the measurement of body shape and the assessment of spinal deformity," in *Proceedings of the 6th International Symposium on Surface Topography and Spinal Deformity*, A. Alberti, B. Drerup, and E. Hierholzer, Eds. Stuttgart: Gustav Fischer, 1992.

[96] N. Oxborrow, "Assessing the child with scoliosis: the role of surface topography," *Arch Dis Child,* vol. 83, pp. 453–455, 2000.

[97] C. Goldberg, D. Moore, E. Fogerty, and F. Dowling, "Surface topography and Cobb angles in idiopathic scoliosis," in *Research into Spinal Deformities 2. Proc. IRSSD 98*, I. Stokes, Ed. Amsterdam: IOS Press, 1999.

[98] C. Griffiths, J. FitzGerald, R. Tweedie, and M. Leonard, "Accuracy and repeatability of spinal asymmetry using surface topography with and without upper body fixation," in *Research into Spinal Deformities 1*, J. Sevastik and K. Diab, Eds. Amsterdam: IOS Press, 1997.

[99] C. Goldberg, E. Fogarty, C. Moore, and F. Dowling, "Scoliosis imaging and the problem of postural sway," in *Research into Spinal Deformities 1*, J. Sevastik and K. Diab, Eds. Amsterdam: IOS Press, 1997.

[100] J. Thometz, X. Liu, and J. Klein, "Functional classification of patients with idiopathic scoliosis assessed by the Quantec System: a discriminate functional analysis to determine the patient group with different curves," in *Research into Spinal Deformities 2 - Proceedings of IRSSD 98*, I. Stokes, Ed. Amsterdam: IOS Press, 1999.

[101] J. Thometz, X. Liu, and R. Lyon, "Axial rotation in idiopathic scoliosis: a comparison of the perdriolle, scoliometer and the Quantec spinal image system," in *Research into Spinal Deformities 2 - Proceedings of IRSSD 98*, I. Stokes, Ed. Amsterdam: IOS Press, 1999.

[102] A. Turner-Smith, R. Roger, and J. Harris, "Shape measurement and scoliosis," Oxford Orthopaedic Engineering Centre, Oxford, Annual report 7, 1980.

[103] A. Turner-Smith and B. De Roguin, "Lateral asymmetry index," Oxford Orthopaedic Engineering Centre, Oxford, Annual report 11, 1984.

[104] A. Turner-Smith, J. Harris, J. Abery, and M. Osborne, "The assessment of scoliosis," Oxford Orthopaedic Engineering Centre, Oxford, Annual report 8, 1981.

[105] I. Weisz, R. Jefferson, A. Turner-Smith, G. Houghton, and J. Harris, "ISIS scanning: a useful assessment technique in the management of scoliosis," *Spine,* vol. 13, pp. 405–408, Apr 1988.

[106] J. Legaye, C. Orban, W. Lokietek, and N. Jacqumin, "The ISIS optic scanner: its use in the evaluation and control of spinal deviations (in French)," *Acta Orthopaedica Belgica,* vol. 58, pp. 66–72, 1992.

[107] F. Berryman, "Fourier transform profilometry for measuring back shape in scoliosis," in *School of Engineering and the Built Environment* Wolverhampton: University of Wolverhampton, 2004, p. 239.

[108] R Development Core Team, "R: A language and environment for statistical computing," R Foundation for Statistical Computing, Austria. ISBN 3-900051-07-0, URL http://www.R-project.org, 2009.

[109] M. Leonardi, M. Cucek-Plenicar, and J. Lenarcic, "Application of Fourier transform measurements of the human back," in *Research into Spinal Deformities 1*, J. Sevastik and K. Diab, Eds. Amsterdam: IOS Press, 1997.

[110] N. Durdle, D. Hill, Z. Zhang, and V. Raso, "A surface modelling system for the study of scoliosis," in *Three dimensional analysis of spinal deformities*, M. D'Amico, A. Merolli, and G. Santambrogio, Eds. Amsterdam: IOS Press, 1995.

[111] H. King, J. Moe, D. Bradford, and R. Winter, "The selection of fusion levels in thoracic idiopathic scoliosis," *The Journal of Bone and Joint Surgery,* vol. 65, pp. 1302-1313, 1983.

[112] C. Goldberg, D. Moore, E. Fogarty, and F. Dowling, "Adolescent idiopathic scoliosis: natural history and prognosis," in *Research into Spinal Deformities 4*, T. Grivas, Ed. Amsterdam: IOS Press, 2002, pp. 59–63.

[113] A. Asher and C. Burton, "Adolescent idiopathic scoliosis: natural history and long term treatment effects," *Scoliosis,* vol. 1, 2006.

[114] R. Jackson and A. McManus, "Radiographic analysis of sagittal plane alignment and balance in standing volunteers and patients with low back pain matched for age, sex, and size," *Spine,* vol. 19, pp. 1611–1618, 1994.

[115] D. Harrison, R. Cailliet, D. Harrison, T. Janik, and B. Holland, "Reliability of centroid, Cobb and Harrison posterior tangent methods; which to choose for analysis of thoracic kyphosis," *Spine,* vol. 26, pp. E227–E234, 2001.

[116] R. Vialle, N. Levassor, L. Rillardon, A. Templier, W. Skalli, and P. Guigui, "Radiographic analysis of the sagittal alignment and balance of the spine in asymptomatic subjects," *Journal of Bone and Joint Surgery,* vol. 87-A, pp. 260–267, 2005.

[117] D. Kolessar, G. Stollsteimer, and R. Betz, "The value of the measurement from T5-T12 as a screening tool in detecting abnormal kyphosis," *Journal of Spinal Disorders,* vol. 9, pp. 220–222, 1996.

[118] K. Singer, S. Goh, P. Leedman, and R. Price, "Reliability of rasterstereography of thoracic kyphosis," in *Research into Spinal Deformities 2 - Proceedings of IRSSD 98*, I. Stokes, Ed. Amsterdam: IOS Press, 1999.

[119] R. Burwell, "The rib hump score: a guide to referral and prognosis?," *Journal of Bone and Joint Surgery,* vol. 64, p. 284, 1982.

[120] J. Mac-Thiong, F. Pinel-Giroux, J. A. D. Guise, and H. Labelle, "Comparison between constrained and non-constrained Cobb techniques for the assessment of thoracic kyphosis and lumbar lordosis," *European Spine Journal,* vol. 16, pp. 1325-1331, 2007.

[121] Dean C. Adams, F. James Rohlf, and D. E. Slice, "Geometric morphometrics: ten years of progress following the "revolution"," *Italian Journal of Zoology,* vol. 71, pp. 5-16, 2004.

[122] C. Brechbuhler, G. Gerig, and O. Kubler, "Parameterization of closed surfaces for 3-D shape description," *CVGIP: Image Understanding,* vol. 61, pp. 154-170, 1995.

[123] A. Kelemen, G. Szekely, and G. Gerig, "Three-dimensional model-based segmentation," in *In Proceedings of IEEE International Workshop on Model Based 3D Image Analysis*, Bombay, India, 1998, pp. 87-96.

[124] D. S. Fritsch, S. M. Pizer, B. Morse, D. H. Eberly, and A. Liu, "The multiscale medial axis and its applications in image registration," *Pattern Recognition Letters,* vol. 15, pp. 445-452, 1994.

[125] P. Golland, W. E. L. Grimson, and R. Kikinis, "Statistical shape analysis using fixed topology skeletons: corpus callosum study," in *In Proceedings of IPMI'99: Information Processing in Medical Imaging*, 1999, pp. 382-387.

[126] C. Davatzikos, M. Vaillant, S. Resnick, J. L. Prince, S. Letovsky, and R. N. Bryan, "A computerized method for morphological analysis of the corpus callosum," *Journal of Computer Assisted Tomography,* vol. 20, pp. 88-97, 1996.

[127] A. M. C. Machado and J. C. Gee, "Atlas warping for brain morphometry," in *In Proceedings of SPIE Medical Imaging 1998: Image Processing*, 1998, pp. 642-651.

[128] J. T. Richtsmeier, J. Cheverud, and S. R. Lele, "Advances in Anthropological Morphometrics," *Annual Reviews in Anthropology,* vol. 21, pp. 283-305, 1992.

[129] J. T. Richtsmeier, V. B. Deleon, and S. R. Lele, "The promise of geometric morphometrics," *Yearbook of Physical Anthropology,* vol. 45, pp. 63-91, 2002.

[130] L. F. Marcus, M. Corti, A. Loy, G. J. P. Naylor, and D. E. Slice, *Advances in Morphometrics*. New York: Plenum Press, 1996.

[131] D. C. Adams, F. J. Rohlf, and D. E. Slice, "Geometric Morphometrics: Ten Years of Progress Following the 'Revolution'," *Italian Journal of Zoology,* vol. 71, pp. 5-16, 2004.

[132] M. E. Piccus, G. A. Smith, B. K. Standley, T. L. Volk, and L. B. Wildes, "Creation of Prototype Aircrew Protection Equipment Based on Face Anthropometry," MS Thesis, Air Force Institute of Technology, USA, 1993.

[133] J. Cheverud, J. Lewis, W. Bachrach, and W. Lew, "The measurement of form and variation in form: an application of three-dimensional quantitative morphology by finite-element methods," *American Journal of Physical Anthropology,* vol. 62, pp. 151-165, 1983.

[134] M. Mochimaru, M. Kouchi, and M. Dohi, "Analysis of 3-D human foot forms using the Free Form Deformation method and its application in grading shoe lasts," *Ergonomics,* vol. 43, pp. 1301-1313, 2000.

[135] F. L. Bookstein, "Principal warps: thin-plate splines and the decomposition of deformations," *IEEE Transactions on Pattern Analysis and Machine Intelligence,* vol. 11, pp. 567-585, 1989.

[136] F. Bookstein, "Foundations of morphometrics," *Annual Review of Ecology and Systematics,* vol. 13, pp. 451-470, 1982.

[137] B. Broadbent, B. Broadbent, and W. Golden, *Bolton standards of dentofacial developmental growth*. Mosby, St Louis, 1975.

[138] C. Rao and S. Suryawanshi, "Statistical analysis of shape of objects based on landmark data," in *Proceedings of the National Academy of Sciences of the United States of America*, 1996, pp. 12132-12136.

[139] J. C. Gower and G. B. Dijksterhuis, *Procrustes Problems*: Oxford University Press, Oxford, 2004.

[140] F. Crosilla and A. Beinat, "Use of generalized Procrustes analysis for the photogrammetric block adjustment by independent models," *ISPRS Journal of Photogrammetry and Remote Sensing,* vol. 53, pp. 195-209, 2002.

[141] J. C. Gower, "Generalized Procrustes analysis," *Psychometrika,* vol. 40, pp. 33-51, 1975.

[142] P. H. Schonemann, "A generalized solution of the orthogonal Procrustes problem," *Psychometrika,* vol. 31, pp. 1-10, 1966.

[143] P. H. Schoenemann and R. Carroll, "Fitting one matrix to another under choice of a central dilation and a rigid motion," *Psychometrika,* vol. 35, pp. 245-255, 1970.

[144] W. Kristof and B. Wingersky, "Generalization of the orthogonal Procrustes rotation procedure to more than two matrices," *Proceedings of the 79th Annual Convention of the American Psychological Association,* vol. 6, pp. 89-90, 1971.

[145] J. M. F. Ten Berge, "Orthogonal Procrustes rotation for two or more matrices," *Psychometrika,* vol. 42, pp. 267-276, 1977.

[146] S. Lele, "Euclidean distance matrix analysis (EDMA): estimation of mean form and mean form difference," *Mathematical Geology,* vol. 25, pp. 573-602, 1993.

[147] S. Lele and T. M. Cole III, "A new test for shape differences when variance-covariance matrices are unequal," *Journal of Human Evolution,* vol. 31, 1996.

[148] S. Lele, "Invariance and morphometrics: a critical appraisal of statistical techniques for landmark data," in *On Growth and Forms: Spatio-temporal Pattern Formation in Biology*, M. A. J. Chaplain, G. D. Singh, and J. C. McLachlan, Eds. Chichester: John Wiley and Sons Ltd, 1999, pp. 325-336.

[149] S. Lele and C. McCulloch, "Invariance, identifiability, and morphometrics," *Journal of the American Statistical Association,* vol. 97, pp. 796-804, 2002.

[150] S. Lele, "Some comments on coordinate-free and scale-invariant methods in morphometrics," *American Journal of Physical Anthropology,* vol. 85, pp. 407-417, 1991.
[151] S. F. Arnold, *The Theory of Linear Models and Multivariate Analysis*. New York: John Wiley and Sons, 1981.
[152] N. L. Johnson and S. Kotz, *Distributions in statistics - Continuous univariate distributions 2*. Boston: Houghton Mifflin Company, 1970.
[153] T. Acharya and A. K. Ray, *Image Processing: Principles and Applications*. New York: John Wiley and Sons Ltd, 2005.
[154] J. M. Bland and D. Altman, "Statistical methods for assessing agreement between two methods of clinical measurement," *Lancet,* vol. 1, pp. 307-310, 1986.
[155] M. A. Schork and R. D. Remington, *Statistics with Applications to the Biological and Health Sciences*, Third ed. New Jersey: Prentice Hall, 2000.
[156] J. C. Gower, "Euclidean distance geometry," *Math. Scientist,* vol. 7, pp. 1-14, 1982.
[157] J. M. Bland, *An Introduction to Medical Statistics*, Third ed. Oxford: Oxford University Press, 2000.
[158] B. O'Neill, *Semi-Riemannian Geometry*. B Street, Suite 1900, San Diego, California, USA: Elsevier Science & Technology, 1983.
[159] I. Dryden, "shapes: Statistical shape analysis," R package version 1.1-3, URL http://www.maths.nott.ac.uk/~ild/shapes, 2009.
[160] J. Claude, *Morphometrics with R*. New York: Springer-Verlag, 2008.
[161] T. M. Cole and J. T. Richtsmeier, "A simple method for visualization of influential landmarks when using Euclidean distance matrix analysis," *American journal of physical anthropology,* vol. 107, pp. 113-124, 1998.
[162] W. J. Krzanowski, *Recent Advances in Descriptive Multivariate Analysis*. New York: Oxford University Press Clarendon Press, 1995.
[163] I. L. Dryden, A. Kume, H. Le, and A. T. A. Wood, "A multi-dimensional scaling approach to shape analysis," *Biometrika,* vol. 95, pp. 779-798, 2008.
[164] S. Lele and J. Richtsmeier, "Statistical models in morphometrics: are they realistic?," *Systematic Zoology,* vol. 39, pp. 60-69, 1990.
[165] J. T. Kent and K. V. Mardia, "Consistency of Procrustes estimators," *Journal of the Royal Statistical Society: Series B,* vol. 59, pp. 281-290, 1997.
[166] F. J. Rohlf, "Statistical power comparisons among alternative morphometric methods," *American Journal of Physical Anthropology,* vol. 111, pp. 463-478, 2000.
[167] F. J. Rohlf, "On the use of shape spaces to compare morphometric methods," *Hystrix - the Italian Journal of Mammalogy,* vol. 11, pp. 9-25, 2000.